

SYNTHESIS OF HYDROXYAPATITE BIOMEDICAL CERAMIC BY SPARK PLASMA SINTERING AND IT'S CHARACTERIZATION

By

Shabbir Ahmed

Student ID- 0416112501

M.Sc. In Mat. Science

This thesis paper is submitted to the department of Materials and Metallurgical Engineering in partial fulfillment of the requirement for the degree of Master of Science in Material Science in the Department of Materials and Metallurgical Engineering

Supervisor:

Dr. Fahmida Gulshan



**Department of Materials and Metallurgical Engineering
Bangladesh University of Engineering and
Technology**

Dhaka-1000, Bangladesh

March 2020

Approval Page

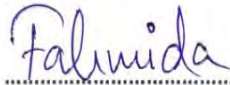
The thesis entitled "SYNTHESIS OF HYDROXYAPATITE BIOMEDICAL CERAMIC BY SPARK PLASMA SINTERING AND IT'S CHARACTERIZATION" submitted by Shabbir Ahmed, Student ID: 0416112501, Session: April 2016 has been accepted as satisfactory in partial fulfillment of the requirement for the degree of Master of Science in Materials Science on 2nd March, 2020.

BOARD OF EXAMINERS




.....
Dr. Fahmida Gulshan (Supervisor)
Professor
Department of Materials and Metallurgical Engineering
BUET, Dhaka

Chairman



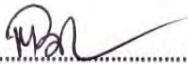
.....
Dr. Fahmida Gulshan (Ex-Officio)
Professor & Head
Department of Materials and Metallurgical Engineering
BUET, Dhaka

Member



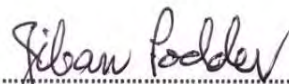
.....
Dr. Ahmed Sharif
Professor
Department of Materials and Metallurgical Engineering
BUET, Dhaka

Member



.....
Dr. Md. Muktedir Billah
Assistant Professor
Department of Materials and Metallurgical Engineering
BUET, Dhaka

Member



.....
Dr. Jiban Podder
Professor
Department of Physics
BUET, Dhaka

Member
(External)

Dedication.....

To the great man Dr. Tofail Syed

Acknowledgements

First of all, thanks to almighty Allah (SWT) for giving me the patience and ability for completing this thesis work.

In completing this thesis work, there are several people I would like to thank:

Prof. Dr. Fahmida Gulshan, my supervisor and advisor for her utmost guidance, continuous encouragement, valuable advices for completing this thesis work and I am really debt to Prof. Tofail Syed for his guidance and help. I have been incredibly fortunate to work with them and have benefited enormously from their knowledge and constant support. I am also grateful to Ehtsham U. Haq for always having time to answer my questions.

My parent continuously encouraged me for completing this thesis work. I won't be able to finish this work without their contribution.

I am really grateful to Garry Warren and Sarah Markham, University of Limerick, Ireland as well as Dr. Muhammad Hassanuzzaman, Assistant Professor, Department of Glass and Ceramic Engineering.

To my friends and former and present colleagues in the department, thank you for creating such a nice atmosphere in the department. Your help and enthusiasm have been highly appreciated and unforgettable, in particularly; Raihan Atahar, Shofikul Islam Nobel, Salim Hoq, Md Mufidul Islam and Asiful Hasan Chy.

I would take the opportunity to thank all my respected teachers and staff at the department of Materials and Metallurgical Engineering, BUET, for making the working environment inspiring.

Shabbir Ahmed acknowledges European Commission Erasmus International Credit Mobility 2015-2020 between University of Limerick, Ireland and Bangladesh University of Engineering and Technology, Dhaka, Bangladesh for a seven months secondment at the Modelling, Simulation and Innovative Characterization (MOSAIC) group of the Bernal Institute of the University of Limerick, where a part of the research leading to the current thesis was conducted. Neither the European Commission nor the University of Limerick holds any responsibility of the content and conclusions of this thesis.

Abstract

This work describes the unique features and controlled sintering ability of modern spark plasma sintering machine for the preparation of transparent hydroxyapatite biomedical ceramic. It also investigated the effect of contact electrical poling to measure and justifies its piezoelectric behaviors. In this research work, highly specialized electric current assisted Spark Plasma Sintering (SPS) technique was used for hydroxyapatite (HA) powder sintering. All the sintering parameters were controlled with high precision by its computerized mechanism that suppressed several limitations of conventional sintering techniques. HA biomedical ceramic pellets were prepared at prolonged temperature ranges around 850°C to 1000°C with calcined and un-calcined HA powder. Transmittances of prepared samples were measured by using UV Vis spectrometer. Phase changes in sintered pellets were analyzed by X- ray diffraction pattern and optical micrograph. XRD analysis confirmed phase purity and crystal orientation of produced samples. Relevant orientation indexes of HA materials were measured from X ray diffraction patterns of planes perpendicular and parallel to the applied pressure direction to identify c-axis elongation so as to evaluate the possibility of introducing piezoelectric property in the HA sample. HA samples prepared at sintering temperature 900°C using calcined powder shows maximum transmittance nearly 75%. On the other hand, HA samples that were prepared from un-calcined powder showed maximum transmittance around 70%. Comparatively, lower sintering pressure 3.9kN was found more favorable for producing transparent HA pellets at temperature 900°C but after crossing 975°C, opposite phenomenon was also observed that is higher pressure was better for producing more transparent HA pellets. Textured transparent HA samples were then applied in high voltage contact electrical poling devices to create a net polarization and therefore to induce piezoelectricity. Here, sufficiently strong electric fields were applied across these ceramics to cause reorientation of spontaneously elongated unit cell into more isotropic alignment along the field lines. Finally, applied field was removed and samples were cooled rapidly to induce a net overall piezoelectric property. Here, the effect of applied voltages and poling temperatures were investigated and found to induce longitudinal piezoelectric coefficient (D_{33}) around 0.8pC and 0.5pC for those sample sintered at temperature 875°C and 975°C when they were polled parallel and perpendicular direction of SPS pressure surface respectively.

Keywords: Hydroxyapatite, Spark Plasma Sintering, Transparent HA ceramic, high voltage contact electrical poling, Piezoelectricity.

Table of Contents

Acknowledgement	IV
Abstract	V
Table of Contents	VI
Nomenclature	VIII
List of Tables	IX
List of Figures	X
Chapter-01 Introduction	01
1.1 Aims and Objectives.....	02
1.2 Research questions.....	03
1.3 Research Hypothesis.....	04
1.4 Structure of the thesis.....	06
Chapter-2 Literature Review	07
2.1 Apatite in natural bone.....	07
2.2 Crystalline Structure of Apatite.....	08
2.3 Hydroxyapatite.....	10
2.3.1 Synthesis of hydroxyapatite powder.....	11
2.3.2 Hydroxyapatite crystal system.....	12
2.3.3 Hydroxyapatite as biomaterial.....	13
2.4 Piezoelectric property of hydroxyapatite.....	14
2.4.1 Ferroelectricity.....	14
2.4.2 Mechanism of Polarization.....	16
2.4.3 Ferroelectricity in Hydroxyapatite material.....	18
2.4.4 Polarizing phenomenon of ferroelectric material	19
2.4.5 Antiferroelectric Materials.....	20
2.4.6 Piezoelectric response of HA.....	21
2.5 Transparent Hydroxyapatite.....	23
2.5.1 Transparency in ceramic materials.	23
2.5.2 Transparent Hydroxyapatite.....	24
2.6 Sintering of Hydroxyapatite.....	25
2.6.1 Comparative sintering methods of hydroxyapatite.	27
2.7 Spark Plasma Sintering Technique.....	29
2.7.1 Structural configuration.....	30
2.7.2 Sintering Mechanism.....	32

Chapter-3	Experimental Procedure	36
3.1	Sintering of hydroxyapatite powder.....	36
3.1.1	Preparing Mold with Fixed amount of powder.....	36
3.1.2	Sintering of HA powder by Spark Plasma sintering Machine....	38
3.1.3	Sintering Chamber.....	39
3.1.4	Control Panel.....	40
3.1.5	Different Programs used in sintering Machine.....	42
3.2	High voltage Polarization of hydroxyapatite pellets.....	44
3.2.1	Design and construction of polarizing apparatus.....	44
3.2.2	Polarizing procedure.....	46
3.3	Characterization Methods.....	49
3.3.1	Optical Characterization using UV visible spectroscopy.....	49
3.3.2	Optical microscopic imaging.....	50
3.3.3	X-ray diffraction.....	36
Chapter-04	Results and Discussion	53
4.1	XRD Characterization.....	53
4.1.1	XRD profile of sintered HA pellets along the perpendicular direction of SPS pressure.....	53
4.1.2	XRD profile of sintered HA pellets in parallel direction of SPS pressure.....	60
4.1.3	XRD for identification of decomposition product.....	63
4.1.4	XRD peak profile- perpendicular and parallel surface of SPS pressure.....	65
4.2	Transparent hydroxyapatite samples.....	66
4.3	Microscopic Images of Transparent, Translucent and Opaque HA samples.....	67
4.4	Measurement of transmittance in UV visible spectrometer.....	76
4.5	Effects of sintering parameters on transmittance.....	83
4.5.1	Effect of Sintering Temperature on Transmittance.....	83
4.5.2	Effect of pressure on Transmittance.....	84
4.5.3	Effect of hydroxyapatite powder on transmittance.....	85
4.5.4	Effect of Sintering Time on transmittance.....	85
4.6	Piezoelectric responses.....	86
Chapter-5	Conclusion.....	91
	Recommended Future Work.....	93
	Reference.....	94

Nomenclature/ Abbreviations:

HA	Hydroxyapatite
FA	Fluorapatite
CA	Chlorapatite
TCP	Tricalcium Phosphate
SPS	Spark Plasma Sintering
ECAS	Electric Current Assisting Sintering
FAST	Field Assisted Sintering
PECS	Pulse Electric Current Sintering
Ps	Saturation polarization
Pr	Remnant Polarization
Ec	Coercive field
HP	Hot Pressing
TEM	Transmission electron microscope
XRD	X-ray Diffraction
SEM	Scanning electron microscope
ST	Sintering Temperature
SP	Sintering Pressure

List of tables

Table-2.1: Calcium phosphate compounds and their Ca/P ratio.....	7
Table-2.2: The structure and symmetries of apatite materials.....	8
Table-2.3: Physical properties of HA material.....	10
Table-2.4: Thermal effects on calcium phosphate.....	28
Table-2.5: Characteristics features of Conventional and SPS Sintering.....	29
Table-3.1: PTN-1 for sintering temperature 900°C.....	42
Table-3.2: PTN-2 for sintering temperature 925°C.....	42
Table-3.3: PTN-3 for sintering temperature 875°C.....	42
Table-3.4: PTN-4 for sintering temperature 850°C.....	42
Table-3.5: PTN-5 for sintering temperature 975°C.....	43
Table-3.6: PTN-6 for sintering temperature 950°C.....	43
Table-3.7: PTN-7 for sintering temperature 825°C.....	43
Table-3.8: PTN-8 for sintering temperature 1000°C.....	43
Table-4.1: XRD data of transparent HA pellets, ST-875 °C, SP-3.9kN, powder type- calcined.....	56
Table-4.2: XRD data of transparent HA pellet, ST-900 °C, SP-3.9, powder type- calcined.....	56
Table-4.3: XRD data of transparent HA pellet, ST-975 °C, SP-3.9KN, powder type- calcined.....	57
Table-4.4: XRD data of translucent HA pellet, ST-850 °C, SP-4.7kN, powder type- calcined.....	57
Table-4.5: XRD data of opaque HA pellet, ST-1000 °C, SP-3.9kN, powder type- calcined.....	58
Table-4.6: XRD data of calcined HA Powder.....	59
Table-4.7: Samples obtained at different sintering temperatures and pressures	66
Table-4.8: Longitudinal piezoelectric constant (D_{33}) before poling.....	86
Table-4.9: Piezoelectric responses of transparent HA pellets (prepared at different sintering temperature) measured by its D_{33} values, under same applied poling condition.....	86

List of figures

Figure-2.1: a) FA, b) F ion replaced with polar OH in HA.....	9
Figure-2.2: Structure of hydroxyapatite unit cell.....	12
Figure-2.3: Biomedical application of HA.....	13
Figure- 2.4- Hysteresis loop for a ferroelectric material and the influence of the electric.... field on the alignment of the dipoles.....	15
Figure-2.5: Atomic polarization.....	16
Figure-2.6: Ionic Polarization.....	16
Figure-2.7: Oriental Polarization.....	17
Figure-2.8: Interface polarization.....	17
Figure- 2.9: Hydroxyl ion orientation and polar -nonpolar orientation in Hydroxyapatite...	18
Figure-2.10: High voltage contact electrical poling.....	19
Figure- 2.11: Characteristic hysteresis loop of antiferroelectric material.....	20
Figure-2.12: SPS sintering technique.....	30
Figure-2.13: Energy dissipation in the microscopic scale.....	32
Figure-2.14: Stages of Sintering.....	43
Figure-2.15: Material Transfer Path during Sintering.....	35
Figure-3.1: Die preparation for SPS machine.....	37
Figure-3.2: Spark Plasma Sintering machine.....	38
Figure-3.3: Sintering Chamber.....	39
Figure-3.4: Control panel of SPS machine.....	40
Figure-3.5: Voltage, Current, time and Pressure Graph.....	41
Figure-3.6: High voltage power supply and desiccators box with locking mechanism.....	44
Figure- 3.7: Interlocked key attached with desiccators.....	45
Figure-3.8: Polarizing Apparatus and Electrodes.....	47
Figure-3.9: UV-Visible spectrometer.....	49
Figure-3.10: Optical microscope.....	50
Figure-3.11: XRD machine.....	51
Figure-3.12: Prepared samples for placing in XRD chamber.....	52
Figure-4.13: XRD direction on HA pellets as per SPS pressure.....	52
Figure-4.1: Transparent HA pellets, ST-875 ^o C, SP-3.9kN, powder type-Calcined....	53
Figure-4.2: Transparent HA pellet, ST-900 ^o C,SP-3.9,powder type-calcined.....	54
Figure-4.3: Transparent HA pellet, ST-975 ^o C, SP-3.9KN, powder type-calcined....	54
Figure-4.4: Translucent HA pellet, ST-850 ^o C,SP-4.7kN, powder type-calcined.....	55
Figure-4.5: Opaque HA pellet, ST-1000 ^o C,SP-3.9kN, powder type-calcined.....	55
Figure-4.6: XRD of calcined HA powder.....	58
Figure-4.7: Transparent HA pellets, ST-950 ^o C, SP-3.9kN, powder type-calcined...	60
Figure-4.8: Transparent HA pellets, ST-850 ^o C, SP-3.9kN, powder type-calcined...	60
Figure-4.9: Transparent HA pellets, ST-900 ^o C, SP-3.9kN, powder type-calcined...	61

Figure-4.10: Translucent HA pellets, ST-875 ^o C, SP-3.9kN, powder type-calcined...	61
Figure-4.11: Opaque HA pellets, ST-975 ^o C, SP-3.9kN, powder type-calcined.....	62
Figure-4.12: XRD peaks and plane taken perpendicular direction of SPS pressure...	63
Figure-4.13: XRD peaks and plane taken parallel direction of SPS pressure.....	63
Figure-4.14: XRD peak of calcined HA powder and prepared HA pellet together.....	64
Figure-4.15: XRD at the perpendicular surface of pellet with respect to SPS pressure	65
Figure-4.16: XRD at the parallel surface of pellet with respect to SPS pressure.....	65
Figure-4.17: Un-calcined powder sintered at pressure 3.9kN, temperature-825 ^o C and sectioned perpendicular to SPS pressure (A) Before etching (B) After etching. Calcined powder sintered at pressure 3.9kN, temperature-825 ^o C and sectioned perpendicular to SPS pressure (C) Before etching (D) After etching.....	69
Figure-4.18: Optical micrograph of SPS sintered opaque milky white HA pellets prepared at 825 ^o C from un calcined powder sintered at (A) 4.7 kN (B) 3.9kN, HA pellets sintered at 850 ^o C from un calcined powder at (D)4.7kN (E)3.9kN, pellets sintered at 1000 ^o C from calcined powder at (D)3.9kN (E)4,7kN and sectioned perpendicular to SPS pressure.....	70
Figure-4.19: Optical micrograph of SPS sintered HA pellets along the edge portion prepared at (A)875 ^o C and 4.3kN (B) 900 ^o C and 4.3kN (C) 925 ^o C and 4.3kN from un calcined powder, (D)825 ^o C and 4.3kN (E) 825 ^o C and 4.7kN (F) 900 ^o C and 4.3kN from calcined powder.....	71
Figure-4.20: Optical micrograph of SPS sintered transparent HA pellets prepared at (A)900 ^o C and 3.9kN (B) 975 ^o C and 3.9kN from un calcined powder (C) 900 ^o C and 3.9kN (D) 975 ^o C and 3.9kN from calcined powder.....	72
Figure-4.21: Optical micrograph of SPS sintered mildly transparent HA pellets prepared at (A)850 ^o C and 4.7kN (B) 875 ^o C and 4.7kN from calcined powder (C) 875 ^o C and 3.9kN (D) 875 ^o C and 4.3kN from un calcined powder.....	73
Figure-4.22: Optical micrograph of SPS sintered (A) translucent HA pellets prepared at 875 ^o C, 4.7kN (B) Opaque HA pellets prepared at 825 ^o C, 4.7kN from un calcined powder sectioned along the parallel direction of SPS pressure.....	74
Figure-4.23: Optical micrograph of SPS sintered transparent HA pellets prepared at(A) 900 ^o C, 3.9kN (B) 900 ^o C, 3.4kN(C) 900 ^o C, 4.7kN(D) 925 ^o C, 4.7kN and sectioned parallel to SPS pressure.....	75
Figure-4.24: Transparent HA pellets from calcined powder (a) SPS pressure-3.9kN (b) SPS pressure4.7kN, sintering temperature 850 ^o C.....	76
Figure-4.25: Transparent HA pellets from un-calcined powder (a) SPS pressure-3.9kN (b) SPS pressure-4.7kN, pellets from calcined powder (c) SPS pressure-3.9kN (d) SPS pressure-4.7kN, sintering temperature 875 ^o C.....	77
Figure-4.26: Transparent HA pellets from un-calcined powder (a) SPS pressure-3.9kN (b) SPS pressure-4.7kN, pellets from calcined powder (c) SPS pressure-3.9kN (d) SPS pressure-4.7kN, sintering temperature 900 ^o C.....	78
Figure-4.27: Transparent HA pellets from un-calcined powder (a) SPS pressure-3.9kN (b) SPS pressure-4.7kN, pellets from calcined powder (c) SPS pressure-3.9kN (d) SPS pressure-4.7kN, sintering temperature 925 ^o C.....	79
Figure-4.28: Transparent HA pellets from un-calcined powder (a) SPS pressure-3.9kN (b) SPS pressure-4.7kN, pellets from calcined powder (c) SPS pressure-	

3.9kN (d) SPS pressure-4.7kN, sintering temperature 950°C.....	80
Figure-4.29: Transparent HA pellets from un-calcined powder (a) SPS pressure-3.9kN (b) SPS pressure-4.7kN, pellets from calcined powder (c) SPS pressure-3.9kN (d) SPS pressure-4.7kN, sintering temperature 975°C.....	81
Figure-4.30: Transparent HA pellets from un-calcined powder (a) SPS pressure-3.9kN (b) SPS pressure-4.7kN, sintering temperature 975°C.....	82
Figure- 4.31: Sintering Temperature Vs Transmittance	83
Figure-4.32: Transmittance of HA pellets prepared from un-calcined powder at different SPS pressures.....	84
Figure-4.33: Changes of transmittance	85
Figure-4.34: Contract Electrical Poling along SPS Pressure Direction.....	87
Figure-4.35: Contract Electrical Poling perpendicular to SPS Pressure Direction...	87
Figure- 4.36: Microstructural changes in sintered sample.....	89

Chapter-1

Introduction

Hydroxyapatite (HA) is a calcium phosphate-based material. It has a wide application as a biomedical material [1-2]. Excellent biocompatibility of HA material is the most important property considered for biomedical application. Hydroxyapatite in the form of hydroxycarbonate apatite is the principal mineral component of bone tissue in mammals. The compositional and structural similarity of synthetic hydroxyapatite to natural bone renders its application to produce artificial bone. It has excellent bone bonding ability which promotes its use in orthopedic applications [3-5]. Its bioactive nature helps to grow bone tissue directly on it without intervening fibrous tissues. Its common applications are bone graft, fillers and as a coating for metal implants. It is comparatively new observation that electrical and optoelectrical properties of hydroxyapatite with higher transparency that may add additional uses to its conventional biomedical application [6]. Such transparent hydroxyapatite would be used in implantable bio-devices for direct observation of biological activities and for the assessment of fundamental cellular functions [7]. It may also be used for direct investigation the behavior of human cell and cultured tissue on material's surface.

Natural bone has been reported to be pyroelectric and piezoelectric [8-9]. The longitudinal piezoelectric co-efficient of bone was measured to be 0.45pC/N [10]. Synthetic and electrically polarized hydroxyapatite has also been found to be piezoelectric, pyroelectric and ferroelectric [11-12]. Piezoelectricity following the mechanical stress influence bone growth. Textured hydroxyapatite reported to show weak ferroelectricity and pyroelectricity but higher (six orders of magnitude) piezoelectricity which is greater than that of bone and of the same order of quartz crystal and uncalcified collagen in tendon [6]. This higher piezoelectric value of synthetic hydroxyapatite makes it physiologically relevant for bone grafting.

Generally used hydroxyapatite is optically opaque and shows milky white appearance. It may show very high level of optical transmittance reported up to 65% [7]. This transmittance of hydroxyapatite arises due to texture, density and crystallographic c-axis orientation. This texture and density are usually controlled by sintering temperature.

1.1 Aims and objectives

The aim of this research work is synthesis of highly transparent hydroxyapatite ceramic using specialized spark plasma sintering technique. In this work, hydroxyapatite powder was sintered at different sintering temperature and pressure. Two types of hydroxyapatite powder calcined and uncalcined were used to know the effect of powder on transmittance of prepared sample. Here, sintering parameter like temperature was changed spontaneously keeping pressure constant and after that pressure was changed keeping the temperature constant. This manner was followed at the temperature range 825°C to 1000°C and pressure 3.9kN to 4.7kN. Throughout the whole process a close focus was given to produce hydroxyapatite that will be transparent, homogeneous in composition with optimal physical, chemical and electrical properties.

After sintering transparent ceramic, a detail analysis was carried out to measure transmittance and responsible causes behind the transmittance. For the measurement of transmittance of transparent hydroxyapatite, UV-visible spectrometer was used after polishing each sample properly. Structural and compositional analysis was carried out using XRD. The electrical and piezoelectric behavior of produced hydroxyapatite pellets were investigated by checking and measuring their piezoelectric properties. These ceramic samples were applied in high voltage contact electrical poling device to see their responses to high voltage polarization process. All the obtain data and information was documented and reviewed with highest scientific standards and methodology.

The aims of this research project:

- I. Synthesis of highly transparent piezoelectric hydroxyapatite biomedical ceramic using SPS technique at different temperatures and pressures.
- II. Structural and compositional analysis of the produced samples to know the effect of sintering parameters.

1.2 Research questions

Hydroxyapatite is the main inorganic compound of human bone and plays an important role for the mechanical work in human body. A lot of biological functions also take place inside the bone. Synthetic hydroxyapatite is already being used in different orthopedic applications like bone grafting, enamel and as a coating material on metallic substances placed in human body.

This research has been carried out by highly specialized Spark Plasma Sintering (SPS) machine to sinter hydroxyapatite powder into transparent hydroxyapatite ceramic pellets so as to diversify the use of hydroxyapatite as biomaterial.

It also investigated the possibility of introducing piezoelectric property in these transparent hydroxyapatite ceramics by applying them in high voltage contact electrical poling device to render its application for few other purposes.

Research purpose to know and investigate the following queries-

1. Possibility of producing highly transparent HA ceramic
2. Effects of sintering parameters over transmittance of hydroxyapatite ceramic.
3. Possible optimum sintering condition for producing highly transparent HA ceramic.
4. Structural and microstructural changes occur during SPS sintering.
5. Possibility of introducing piezoelectricity in transparent HA ceramic by high voltage contact electrical poling technique.

1.3 Research hypothesis

The origin of transparency in HA is still unclear. Several studies have been carried out to know the reasons behind the transmittance of hydroxyapatite but still there is a lack of experimental proof. It is considered that optical transparency is influenced considerably by local discontinuities in the refractive index, this discontinuity is the result of grain boundaries, compositional heterogeneities and even it would be the result of microstructural defect such as porosity [13-14]. This discontinuity may also be the result of different orientation of adjacent grain. Those ceramics composed of noncubic, uniaxial or biaxial crystallites as a randomly orientated polycrystalline structure usually show higher level of mismatch between ordinary and extra-ordinary optical axes of the neighboring grains [14]. In some experimental work, very high level of crystallographic c-axis orientation has been observed in transparent hydroxyapatite sintered by spark plasma sintering technique [15].

It is described that the general unit cell of calcium apatite consists of pseudo-hexagonal network of PO_4 tetrahedra with Ca^{2+} ions in the interstitial sites and columns of anions, oriented along the c-axis [8]. In the structure of fluorapatite (FA), the fluorine ions sit in the center of the plane of the PO_4 tetrahedra and in the center of the calcium triangle. Whole structure of FA which has been described to have a hexagonal structure and $\text{P6}_3/\text{m}$ space group with the cell parameter, $a=9.397\text{\AA}$, $b=6.878\text{\AA}$ [9]. The unit cell parameter a of the structure increases as the ion within the calcium channel get larger.

On the other hand, in hydroxyapatite, hydroxide ion cannot fit within the Ca^{2+} triangle, that is why for approximation of HA structure a monoclinic structure was proposed by Elliot and Young derived from the hexagonal structure of fluorapatite with a doubling in the b-axis [9, 16]. If OH ions stack exactly at the middle of Ca^{2+} triangle due to rapid cooling after high temperature and pressure assisted sintering, then there may raise some discontinuities in other plane. It would be one of the causes of transparency in HA material. Transparency of ceramic is also influenced by texture and densification. Therefore, transmittance in HA would be a combined effect of densification and texture through an in-plane c-axis orientation. Crystal structure plays an important role in determining whether a ceramic can be optically transparent or not. In ceramics of optically anisotropic crystals, an additional scattering of light arises at the boundaries when the light travels from one grain to another. This is the reason why transparent ceramics generally have a cubic lattice structure, which is isotropic, such as MgO , Y_2O_3 , YAG, and MgAl_2O_3 (spinel), but in the case of HA the reason behind the transparency is different because it has non-cubic crystal symmetry.

S.F Wang and J. Zhang reported in their studies that high densification may lead the ceramics materials toward transmittance [17]. As electric current assisted SPS technique offers high densification nearly equal to the theoretical density. Therefore, high densification through the optimization of SPS sintering parameter in SPS machine may introduce transmittance in highly purified and dense hydroxyapatite ceramic pellets.

Some measurement showed that the dielectric properties of HA as anti-ferroelectric and the then time this property was considered dielectric anomaly [18]. To discuss ferroelectric behavior of HA, Tofail et al. proposed two structures of HA, P₆₃ and P₂₁, that have a non-centrosymmetric, polar configuration, allowing for piezoelectricity of the materials. The P₂₁ structure derived from the size of the hydroxyl anions that fit slightly above and under the [0 0 ¼] and [0 0 ¾] planes. This causes the PO₄ tetrahedrons in one column to tilt in one direction and the adjacent tetrahedron to tilt in the opposite direction [16, 19]. The presence of these two planes will determine the polarity and polarizability inside the Hydroxyapatite ceramic material.

In this research work, highly transparent hydroxyapatite ceramic pellets were intended to synthesize optimizing sintering condition in modern spark plasma sintering machine, and then investigated the possibility of polarization to induce piezoelectricity in these optically transparent ceramic pellets applying high voltage in contact electrical poling device.

1.4 Structure of the thesis

This book apparently contains five sections- Introduction, Literature review, Experimental part, Results and discussion and Conclusion.

Introduction section contains the outline of this research work. It describes the aim and objectives of this work specifying the research questions. Research hypothesis includes purposes and possible reasons behind this research. Methodological approach for investigation has also been included in this part.

The second part of this work is a detail literature review that focuses to compile all literature relevant to this investigation. It upholds a brief description over scholarly papers, theoretical and methodological approaches and contribution on the preparation of transparent hydroxyapatite ceramic and its piezoelectric properties. Brief descriptions on the instrument and its working principle have been incorporated in this section.

The experimental section provides detail description on the activities carried out for synthesis and characterization of transparent ceramic of hydroxyapatite. It also includes polarizing instrument and related steps to polarize synthesized samples.

All the obtained experimental results and relevant explanations have summarized in the results and discussion section. Finally, a conclusion section has been drawn from the main experimental results, hope that will add a novel outcome to this field of study.

Chapter-2

Literature Review

2.1 Apatite in natural bone

Approximately, 90-95% inorganic component of bone consists of collagen and this inorganic component consists primarily of calcium and phosphate, mainly in the form of calcium apatite [20]. Apatite is highly specialized and complex tissue that not only forms skeleton but also provides mechanical support and work as reservoir for minerals. A lot of biological function happens inside the bone. Bone apatite is a dynamic tissue as it has the capability of generating and remodeling throughout the lifetime. Most important calcium phosphates are hydroxyapatite (HA), chlorapatite (CIA) and fluorapatite (FA). These calcium phosphate-based materials are main constituents of hard tissues of most living creatures like mammals. The structure of the Ca-P solid phase in bone was first identified by DeJong in 1926 as a crystalline calcium phosphate similar to geological apatite by chemical analyses and most importantly by X-ray diffraction [21]. The compositions of synthetic calcium appetites are very complex, and in most cases more complex than in biological apatite, due to multiple lattice substitutions and by the presence of varying numbers of ion vacancies [22]. The most relevant of these substitutions in biological apatite are the replacement of the PO_4^{3-} anions by bivalent species. Chemical analyses of synthetic calcium apatite have revealed a common charge compensation mechanism containing these bivalent ions which are created by two ionic vacancies: one of which is on a cationic site and the other on a monovalent anionic site according to the general chemical formula: $\text{Ca}_{10}(\text{PO}_4)_6(\text{X})_2$ [23]. The cationic vacancy has been shown to occur mainly on the Ca (II) ions site in close proximity to monovalent anionic sites suggesting the existence of clusters of vacancies that are often observed in compounds with a large number of vacancies in accordance with Pauling's rules of the local charge compensation in the lattice [24].

Table-2.1: Calcium phosphate compounds and their Ca/P ratio [25]

Ca/P molar ratio	Calcium phosphate	Formula	Acronym
2.0	Tetracalcium phosphate	$\text{Ca}_4(\text{PO}_4)_2$	TTCP
1.67	Hydroxyapatite Chlorapatite Fluorapatite	$\text{Ca}_{10}(\text{PO}_4)_6(\text{OH})_2$ $\text{Ca}_{10}(\text{PO}_4)_6(\text{Cl})_2$ $\text{Ca}_{10}(\text{PO}_4)_6(\text{F})_2$	HA CIA FA
1.33-1.67	Calcium deficient apatite	$\text{Ca}_{10-x}(\text{PO}_4)_{6-x}$ $x(\text{HPO}_4)_x(\text{OH})_{2-x}$	Ca-dAp
1.5	β -Tricalcium phosphate	$\beta\text{-Ca}_{10}(\text{PO}_4)_6$	β -TCP
1.5	α -Tricalcium phosphate	$\alpha\text{-Ca}_{10}(\text{PO}_4)_6$	α -TCP
1.5	Υ -Tricalcium phosphate	$\Upsilon\text{-Ca}_{10}(\text{PO}_4)_6$	Υ -TCP
1.33	Octa calcium phosphate	$\text{Ca}_4\text{H}(\text{PO}_4)_3 \cdot 3\text{H}_2\text{O}$	OCP

2.2 Crystalline structure of apatite

Calcium apatite has the general formula $\text{Ca}_5(\text{PO}_4)_3\text{X}$ where X denote ionic end member. In the case of hydroxyapatite, the end member is hydroxyl group (OH) and then the formula becomes $\text{Ca}_5(\text{PO}_4)_3\text{OH}$. This structure of hydroxyapatite is tolerant to different form of substitutions within the crystalline structure. When the end member is substituted by fluorine the structure become fluorapatite (FA) $\text{Ca}_5(\text{PO}_4)_3\text{F}$, if the end member is substituted by chlorine ion then it will be chlorapatite (CIA) $\text{Ca}_5(\text{PO}_4)_3\text{Cl}$ [9]

The unit cell of calcium apatite in general is described as consisting of a pseudo-hexagonal network of PO_4 tetrahedra with Ca^{2+} ions in the interstitial sites and columns of anions, oriented along the c-axis [17]

Table-2.2: The structure and symmetries of apatite materials can be presented as follows-

Materials	Structure	Cell parameters	Position of anion	Nature of dipoles	Symmetry	Dielectric properties	Reference
FA	Hexagonal $\text{P6}_3/\text{m}$	a= 9.397 Å c= 6.878 Å	Equiplanar to Ca^{2+} triangles	No dipoles	Centro symmetric non-polar		
CIA	Monoclinic $\text{P2}_1/\text{b}$	a=9.628 Å b=2a c=6.764 Å	Above or under Ca^{2+} triangles	$\text{Cl}^-/\text{Ca}^{2+}$ triangle		Anti-ferroelectric	Elliott 2013 Hughes 2015
HA	Monoclinic $\text{P2}_1/\text{b}$	a=9.4214Å b=2a c=6.8814 Å	Above or under Ca^{2+} triangles	Hydroxide ions		Anti-ferroelectric	

Here, Fluorapatite is described to have a bipyramidal hexagonal structure that is centrosymmetric at room temperature with two formula units per unit cell and is usually taken as a model for apatite material [26]. The unit cell of fluorapatite contain two fluoride anions, positions along the c-axis at $z=1/4$ and $z=3/4$ i.e. along the two symmetry planes. They are both surrounded by a triangle of calcium ions. The two triangles of calcium ions are rotated by an angle of 60° along the c- axis, forming a channel along the c-axis with a fluoride anion positioned in the center of the channel. The fluoride anions fit within the center of the triangle, forming a non-polar structure [26]

The unit cell parameter $-a'$ increases as the ion within the calcium channel gets bigger. However, the hydroxide and chloride anions do not fit within the Ca^{2+} triangles. The dipoles formed in HA and CIA have identical orientation within the given channel. The monoclinic structure of hydroxyapatite and chlorapatite proposed by Elliot and Young is derived from the hexagonal structure of fluorapatite with a doubling in the b-axis due to alternating order of large dipoles in the adjacent channels.

Fluoride ion sits centered between the planes of the PO_4 tetrahedra and in the center of the calcium triangles that run throughout the FA structure. The position of the F^- ion creates a mirror plane in the hexagonal $\text{P6}_3/\text{m}$ structure. This mirror plane is located at both $z=0.25$ and $z=0.75$, as shown in figure-2.1.

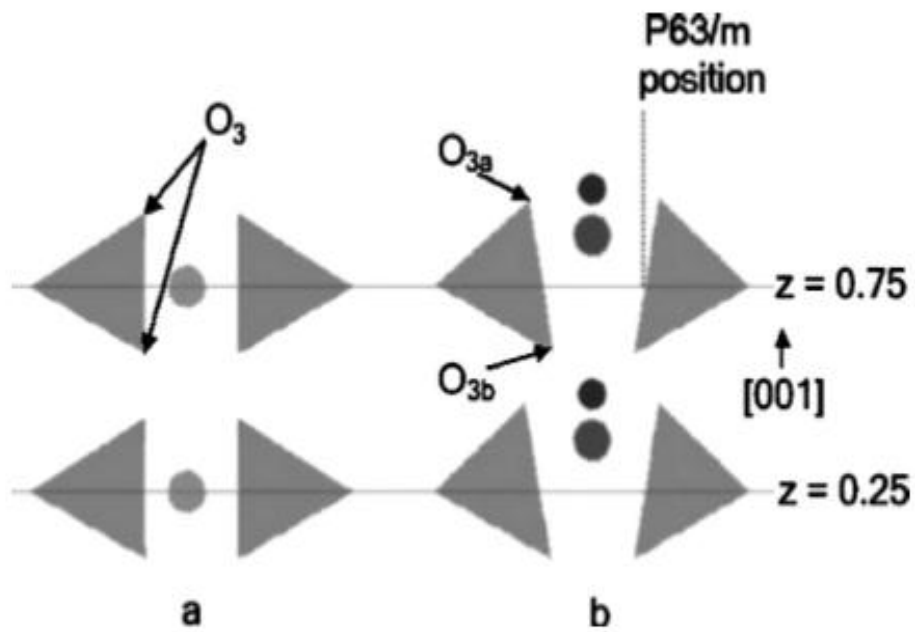


Figure-2.1: a) FA, b) F ion replaced with polar OH in HA [12]

2.3 Hydroxyapatite

The mineral phase of bone comprises of two third of bone apatite, an impure and non-stoichiometric hydroxyapatite phase [26], accompanying some other salts of calcium and phosphate. It has similar chemical composition and crystal structure to apatite in the human skeletal system thus it is very suitable for bone substitution and reconstruction [27] and has been using widely for years for clinical applications like implant and coating. Its non-toxic, non-inflammatory biocompatibility renders preferentially its application as biomaterial. HA plays a vital role in the orthopedic application due to its favorable osteoconductive and bioactive properties [28-29]. HA can adhere directly to hard tissues, such as bone and teeth, as well as to soft tissues, such as skin and muscular tissues, without the formation of an intermediate layer [30]. It's the most common naturally occurring mineral with the formula $\text{Ca}_5(\text{PO}_4)_3(\text{OH})$ or $\text{Ca}_{10}(\text{PO}_4)_6(\text{OH})_2$ here, OH ion can be replaced by fluoride, chloride or carbonate to form fluorapatite, chlorapatite. Up to 50% by volume and 70% by weight of human bone is modified form of hydroxyapatite and referred as bone mineral [31]. A brief overview on the physical properties of hydroxyapatite has been shown in the table-2.2

Table-2.3: Physical properties of HA material.

Composition	Hydroxyapatite
Formula	$\text{Ca}_{10}(\text{PO}_4)_6(\text{OH})_2$
Bulk density	0.6-0.7 g.cm^{-3}
Specific weight	<2 gms
Porosity	70%-75%
Pore size (by SEM micrograph)	100-300 μm
Unit volume	3-4 cm^3
Flexural strength for solid HA	>25MPa
Compressive strength for solid HA	>120 MPa
Sizes	Any size(14, 16, 18, 20mm...)
Shapes	Spherical, conoidal, or any other
Types	Evisceration, enucleation

2.3.1 Synthesis of hydroxyapatite powder

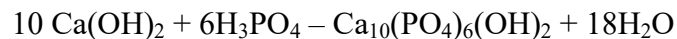
There are several methods have been using for synthesis of HA powder.

- Wet chemical methods(precipitation)
- Hydrothermal techniques
- Sol-gel
- Hydrolysis of calcium phosphate

Most widely used techniques are wet chemical precipitation and hydrothermal treatment-

Wet chemical production method

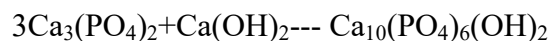
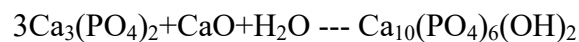
The most common hydroxyapatite nanocrystal suspension preparation by wet chemical route was proposed by Yagai and Aoki that follows the reaction.



In this process, orthophosphoric acid solution is added in a dropwise manner to a dilute suspension or solution of calcium hydroxide of pH greater than 9. It is a very control process where acid is added at a control rate maintaining a string throughout the process. Temperatures of reaction are usually kept in the range 25°C to 90°C. High temperature produces high crystallinity product, though total precipitation is a slow process.

Hydrothermal techniques

In general, di-calcium phosphate anhydrous (CaHPO_4) and calcium carbonate (CaCO_3) by the hydrothermal method at temperature 120°C to 180 °C produces hydroxyapatite. A new way of producing hydroxyapatite powder was proposed by P. Hui et al., where a stoichiometric amount of calcined eggshell was dispersed in well-degassed distilled water [32]. Under vigorous stirring reagent grade tri-calcium phosphate solution was mixed into calcined eggshell solution to produce a suspension and finally hydroxyapatite powder by hydrothermal technique following the reaction.



2.3.2 Hydroxyapatite crystal system

There are of two types non-stoichiometric or calcium deficient hydroxyapatite and stoichiometric apatite. Non-stoichiometric or calcium deficient hydroxyapatite having the formula $\text{Ca}_{10-x}(\text{PO}_4)_{6-x}(\text{HPO}_4)_x(\text{OH})_{2-x}$ (where the value of x is between 0 and 1) has a Ca/P ratio between 1.67 and 1.5[25]. On the other hand, stoichiometric hydroxyapatite has a Ca/P ratio 1.67. The nonstoichiometric structure has cation (Ca^{2+}) and anion (OH^-) vacancies. This gap or interstitial sites usually occupied by phosphate and hydrogen phosphate groups. Hydroxyapatite has hexagonal crystal system and its crystal class is dipyramidal (6/m). The parameters of the unit cell of hydroxyapatite are $a=9.41\text{\AA}$, $c=6.88\text{\AA}$ and $z=2\text{\AA}$ [17,19,26]

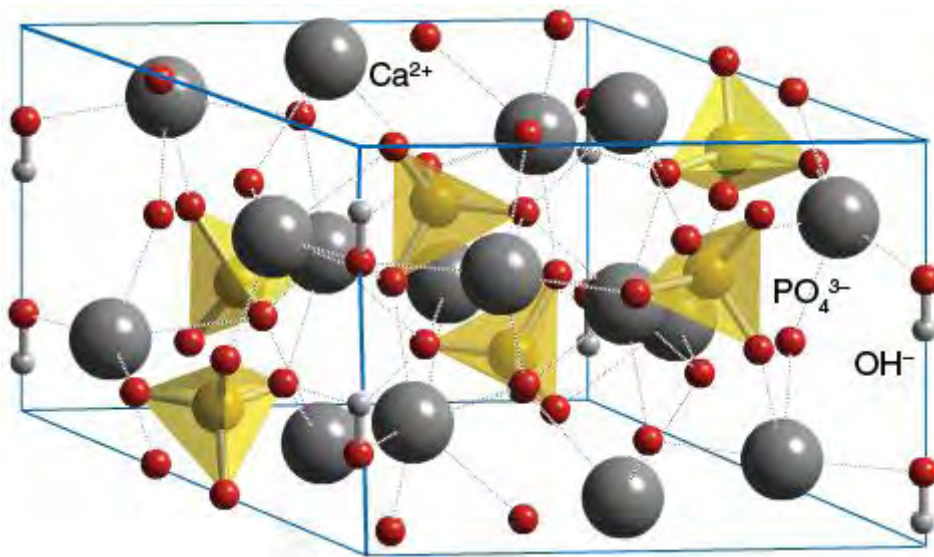


Figure-2.2: Structure of hydroxyapatite unit cell

According to least square refinements of diffraction data of HA, two phases have been suggested- a disordered hexagonal structure with $P6_3/m$ symmetry, space group 176 and a monoclinic structure with $P2_1/b$ symmetry, space group 14 [33]. Here, the monoclinic unit cell is derived from two hexagonal unit cells with b parameter twice that of the hexagonal value and involves an ordered arrangement of the anion columns. It has been recommended that monoclinic phase is associated with stoichiometric apatite [33]

Most investigators were satisfied to hexagonal $P6_3/m$ symmetry as it gives a good least square fit to x-ray diffraction data [19, 34, 35]. Impurities within nonstoichiometric hydroxyapatite raises disordered arrangement of OH^- ions and the structure is expected to adopt a monoclinic ordered arrangement [36]. Generalized gradient approximation density function theory proposed $P6_3/m$ and $P6_3$ hexagonal structure models to be energetically unfavorable as compared with previously proposed $P2_1/b$ symmetry and newly proposed monoclinic $P2_1$ structure model [33]. Rietveld analysis reported on synthetic HA that to be predominantly hexagonal at room temperature and diffraction pattern of this material interpreted as a mixed monoclinic phase of $P2_1/b$ and $P2_1$ [33].

2.3.3 Hydroxyapatite as biomaterial

Hydroxyapatite is the principal mineral component of bone tissue of mammals. Naturally synthesized hydroxyapatite as a calcium phosphate is similar to human hard tissues in morphology and composition [37]. Its Ca/P ratio is 1.67, identical to bone apatite [38-39]. It is biocompatible, bioactive, osteoconductive, non-toxic and non-inflammatory in nature, which allows bone tissue to grow directly on it when placed in human body without intervening fibrous tissue [39]. Thermodynamically, HA is considered most stable material or calcium phosphate compound under physiological condition like temperature, pH and even composition of body fluid [38]. That is why it has been using as prominent biomaterial in medical science. The most common uses of this HA material are bone grafts, fillers and coating for metal implant. Continuous stride of diversifying its application in some other biomedical application is still ongoing.

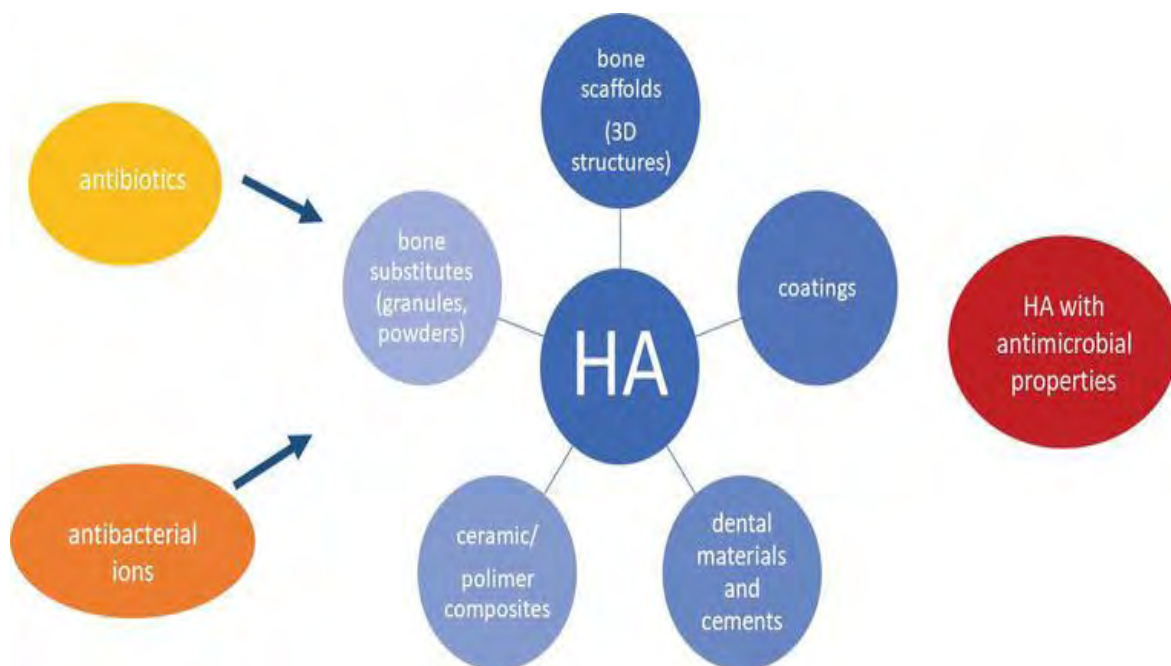


Figure-2.3: Biomedical application of HA

2.4 Piezoelectric property of hydroxyapatite

Pyroelectric, piezoelectric and ferroelectric natures of bone were reported in various studies [8-9]. A piezoelectric material is a kind of dielectric material which shows electrical polarization when submitted to mechanical stress. Pyroelectric material exhibit polarization when submitted to the change of temperature. The piezoelectric effect in bone material is believed to affect bone growth via transportation of ionic fluid within structure [40-41]. The longitudinal piezoelectricity of bone was measured to be 0.45pC/N [18]. This effect was attributed to collagen and hydroxyapatite crystal [42]. Synthetic HA is a good candidate as a bone substitute. It is highly biocompatible, structurally similar to bone, bio resorbable and has a surface which facilitate bone growth [43]. Abbasi A. Gandhi et al. reported that direct current electrical poling of textured hydroxyapatite ceramic exhibit weak ferroelectricity and pyroelectricity, but six order higher piezoelectricity and piezoelectric charge coefficient was reported to have higher value than bone and three orders higher than tendon.

Piezoelectricity means electricity resulting from pressure and latent heat. Piezoelectricity is a property of non-centrosymmetric crystalline materials whereby an applied mechanical stress produces an electric displacement; this is known as direct piezoelectric effect. Alternatively, when an electrical charge is applied to a material it produces a mechanical strain and this is known as the converse piezoelectric effect.

Firstly, to understand the mechanisms behind the piezoelectric materials, it is necessary to understand ferroelectric materials as all ferroelectric materials are generally piezoelectric but not all the piezoelectric materials are ferroelectric.

2.4.1: Ferroelectricity

A ferroelectric material has spontaneous polarization due to an electron, molecule or atom being displaced from its symmetry-defined position, thus forming a dipole in the structure. In perovskite-type ferroelectrics, the spontaneous polarization occurs when they are cooled down through their para-electric to the ferroelectric phase transition temperature, called the Curie temperature (T_c). At the phase transition a group of aligned dipoles are formed, called ferroelectric domains. When an external electric field is applied, the domains switch their direction to the direction of the field. The domains can keep their alignment and maintain the polarization when the external field is removed, this is called remnant polarization. Ferroelectric materials are usually characterized by their remnant polarization, dielectric and piezoelectric properties, and by their ferroelectric-to-paraelectric phase transformation temperatures, i.e. their curie temperatures (T_c) [44-45]. The curie point is defined by following change in the dielectric constant and loss during heating and cooling across the phase transition temperature. In the crystal structure of ferroelectric ceramics, one atom is displaced a small distance (0.1 Å) from its centrosymmetric position, thus giving rise to an electrical dipole (spontaneous polarization). When an external electric field is applied to the material, the polarization follows the external field according to a hysteresis loop. A typical hysteresis loop together with the changes of the dipole alignments is shown in Figure-2.4. When saturation polarization (P_s) is reached, all the dipoles are aligned. When the field is removed, the material is still partly polarized, to an extent that is called remnant polarization (P_r), and the external field in the opposite direction needed to remove the polarization is

called the coercive field (E_c). If the field is further increased, the polarization becomes saturated in the opposite direction.

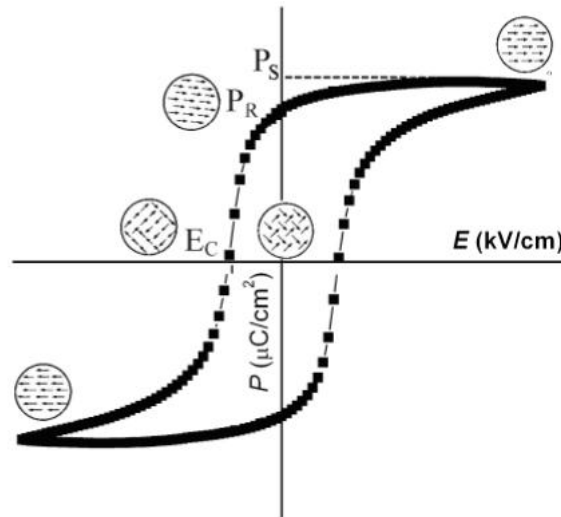


Fig 2.4- Hysteresis loop for a ferroelectric material and the influence of the electric field on the alignment of the dipoles, modified from ref. [45]

All ferroelectric material exhibit piezoelectricity due to the lack of symmetry so ferroelectricity is considered as a kind of piezoelectricity, in ferroelectric materials polarization of dipole occurs spontaneously and they can also be reversed [8]. Domain region exists within ferroelectric structure; these are the regions that separate two distinctively polarized areas. The electric orientation of molecule in the ferroelectric and piezoelectric material is defined as polarization and the reorientation of this domain is caused due to polling process. Ferroelectric polar domain can be aligned within an electric field, in similar way how ferroelectric material can be aligned in a magnetic field. Ferroelectric materials demonstrate a spontaneous nonzero polarization after entrainment even when the applied field E is zero. Most distinguishing feature of ferroelectrics is that the spontaneous polarization can be reversed by a suitably strong applied electric field in the opposite direction. However spontaneous and switchable polarization is necessary for all ferroelectric materials and therefore it must contain spontaneous and switchable dipoles. Usually ferroelectrics materials are pyroelectric in nature and can be re oriented.

2.4.2: Mechanism of Polarization

Polarization has four basic mechanisms-

Atomic Polarization

This type of polarization arises in materials due to the change in dipole moment during the stretching of chemical bond of unlike atoms or molecules. This involves the separation of the center of the electron cloud around an atom with respect to the center of its nucleus under the application of electric field.

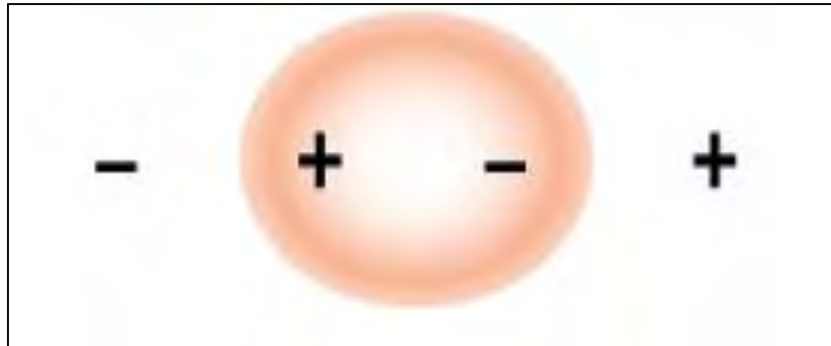


Figure-2.5: Atomic polarization

Ionic Polarization

Ionic polarization occurs in ionic materials. It occurs when an electric field is applied to an ionic material then cations and anions get displaced in opposite directions giving rise to a net dipole moment. In solids, ionic bonding automatically has dipoles, but it gets cancelled due to symmetry of the crystals. Here, external field leads to small displacement of ions from their equilibrium positions and hence induce a net dipole moment.

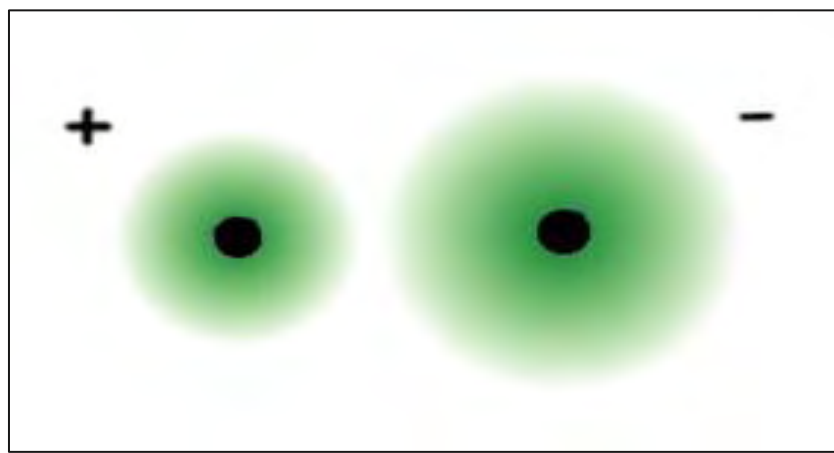


Figure-2.6: Ionic Polarization

Orientation Polarization

This is primarily due to orientation of molecular dipoles in the direction of applied field which would otherwise be randomly distributed due to thermal randomization. In case of dipolar polarization, some materials where the dipoles are present independent of each other, i.e. they don't interact, and they can be rotated freely by an applied field unlike in case of ionic polarization.

For example, H_2O molecule has a dipole moment and these dipole moments are free to rotate and can have any orientation with respect to neighboring molecules. Due to the ability of molecules to move around randomly, liquids like water have very limited dipolar polarization contribution despite having a permanent dipole moment for each molecule.

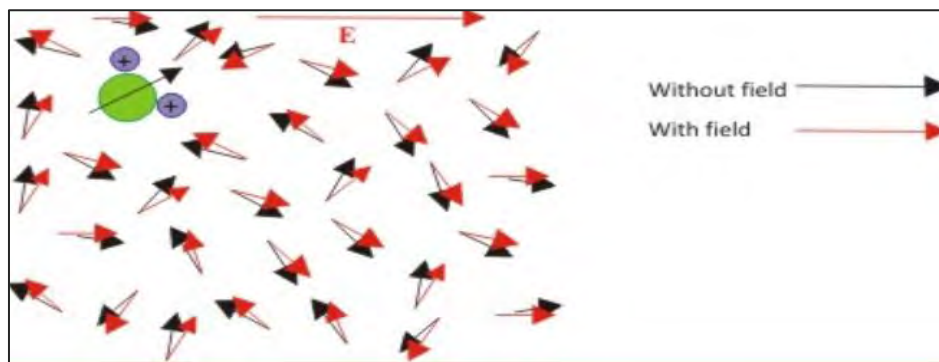


Figure-2.7: Oriental Polarization

Interface or space charge polarization

This involves limited movement of charges resulting in alignment of charge dipoles under applied field. This usually happens at the grain boundaries or any other interface such as electrode-material interface. In this polarization charge carrier migrate appreciable distance through dielectric which become trapped or cannot discharge at electrode.

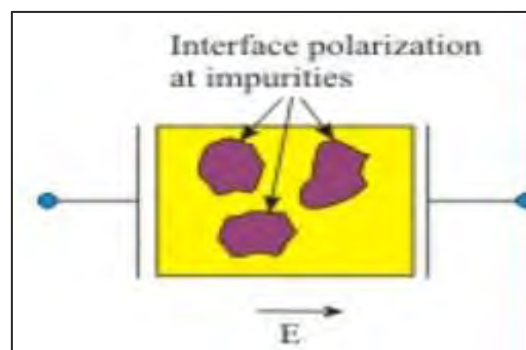


Figure-2.8: Interface polarization

Ferroelectric polar domain can be permanently aligned within an electric field in the similar way as the ferroelectric material aligned in the magnetic field. Only thing that compulsory for all ferroelectric material is spontaneous and switchable polarization. Net permanent electric dipole is induced within of ferromagnetic materials from the vector sum of all the individual dipole moment in each unit cell. In ferromagnetic material, each unit cell is an electrical dipole and shows spontaneous and reversible polarization.

2.4.3 Ferroelectricity in Hydroxyapatite material

In hydroxyapatite, hydroxyl ion cannot fit inside the calcium triangle because of its large size thus it goes slightly above or below the triangle and this phenomenon causes the phosphate tetrahedrons in one column to tilt in one direction and the adjacent tetrahedrons to tilt in the opposite direction [12,16,19]. This tilt or relaxation produces a non-centrosymmetric polar configuration in the hydroxyapatite structure. Hydroxyl ion orientation and possible polar and nonpolar symmetries in hydroxyapatite can be represented as shown in Figure 2.9. Hydroxyl ions above and below the phosphate triangles mirror plane constitute a crystal structure which is ferroelectric in nature. Antiparallel arrangement of the hydroxyl ions creates a lattice structure with no overall net charge, thus non-ferroelectric.

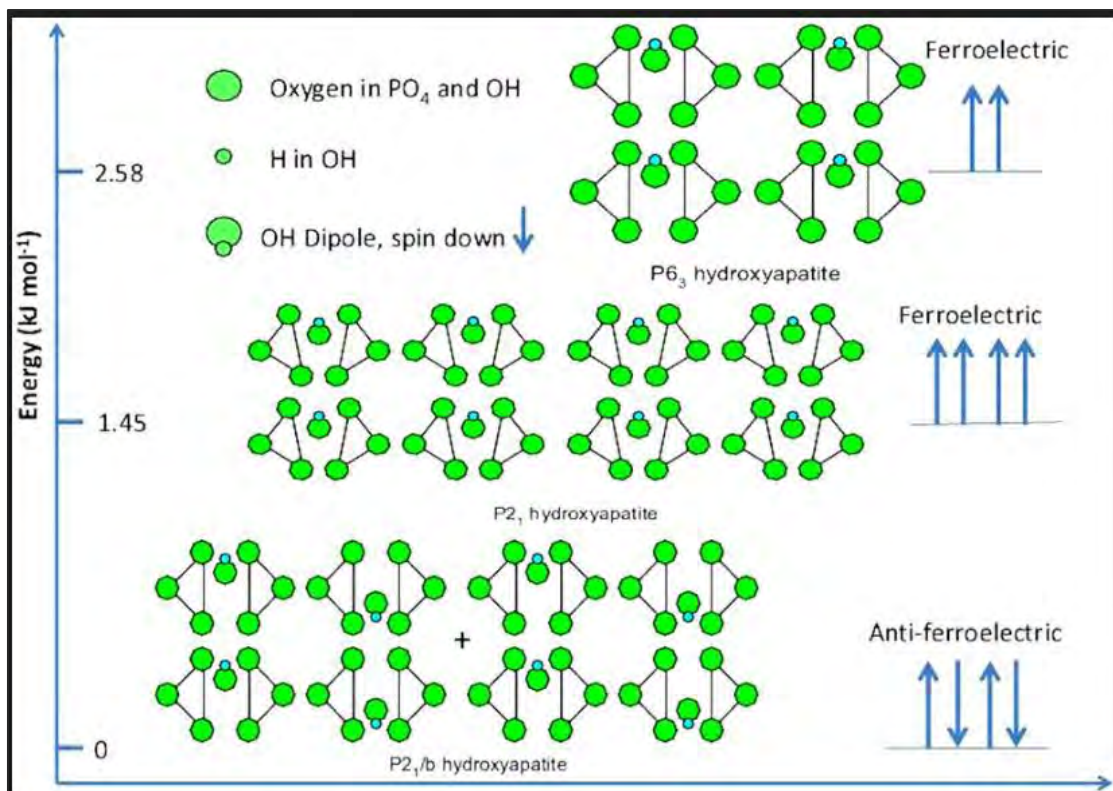


Figure- 2.9: Hydroxyl ion orientation and polar -nonpolar orientation in Hydroxyapatite [41]

2.4.4 Polarizing phenomenon of ferroelectric material

Cooling down of ferroelectric material from its curie temperature forms domain of continuous crystallographic orientation and thus causes polarization. When this cooling take place in the absence of electric or magnetic field, these domains form an anisotropic manner because of this, there is no net polarization throughout the sample hence no piezoelectric effect observe at the macroscopic scale. A process known as poling is used to create a net polarization and therefore induce piezoelectricity within ferroelectric ceramics. Here a sufficiently strong electric field is applied across the ceramics which can cause reorientation of spontaneously polarized unit cell into more isotropic alignment along the field lines. Microstructurally, the spontaneous polarization reorientation occurs through the motion of domain walls, or the boundaries that separate different domains. When field is removed, it induced a net overall polarization and form ferroelectric structure that will give piezoelectric response when tested. Along with electrically poling ceramic there are a number of different factors can affect the degree of polarization and resulting piezoelectric properties of the material such as the chemical modification of the structure and doping, as this affects the point defect structure in material [18]. Mechanical stress has also found to have an influence on the degree in which domain wall is oriented during poling process [19]. Defect or trapped charges are also found to have influence on the orientation of this domain [16]

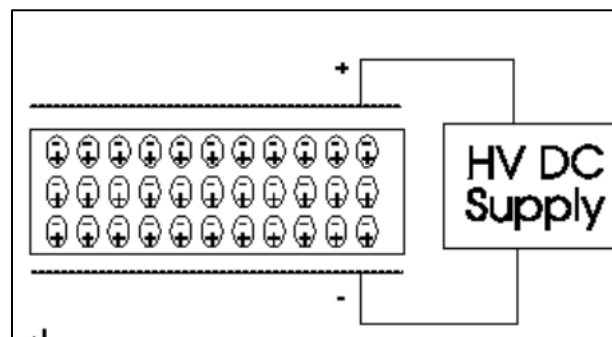


Figure-2.10: High voltage contact electrical poling

However, the temperature at which the poling is performed has been shown to be one of the most influential parameters in the poling process. As the domain wall orientation has been shown to be thermally activated, the poling process is often performed at an elevated temperature. This allows a higher degree of orientation, a larger net polarization in ceramic and thus obtains higher value of piezoelectric coefficient [16]. Poling of ceramic is only possible in ferroelectric materials. Quartz is a piezoelectric material, but it is non-ferroelectric with randomly oriented grains that cannot be poled in electric field but still exhibits macroscopic piezoelectric properties. In ferroelectric materials, remnant polarization will remain even after the removal of poling field. There are many different factors affect the strength of this remnant polarization some of them are available domain states, electromechanical boundary conditions at grain boundaries, sample surface and imperfections as well as elastic and charge defects in the materials [27]. Reversal of polarization is another most important characteristic of ferroelectric material caused by an applied electric field. An application of electric field across a ceramic can reduce domain walls and allows for a reversal of polarization. This domain wall switching creates a ferroelectric hysteresis loop. Polarization of crystal increases linearly with field amplitude [27].

2.4.5 Antiferroelectric Materials

Antiferroelectricity is a physical property closely related with ferroelectricity. It has ordered crystal dipole, but adjacent dipoles are oriented in opposite direction. Antiferroelectricity can appear and disappear depending on temperature, pressure, growth method, external electric field. When temperature is raised to curie point, antiferroelectricity get totally disappeared. Antiferroelectric property is steadier than ferroelectric property.

Entire macroscopic spontaneous polarization in antiferroelectric material is zero because closest opposite dipole cancels each other. The antiferroelectric property is not piezoelectric, that means there is no change in mechanical character of the material by the application of external field. Antiferroelectric material shows characteristic hysteresis loop, as shown in the figure-2.11. The reversal of spontaneous polarization of these materials gives a double hysteresis loop.

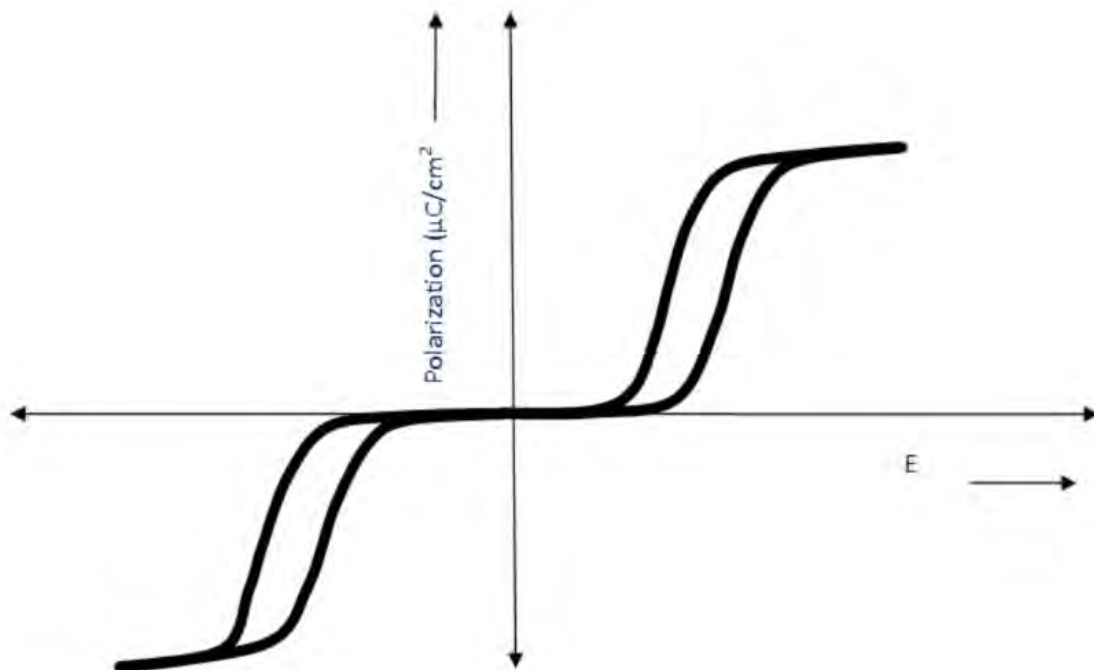


Figure- 2.11: Characteristic hysteresis loop of antiferroelectric material.

2.4.6 Piezoelectric response of HA

The HA granule has been used as an adsorbent of chromatographic support for the purification and separation of biological molecules in which the crystal morphologies of HA are of great important, here, the *a*- plane can adsorb a considerable amount of proteins compared with the *c*- plane due to the differences of electrostatic interactions[46-47]. It indicates that the ability of cell attachments is different on *a* and *c* planes since the interfacial interaction between cells and substrates is strongly dependent on the intervenient proteins that the cells produces. All biological processes occurring in the bones are accompanied by electrical phenomena connected with their piezoelectric properties. Conducted bio-mineralogical studies indicate piezoelectric properties of apatite, which is one of the major components of bone[48], these piezoelectric phenomena have long been of interest both in biochemical and electrical terms [48-49] as well as in a practical sense, mainly in relation to bone healing and acceleration of fracture unions [49]. Elements of bone such as bone marrow, body fluids, cells and others get in contact with bone collagen containing micro-crystals of hydroxyapatite. On this contact point, there is constant physicochemical equilibrium between the "biological world" and the "mineral world" of bone[48]. Generated "bone" currents through mechanical bone stress can affect bone collagen itself, especially the binding between collagen and hydroxyapatite. It appears that currents generated during stress (during walking) promote stability of these bonds. Absence of these currents can probably cause the bindings (ionic: apatite - collagen) to weaken or be broken. The effect is loosening and weakening of the bone structure. The bone system like bone marrow and other elements including vessels, nerves, etc. are a system of physicochemical equilibrium. It changes throughout life from youth to old age. Its function is to transfer elements from the "biological part" to the "mineral part" and vice versa [50]

Research on the piezoelectric properties of bones opens new prospects for understanding many biochemical phenomena in bones and other organs [51]. Here, for example, dense transparent HA sintered bodies with high crystal orientation would be used in confocal microscopy for direct observation of the bio-interfacial reactions with improved spatial and temporal resolution [52-53].

A study carried out by Elliot and Young et al, Rausch, Bauer and klee about the dielectric properties and measurement of Chloro-Apatite(CIA), this observation can also be applied to explain piezoelectric response and durability of polarized HA sample. In their study, they found CIA hysteresis loops with a shape characteristic of a ferroelectric substance and not a butterfly type, which might be expected from an antiferroelectric crystal.

To explain or justify this incident, they proposed two models-

Bauer and Klee (1992) vacancy model:

When high electric field >1300 V/mm applied on CIA then it interacts with chloride ions which are located near vacancies and excites Cl ions to jump across the vacancy, while other chloride ions remain in their positions. This creates a temporary crystal structure which was ferroelectric in behavior with the space group reducing from $p2_1/b$ to $p2_1$.

Second Model:

It suggests that CIA has a permanent ferroelectric phase. In this ferroelectric phase all the local calcium chloride dipole is aligned in the same direction and the crystal become ferroelectric with space group $p6_3$. Bauer and klee found that the application of a sufficiently strong electric field 5000 volt/mm caused the local chlorine-calcium dipoles within the

crystalline structure of bulk chlorapatite to all aligned in the same direction. By applying this high electric field, the crystal structure become ferroelectric with space group $p6_3$. This analysis was carried out by studying the hysteresis loop created in an alternating electric field. It was noticed in different studies that-

1. Prolonged retention of piezoelectric response confirms the presence of a ferroelectric phase
2. While a reduction of piezoelectric response rapidly over time may indicate the relaxation of chloride ions in ClA from the high energy vacancy filled position to the lower energy anti-ferroelectric positions.

2.5: Transparent Hydroxyapatite

2.5.1 Transparency in ceramic materials

Transparency is a physical property of material. In the field of optics, transparency (also known as pellucidity or diaphaneity) is the property of materials of allowing light to pass through it without being scattered. When light encounters a material, it can interact with it in several different ways. These interactions depend on the wavelength of light and the nature of material. This interaction is considered as some combination of reflection, absorption and transmission and causes transparency or opacity. Materials that allow light to pass through it without being scattered following Snell's law are transparent materials. Translucency is a superset of transparency; it allows light to pass through but does not necessarily follow Snell's law. When photon strikes into the material, it interacts with its constituents. This interaction can be divided into two contributions, one of them is elastic and is the source of the index of refraction where photon gets slow down while the other one is inelastic where photon gets absorbed by an atom. Material which do not transmit light are called opaque, they have their own absorption center. There is also some other material selective to their absorption characteristics and they can absorb certain portion of visible spectrum. The frequencies of the spectrum which are not absorbed are either reflected or transmitted for our physical observation. Generally, when light strikes on the surface of solid material, it bounces off in all directions due to multiple reflections by the microscopic irregularities like grain boundaries of polycrystalline material and for the rough surface [54].

Many ceramic crystalline and glassy have found to show optical transparency in various forms from bulk solid-state component to high surface area forms [55]. Optical transparency in polycrystalline materials is limited by the amount of light which is scattered by their microstructural features. Light scattering depends on the wavelength of the light more specifically frequency of the light wave and the physical dimension of the scattering center. Primary scattering centers in polycrystalline materials include microstructural defects such as pores and grain boundaries [55]. In addition to pores, most of the interfaces in a typical metal or ceramic object are in the form of grain boundary which separate tiny regions of crystalline order. When the size of the scattering center is reduced below the size of the wavelength of the light then light is being scattered

In polycrystalline materials that would be metals and ceramics, the size of the crystalline grains is determined largely by the size of the crystalline particles present in the raw material during formation of the object. The size of the grain boundaries directly related with particle size so reduction of the original particle size well below the wavelength of visible light range eliminates much of light scattering, resulting in a translucent or even transparent material [56].

There are several single crystal ceramics having various sites to scatter light, including mainly residual pores within the grains and at the grain boundaries, second phases (impurities) at the grain boundaries and double refraction from birefringent materials.

2.5.2: Transparent Hydroxyapatite.

It was observed that hydroxyapatite (HA) would also be transparent despite of its non-cubic crystal symmetry when it is sintered using spark plasma sintering technique at the temperature range 800 to 1300°C under a uniaxial pressure of 30-50 MPa and a total sintering time of 5-10 min [57]. The presence of fine grains and low porosity in HA ceramics improves its optical properties. HA is an optically anisotropic material with a refractive index of 1.651 and 1.644 depending on the polarization and propagation direction of light [58]. Low birefringence (0.007) compared to the refractive index along with fine and dense microstructure can increase the transparency by reducing light scattering from both the grains and pores, as in the case of alumina[59]. But, the origin of high transparency in HA is still under debate. Sometimes higher densification reduces porosity and other light scattering center and makes ceramics materials highly transparent [60]. Some studied reported that local discontinuities in the refractive index originated from the presence of grain boundaries, compositional heterogenetic, microstructural defects and porosity are tremendously responsible for optical transparency [60]. Although transparent hydroxyapatite reported to show very high level of crystallographic c- axis orientation sintered by spark plasma sintering [61]. Transparency may also be affected by discontinuities in the refractive index generated by grains having different crystallographic orientation. Watanabe et al. reported to exhibit over 65% optical transparency at 700 nm wavelength in textured HA sintered by spark plasma sintering. Those samples are usually sintered at higher temperature and for a longer time usually show higher optical transmittance rather than those samples sintered for limited time [62-63].

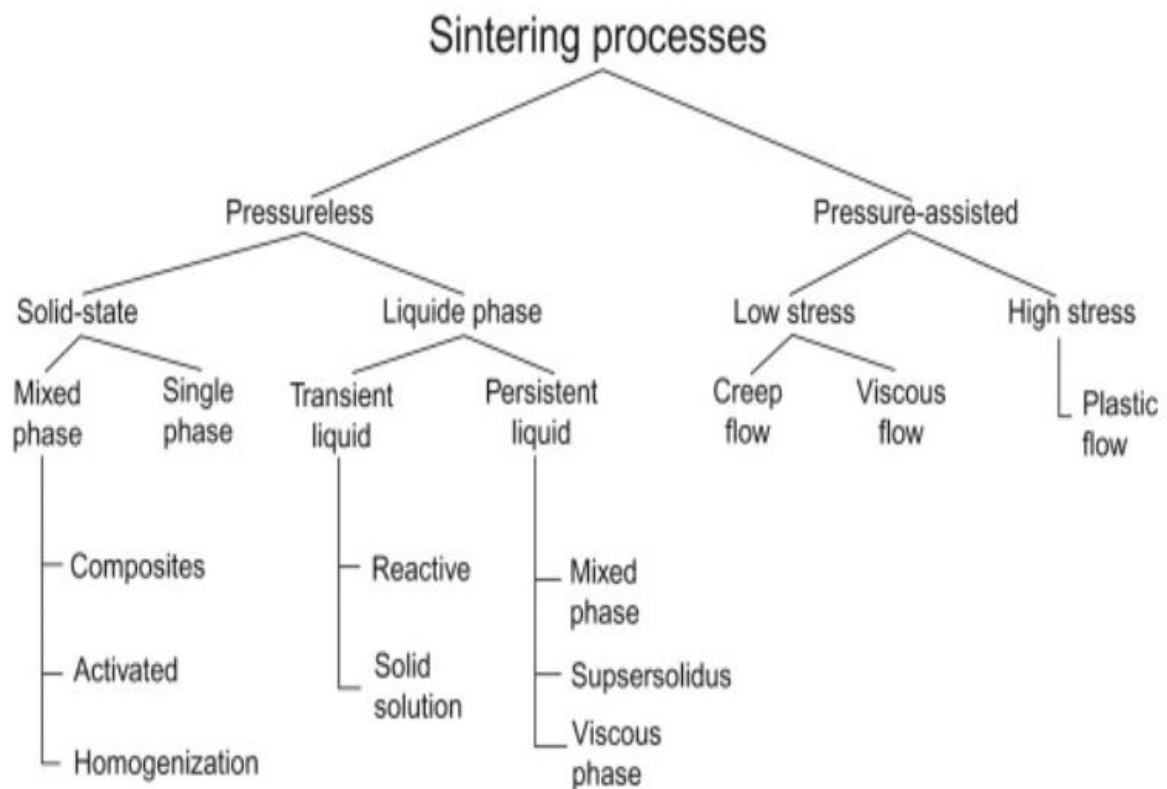
In some studies, it was found that applying of high pressure is beneficial for attaining dense HA. This high density and homogeneous grained structure introduced high transparency in produced HA ceramics besides the unique intrinsic optical properties in HA crystal, i.e. its low refractive index and very small birefringence. Full densification at the minimized sintering temperature allows for the preparation of transparent HA ceramics with stoichiometric composition, i.e. avoiding the loss of structural water that commonly takes place during the conventional ways of sintering [64].

Osteoblast proliferation was reported to be significantly higher on nanophase HA than on conventional coarse-grained HA ceramic[65] Therefore, the preparation of transparent polycrystalline HA ceramics with nanosized grains is important for direct observations of the in vivo interactions with proteins and/or cells [66]. Transparent HA ceramics with fine and dense microstructures have been achieved using nanosized HA powders through hot isostatic pressing [67-68], microwave sintering [69] and spark plasma sintering (SPS) [57-61]. During SPS, the grain growth and decomposition of HA were suppressed by sintering at relatively low temperatures for a short time. The resulting HA ceramics exhibited higher transparency than that of existing HA ceramics including high-pressure sintered samples [70]

2.6 Sintering of hydroxyapatite

Sintering is a process or treatment implemented by thermal action for creating bonds in particles to form a coherent, predominantly solid structure via mass transport events that often occur on the atomic scale. It lowers the surface energy by reducing surface area through the formation of interparticle bonds. Bond formation occurs at the atomic level. Several parameters like time, temperature, pressure and rate of sintering play the important roles in whole process. Holding time at peak temperature increases sintering but longer sintering time causes microstructural coarsening. Temperature increases atomic motion to ensure adequate diffusion. Sintering theory is accurately explainable in the case of solid-state diffusion mechanism but in practice, its applications involve multiple phases and liquids.

To classify sintering process, pressure is considered first differentiation and thus classified as pressure assisted and pressure less. Pressure assisted sintering process includes hot isostatic pressing, hot pressing and spark plasma sintering. Here, pressureless sintering techniques can also be classified primarily into two groups- liquid phase and solid state. A brief categorization is shown below-



For most materials, diffusion along the grain boundaries is most important. Alternatively, particle melting occurs during liquid phase sintering, resulting in a solid–liquid mixture that sinters by viscous flow. The liquid phase provides bonding, contributes a capillary force and enhances mass transport.

On the other hand, pressure less sintering includes solid state sintering and liquid phase sintering. Single phase solid-state sintering is the best understood form of sintering. Among the solid-state processes, there are options involving mixed phases, such as those to form composites or alloys. Compact homogenization occurs when sintering mixed powders that are soluble in each other and produce an alloy. Activated sintering is a special treatment involving small quantities of insoluble species that segregate to the grain boundaries to accelerate sintering. Mixed phase sintering is often employed to form composites, where one phase is dispersed in a matrix phase. Another variant occurs when a material is intentionally sintered in a two phase field, such as when steel is sintered at a temperature where both body-centered cubic and face-centered cubic phases coexist.

Commonly, sintering involves a liquid phase that improves the sintering rate. Most industrial sintering involves forming a liquid phase, accounting for nearly 90% of the value of all sintered products. The two forms involve persistent or transient liquids. Persistent liquid phases exist throughout the high temperature portion of the sintering cycle and can be formed using pre-alloyed powder or from a mixture of powders. Transient liquid phase sintering produces a liquid during heating, but that liquid subsequently dissolves into the solid. In some cases, an exothermic heat release also occurs and leading to reactive liquid phase sintering.

2.6.1 Comparative sintering methods of hydroxyapatite

Bulk HA compacts sintered by conventional sintering method is difficult to use as nonstructural implants because of low strength [71]. According to thermodynamic standpoint, sinter bonding is driven by the surface energy reduction. Therefore, small particles have more surface energy which renders its sinter more first and consume comparatively little time. Since atomic motion increases with temperature, sintering process gets accelerated. When sintering conditions and parameters in conventional sintering of HA are optimized, the fracture strength could increase with higher density but, the limited stability of HA at high temperatures create several problems, HA get dissociate into tricalcium phosphate and tetra calcium phosphate at 1300°C in air or 1000°C in vacuum [72]. At the same time, high temperatures and extended sintering time for consolidation of HA powders often result in extreme grain coarsening or surface contamination, which can degrade the desired mechanical properties. Various sintering methods have been frequently testing for the consolidation of powder HA materials to find out the most suitable route for achieving high-density and improved mechanical strength. Conventional pressureless sintering and pressure assisted hot pressing or microwave sintering are the most commonly used methods employed for consolidation of HA powder.

The conventional pressure less sintering requires a high heating temperature in extended time period which leads to waste of energy and time and to weakening of mechanical properties. These energy losses and weaken mechanical properties of HA materials happen due to extreme abnormal grain growth over long periods of time [72]. As sintering occurs without pressure, therefore, requires excessive times, sometimes it becomes a matter of hours, that's why, demands high cost of operation and sometimes non-competitive as well. Appreciable amount of pore removal is not also possible by conventional sintering process.

In hot pressing sintering process, powder is uniaxially pressed between two graphite die and heated in a definite atmospheric condition. It is a single step process where powder compaction and sintering occur at a same time. Graphite heating elements surround the pressing tools and transfer heat to the compact powder by radiation or convection. In this process, mold would also be heated by resistant or induction heating. Finally, mold is cooled slowly under pressure. This method offers high mechanical strength in HA pellets but can't resist decomposition of HA because of high temperature exposes for extended time period.

Microwave sintering is a fast sintering processes comparing hot pressing technique, that's why can ensure high efficiency in reaching the high-density without any excessive grain growth. But high temperature exposure can't resist decomposition appreciably.

These limitations can be alleviated by using spark plasma sintering to avoid exposing the compacts to high temperatures for a long duration. Comparing to the conventional sintering, spark plasma sintering (SPS) makes possible sintering and sinter-bonding at lower temperatures and shorter duration by charging the intervals among powder particles with electrical energy and efficiently applying a high temperature spark plasma momentarily [73]. This enables compacted powder to be sintered under uniform heating to high density at relatively lower temperature and in a much shorter sintering duration, typically a few minutes

compared to conventional sintering [74]. The short sintering duration for the SPS process would be advantageous in suppressing exaggerated grain growth [75].

Table-2.4: Thermal effects on calcium phosphate [76]

Temperature(°C)	Reaction
25-200	Evaporation of absorbed water
200-600	Evaporation of lattice water
600-800	Decarbonation
800-900	Dihydroxylation of calcium apatite
1050-1400	Decomposition to form β -TCP and TTCP
Above 1120	β -TCP is in the stable form
1120-1470	β -TCP converts to α -TCP
1550	Melting temperature of calcium apatite
1630	Melting temperature of TTCP, leaving behind CaO
1730	Melting of TCP

2.7. Spark Plasma Sintering Technique.

Spark Plasma sintering is relatively new technique to sinter powder materials as it was only developed in the mid of 1980s and has some similarities with traditional hot-pressing method [77-78]. It is an electric current assisting sintering (ECAS) process which avoids binders leads direct sintering, so no need pre-pressing and green compact. Molds are designed for final part shape because cavity is filled under pressure and hot pressing. This is most common for this technique. This technique is also known as Field Assisted Sintering Technique (FAST) or Pulse Electric Current Sintering (PECS). High electricity is passed through the graphite die for sintering in this process. Sintering techniques assisted by pressure such as hot pressing or hot isostatic pressing enable 200–400 K lower processing temperatures than in conventional sintering and reductions of sintering time by few hours, which results in finer microstructures [44]. Significant improvements of sintering kinetics are also observed when the process is assisted by electric current or electromagnetic field [79-80]. Here, SPS heating system is internal and joule heating plays the dominant role to raise internal heat for sintering. Joule heating may lead the sintering materials toward its theoretical density at lower sintering temperature comparing conventional sintering process [80]. Its internal heating and cooling rate are very high which is conventional for suppressing the grain growth. SPS sintering technique provide a lot of advantage over conventional sintering method because of its hot pressing or hot isostatic pressing. It has accurate and easy controlling facilities, high speed, high reproductivity, safety as well as reliability [80].

Table-2.5: Characteristic features of Conventional and SPS Sintering

Characteristics features	Conventional Sintering	SPS sintering
Heating type	External	Internal joule heating
Sintering time	Few hours	Only few minutes
Heating rate	low	Very high
Heating element	Located inside the reaction chamber	No heating element

2.7.1 Structural configuration

A typical Spark Plasma Sintering is displayed in the figure-2.12. SPS sintering machine is designed with uniaxial pressure devices for ensuring uniform force throughout the whole part of sample powder applied for sintering. It has pulse direct electrical current (DC) generator and controlling devices for ensuring high speed consolidation of powder under low atmospheric pressure. This uniaxial pressure device, in which water-cooled graphite punches serves also as electrodes. This water-cooled reaction chamber that can be evacuated or back filled with a gas. It has also a z-axis position dilatometer and a temperature regulation system.

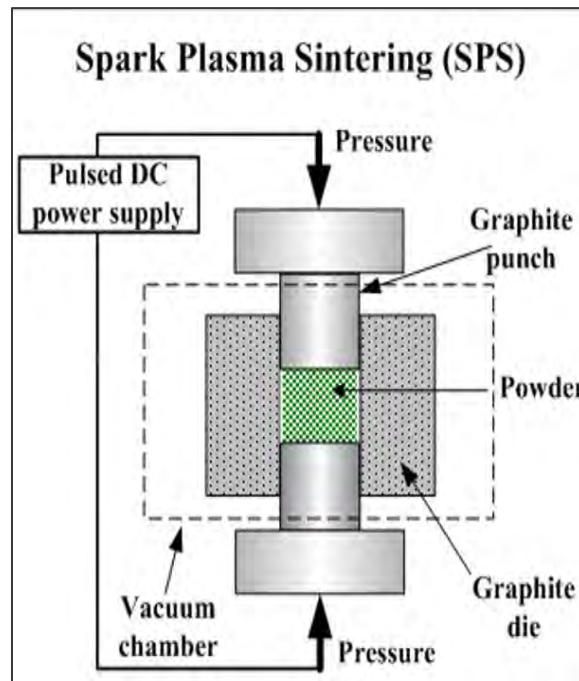


Figure-2.12: SPS sintering technique [60]

SPS chamber is connected with a computer-based process controller which records the shrinkage, temperature, pressure, average voltage and current during the process.

Different type of dies for different shape and size are used to prepare sample as per the requirement of characterization technique. Powder for preparing samples are usually wrapped with carbon lining to avoid thermal shocking.

Spark plasma sintering technique apparently like the conventional hot-pressing method that is widely used for preparing ceramic sample. In the time of sintering powder material is loaded into graphite die and graphite punches placed into both ends. A uniaxial pressure is then applied to the punches during the sintering process. The SPS machine uses a pulsed direct current which can pass through the graphite die and punches. As there is high conductivity throughout the graphite a low voltage nearly 15V and a high current nearly 5500A are used during this sintering. High current passing through both the powder and the graphite die causes heating of the sample through electrical resistance or joule heating. This method allows for heat to be internally generated and relatively evenly distributed throughout the sample compared to that of hot pressing. This feature of the SPS machine allows for possibility of having a very first heating rate and short holding times. However, the heating

rate of the sample is limited by the size of die used and the temperature distribution throughout the sample. Another advantage of the SPS process over the traditional sintering processes is a very large uniaxial pressure that can be applied throughout the sintering process. The combination of these features in SPS process allow for the creation of a ceramic of high quality in a shorter time compared to that of conventional sintering. The consolidation rate using SPS method is greatly enhanced and the sintering temperature can be few hundred degrees lower than conventional hot press sintering process.

It is possible to have high heating rates in the SPS (up to $1000\text{ }^{\circ}\text{C min}^{-1}$). The highest possible temperature so far used is $2200\text{ }^{\circ}\text{C}$. Both maximum temperature and heating rate are limited by the size of the die, a larger die needs higher current than a small die to be heated to the same temperature. It is also important to consider that the higher heating rate affects the temperature distribution in the die and sample.

There are few factors directly contribute to the consolidation rate-

1. Rapid heating and cooling rate
2. Use of joule heating rather than external heat sources
3. High uniaxial pressure throughout the process
4. Pulse DC current

2.7.2 Sintering Mechanism

Direct way of heating in SPS allows very high heating and cooling rates, increasing densification over grain growth promotes diffusion mechanism. Heating power in this process is not only distributed over the volume of the powder compacts homogeneously in macroscopic scale, but moreover the heating power is dissipated exactly at the locations in the macroscopic scale where the energy is required for sintering process, namely at the contact points of the powder particles.

It was claimed at the very beginning of using SPS technique that plasma is formed between the particles but there is no experimental evidence that proves this statement. Applying simulation work it was noticed that very little current is actually passing through non-conductive material, thus eliminating the possibility of plasma formation [81]. Later, Groza et al. and Kim et al. showed in their experiments that the particles experienced a “cleaning” of the surface when the particles were exposed to high current densities, which in turn promoted the breakdown of the oxide layer on their surface and promoted neck growth and plastic deformation [82-82]. The presence of an electric current and/or field may give rise to changes in phase transformation temperatures, nucleation rates and grain growth rates, reactions patterns and deformation behaviors of different materials [84-86]. The proposed explanations invoke variations of dielectric, magnetic properties of materials [87], increased diffusion rates, enhanced annihilation of dislocations, and changes in mobility of dislocations and vacancies [85]. Even though, it is very difficult to separate the effect of current from temperature in SPS. It is quite certain that materials sintered in SPS are exposed to high electric and magnetic fields during sintering which most probably influences the sintering, process and properties of sintered material.

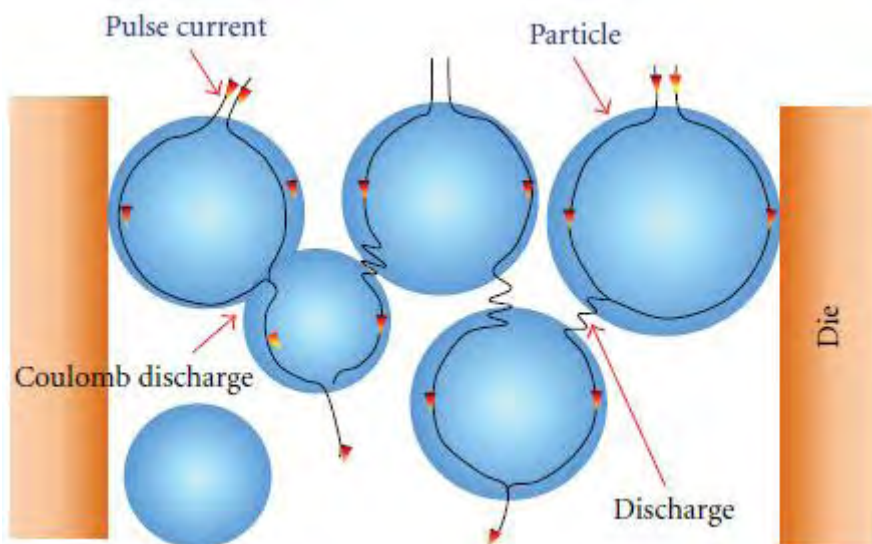


Figure-2.13: Energy dissipation in the microscopic scale [60].

Here, the hydroxyapatite powder is loaded into a graphite die and graphite punches are placed into both ends. A uniaxial pressure is then applied to the punches during sintering process. The SPS machine uses a pulsed direct current which can pass through the graphite die and

punches. Graphite is highly conductive material and allows very high current up to 5500A at low voltage (15V). This High current pass through the powder and graphite die causes heating of the sample using electrical resistance on Joule heating. Ultimately it can be said that the heat is internally generated and evenly distributed throughout the sample compared to hot pressing. This ability of SPS machine allows very fast heating rate and short holding time.

Material Transfer Path

Sintering of powder material inside the mold involves elimination of porosity inside the powder sample accompanying the suppression of grain growth. Ceramic are sintered into solid without melting, solidification and cold working because-

1. Higher melting temperature of ceramic.
2. Micro-structure cannot modify through plastic deformation and recrystallization due to their brittleness
3. Low thermal conductivity causes larger thermal gradient which may causes stress shock in melting -solidification process.

Sintering commonly occurs in ceramic at elevated temperature, usually at $T > 0.5T_m$ here, T_m refers melting temperature at which diffusional mass transport occurs. Successful powder ceramic sintering usually results in dense polycrystalline sample with reduced porosity. In solid state sintering, densification achieve through the change in particle shape without particle rearrangement.

The sintering of the powder sample into a solid ceramic is accompanied by many different changes within sample, some of which are desirable and others undesirable. Changes that occur include a change in strength, hardness, electrical and thermal conductivity, permeability, average grain number, size, shape, distribution of grain size and shape, chemical composition and crystal structure of ceramic. To produce a ceramic with optimum physical and chemical properties it is therefore necessary to fully understand the sintering process.

Solid state sintering occurs in three stages each with their distinctive process as shown in the figure-2.13. In the initial stage of sintering the powder particle morphology begin to change with the smoothing of surface, this is also accompanied by local point contact of individual particle with one another. When initial stage of sintering occurs no shrinkage of ceramic is noticeable.

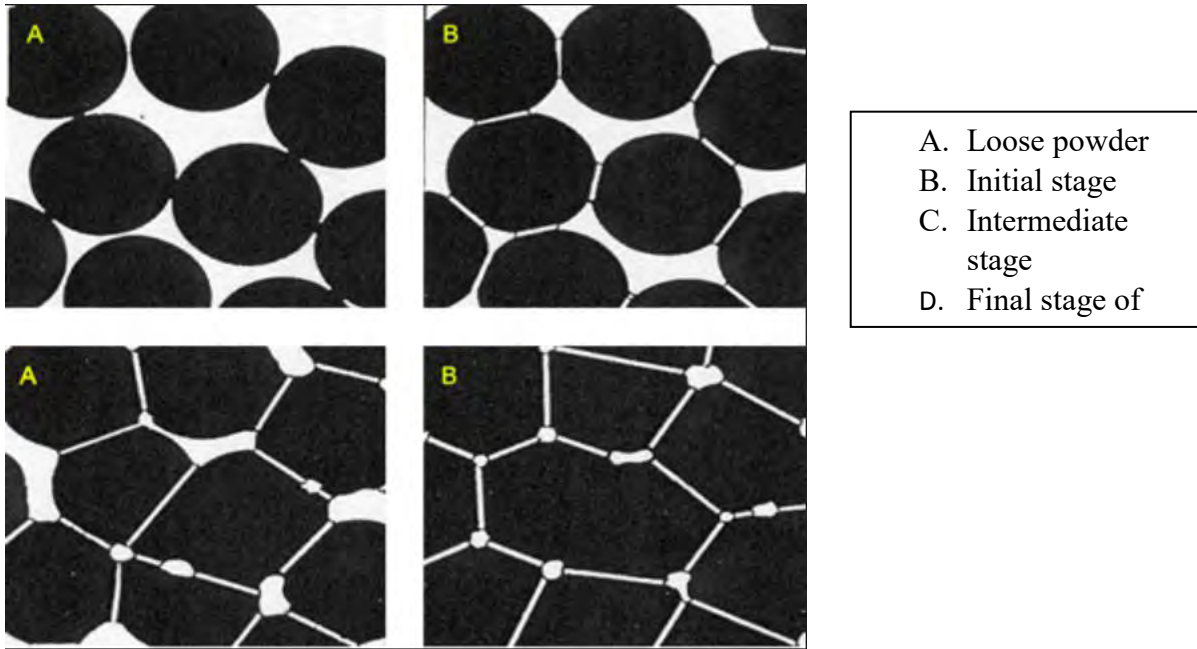


Figure-2.14: Stages of Sintering

After establishing contact between particles necks begin to form between particles. This process results in densification of sintering component. Densification in the initial stage reaches higher value after exposing the powder to high temperature, due to large surface area and the driving force for sintering. Second stage or the intermediate stage of sintering involves further neck growth with pores forming array of interconnected cylindrical channels and these centers approaches one another with resulting compact shrinkage.

The total shrinkage during intermediate stage can result in addition densification by as much as 25% or total of about 95% of the theoretical density. However, shrinkage does not necessarily have to take place during intermediate stage of sintering. For example, shrinkage would not occur if matter was transported from the particle surface and proceed through either gas or along interface as surface diffusion.

If the only material transport mechanism originates on the surface of particles no compact shrinkage takes place in such case a change of the shape and size of pores and particle is observed and commonly defined as grain growth or coarsening. Grain growth/coarsening depletes the system of surface energy and effectively stops the densification of the compact. The coarsening process decreases the driving force for sintering and therefore the sintering rate express as shrinkage versus time that decreases in the intermediate stage.

Densification in intermediate stage takes place only if the mass is transported from the particle volume, here, mass is transported from grain boundary and proceeds through the solid as volume diffusion or along a boundary as grain boundary diffusion towards the neck forming between the sintering particle.

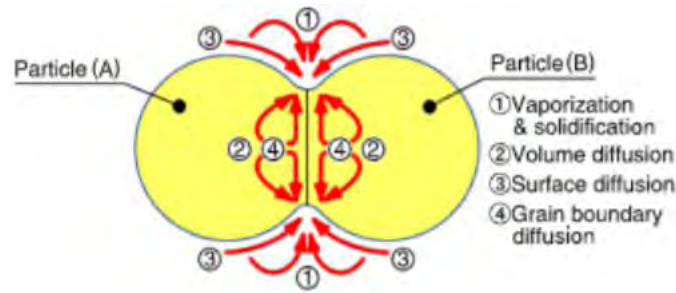


Figure-2.15: Material Transfer Path during Sintering [7]

The origin of mass transport during sintering determines the ability of compact to shrink and eliminate porosity. There are system where sintering proceeds vigorously through evaporation/condensation or through surface diffusion without any shrinkage of the compact. In most cases this is undesirable phenomenon whenever residual porosity is undesirable.

The final sintering stage begins at about 93-95 % of theoretical density at the end of this stage all porosity is almost fully eliminated. This situation happens only if the pores follow the movement of grain boundaries and are not trapped within grains.

Tapping of pores can occur when discontinuous grain growth happens, a small number of grains growing at very large rate at the expense of all other grains, trapping porosity in their path. In this stage of sintering, pores that are attached to grain boundaries move together and reduce surface energies. Grain boundary movement is also accelerated leading eventually to dissentionous grain growth. This leads to rapidly moving grain boundaries that consume small grain and increased grain growth [88]

Chapter-3

Experimental Methods

This chapter discusses experimental steps that were followed during this research work. It describes synthesis and sintering technique of hydroxyapatite ceramics, contact electrical poling and characterization methods followed for total characterization. This section also evaluates and justifies the parameters used in investigation and characterization as well as different necessary steps taken during research work.

3.1 Sintering of Hydroxyapatite Powder

3.1.1 Preparing Mold with fixed amount of powder

Mold preparation is primarily the most important part of spark plasma sintering where predetermined amount of powder calculated out and poured in carbon paper wrapped graphite mold. At very beginning, HA powder was properly screened and dried out to avoid moisture and coarse powder particle then weighted out as per the calculated amount depending on the diameter and thickness of expected sample pellets following the equation-

Weight of powder for one sample = $\pi (D^2/4) H \rho$

For hydroxyapatite,

Density, $\rho = 3.16 \text{ g/cm}^3$

Diameter of Die, $D = 10 \text{ mm}$

$= 1 \text{ cm}$

Expected Thickness of sample = 2 mm

$= 0.2 \text{ cm}$

Therefore, Weight required for one sample = $3.1416 (1/4) 0.2 \times 3.16$

$= 0.496 \text{ g (Approximately)}$

Here, carbon paper is used to wrap the inside of mold cavity that helps to avoid direct contact of powder and mold during sintering which may have caused infusion of foreign particle inside the sintered body. Conducting nature of carbon paper is helpful to transmit electric current uniformly throughout the powder taken inside the mold for sintering. This paper also helped to eject out sintered material from the mold cavity. To avoid unexpected powder loss during pouring operation and grinding of powder inside the cavity extra 0.20 g HA powder was added with calculated amount. Therefore 0.7 g of powder was weighted out for every single sample. Before pouring HA powder inside the graphite die, carbon paper was placed properly inside the cavity and rubbed by round strict to attach the paper with the mold to ensure proper contact. After pouring powder inside the cavity of mold, carbon strip was placed above and below the powder level to avoid direct contact of electrified punch with HA powder. Then the mold was placed exactly at middle of SPS chamber to ensure uniform pressure throughout the whole die.

Steps involved in SPS sintering-

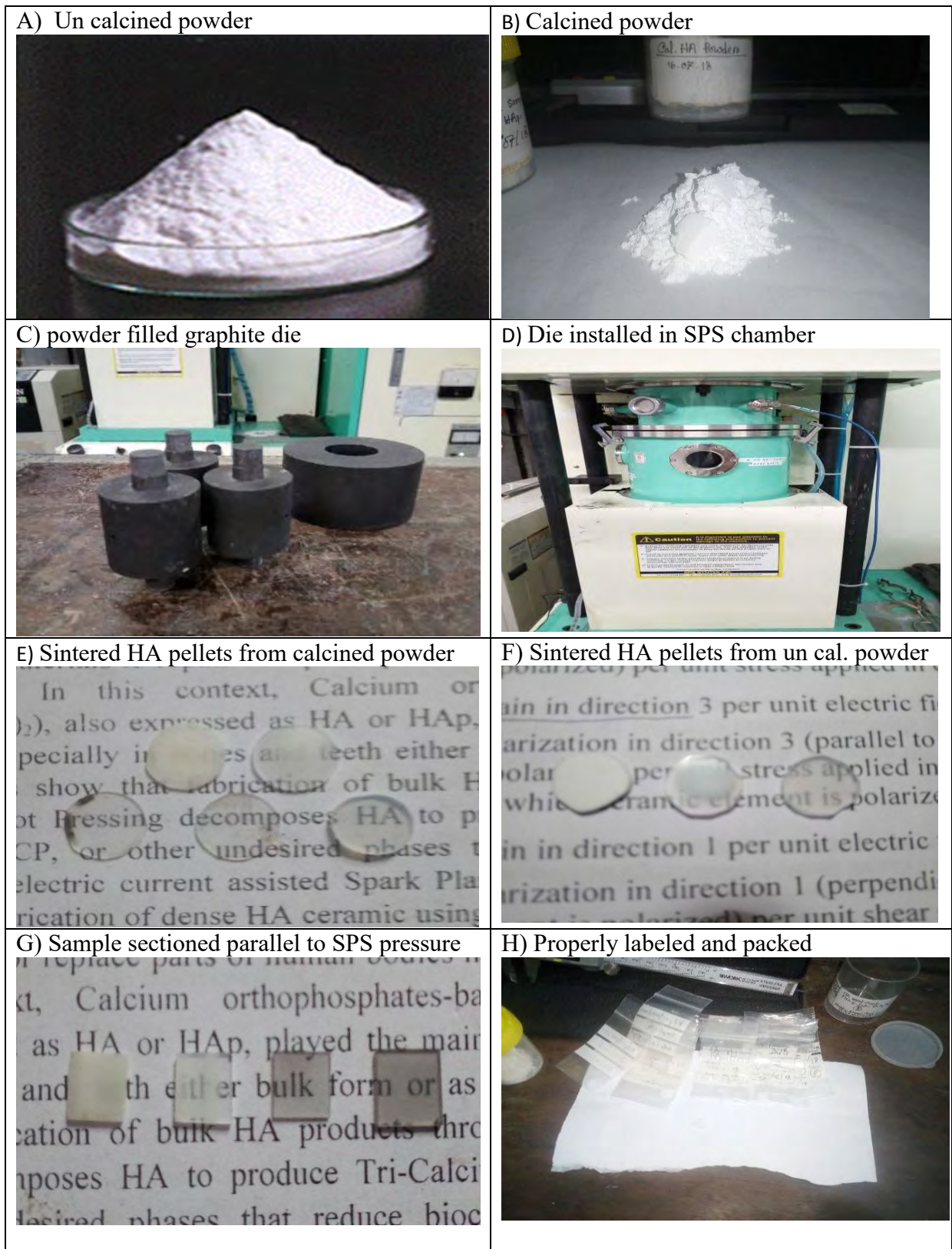


Figure-3.1: Different steps involved in SPS technique.

3.1.2 Sintering of HA powder by Spark Plasma sintering Machine

Hydroxyapatite powder was sintered into ceramic pellets using spark plasma sintering furnace (Dr. Sinter, SPS-515S, SPS Syntax Inc., Kawasaki, Japan). Powder was loaded into a graphite die (10mm in diameter) and punches inserted through the top and the bottom of the die, as shown in figure-3.1(E). A thermocouple was inserted a few mm inside the sintering die instead of a pyrometer that usually focused on the sintering die hole to monitor the temperature. The upper temperature limit of the K-type thermocouple is 1000°C, and the temperature range for the pyrometer is $T > 600^{\circ}\text{C}$. Energy output in SPS automatically increases when pyrometer is used, and when the temperature reaches 600°C then the temperature is regulated via the output from the pyrometer. In order to avoid overshoot it is possible to limit the energy output. The recorded shrinkage values (ΔL) can be converted to density values, as the sample has constant mass and diameter. The linear shrinkage and shrinkage rate are defined as $-\Delta L/L_0$ and $d(\Delta L/L_0)/dt$, respectively, where L_0 is the initial height of the specimen.

Sintering temperature of hydroxyapatite powder was considered in temperature range 825°C to 1000°C. Uniaxial pressures of 3.9 to 4.7kN were applied through the punches. Sintering chamber was kept in vacuum state of 6×10^{-3} Pa throughout the whole sintering time. During the sintering process, a constant force was continued on HA powder through upper and lower punches.



Figure-3.2: Spark Plasma Sintering machine

SPS sintering machine ensures uniform force throughout the whole part of sample powder inside graphite mold. It's pulses direct electrical current (DC) generator and controlling devices ensures high speed consolidation of powder under low atmospheric pressure. Here,

uniaxial pressure device contains water-cooled graphite punches serve also as electrodes. This water-cooled reaction chamber that can be evacuate or back filled with a gas

3.1.3. Sintering Chamber

High electric current and low voltage were applied through the mold placed inside SPS sintering chamber as shown in figure- 3.3. This power source module of sintering machine is connected with control panel. High current across the graphite die caused joule heating to sinter the powder inside graphite die. The amount of current passing through the sample controls the heating rate, holding temperature and cooling rate. SPS pressure was increased slowly in the temperature range 200°C to 250°C and decreased slowly after sintering when temperature got below 800°C.

This direct way of heating allows very high heating and cooling rates by increasing densification over grain growth promotes diffusion mechanism. In this process, the heating power is not only distributed over the volume of the powder compacts homogeneously in macroscopic scale, but moreover the heating power is dissipated exactly at the locations in the macroscopic scale where the energy is required for sintering process, namely at the contact points of the powder particles.



Figure-3.3: Sintering Chamber

In the initial stage of sintering, the powder particle morphology begins to change with the smoothing of surface of the powder particles and this is accompanied by local point contact of individual particle with one another. At the initial stage of sintering no shrinkage of ceramic is noticeable. After establishing the contact between particles, necks begin to form between particles. This process results in densification of sintering component. The densification in the initial stage is reached after exposing the powder to high temperature, due to large surface area and the driving force for sintering. The second stage or the intermediate

stage of sintering involves further neck growth, with pores forming array of interconnected cylindrical channels and these centers approaches one another, with resulting compact shrinkage.

3.1.4 Control Panel

Spark Plasma Sintering machine works according to the set-up program and fully computerized and automatic way. It has a control panel to control and monitor everything very precisely shown in fig 3.4. All information is recorded and displayed in computer screen, as shown in the figure-3.5. Once the temperature reached at predetermined sintering temperature, the samples were hold in this point for 3 min. After sintering, electric current got reduced automatically but pressure kept constant until temperature got reduced to 700°C. When the temperature downed to 700°C, current passing through the sample was completely turned off and the sample was allowed to cool down to room temperature using water coolant system. Finally, the pressure was released, and the sample was allowed to cool further to room temperature.



Figure-3.4: Control panel of SPS machine

Computer connected with control panel converts recorded shrinkage values (ΔL) to density values, as the sample has constant mass and diameter. The linear shrinkage and shrinkage rate are defined as $-\Delta L/L_0$ and $d(\Delta L/L_0)/dt$, respectively, where L_0 is the initial height of the specimen. All the density and deformation curves presented have been corrected for the graphite expansion.

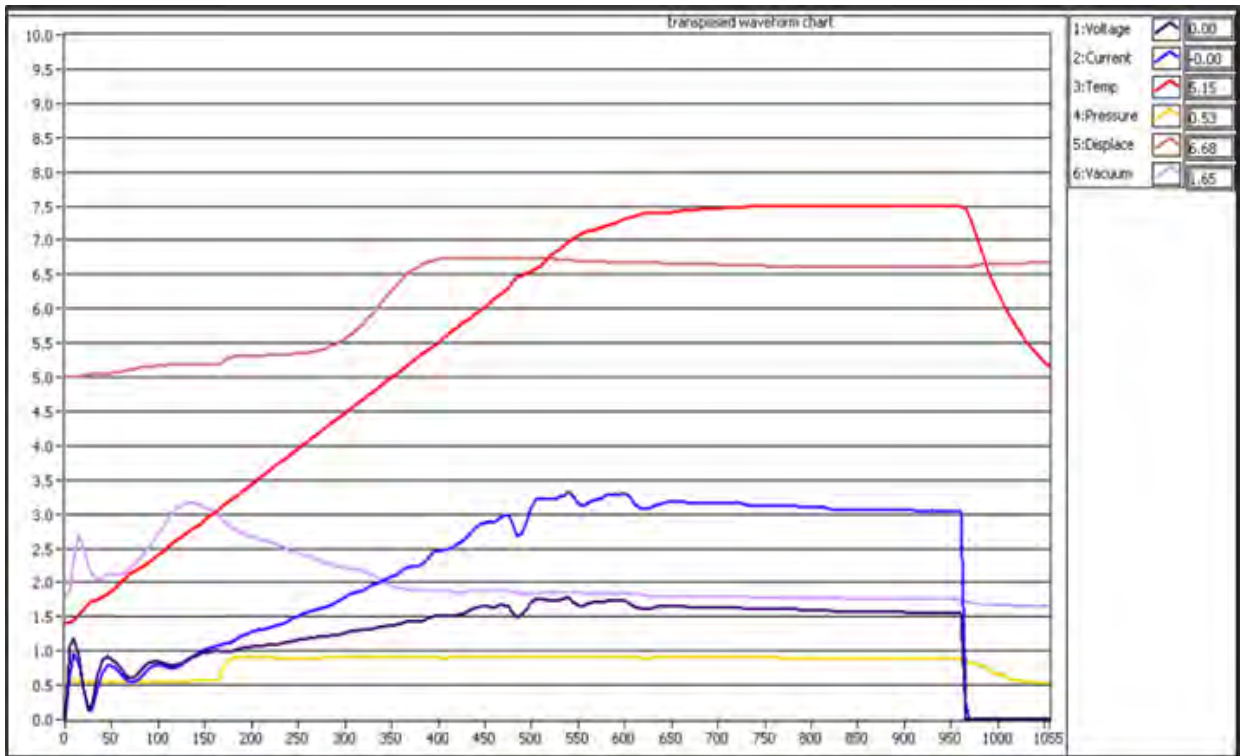


Figure-3.5: Voltage, Current, time and Pressure Graph.

3.1.5. Tables of different Pattern (programs) used in sintering Machine:

Table-3.1

PTN-1: Sintering temperature-900°C

Heating range(°C)	Time(min)	Change(Per min)
0-840	8	100.4
840-880	1	40
880-890	1	10
890-897	1	7
897-900	1	3
900-900	3	0

Table-3.2

PTN-2: Sintering temperature-925°C

Heating range(°C)	Time(min)	Change(Per min)
0-870	9	96.67
870-900	1	30
900-920	1	20
920-923	1	3
923-925	1	2
925-925	3	0

Table-3.3

PTN-3: Sintering temperature-875°C

Heating range(°C)	Time(min)	Change(Per min)
0-800	8	100
800-850	1	50
850-868	1	18
868-872	1	4
872-875	1	3
875-875	3	0

Table-3.4

PTN-4: Sintering temperature-850°C

Heating range(°C)	Time(min)	Change(Per min)
0-790	8	98.75
790-835	1	45
835-847	1	10
847-849	1	2
849-850	1	1
850-850	3	0

Table-3.5

PTN-5: Sintering temperature-975°C

Heating range(°C)	Time(min)	Change(Per min)
0-900	9	100
900-950	1	50
950-965	1	15
965-973	1	8
973-975	1	2
975-975	3	0

Table-3.6

PTN-6: Sintering temperature-950°C

Heating range(°C)	Time(min)	Change(Per min)
0-890	3	111.25
890-930	1	40
930-943	1	13
943-946	1	3
946-948	1	2
948-950	1	2
950-950	3	0

Table-3.7**PTN-7: Sintering temperature-825°C**

Heating range(°C)	Time(min)	Change(Per min)
0-775	8	105
775-800	1	25
800-820	1	20
820-823	1	3
823-825	1	2
825-825	3	0

Table-3.8**PTN-8: Sintering temperature-1000°C**

Heating range(°C)	Time(min)	Change(Per min)
0-915	9	114.37
915-970	1	55
970-985	1	15
985-997	1	13
997-1000	1	3
1000-1000	3	0

3.2 High voltage Polarization technique of HA pellets

Hydroxyapatite pellets sintered by SPS process were then taken through high voltage contact electrical poling or polarizing process. It was carried out with an aim of creating a net polarization amongst the crystallographic domains and to induce piezoelectricity in HA ceramic pellets. When sufficiently strong electric field is applied across the ceramic it can cause reorientation of the spontaneously polarized unit cells into a more isotropic alignment along the field lines. As very high voltages (up to 5000V) would be applied during the polarizing process, it was necessarily designed and constructed in an insulated container as a house of the polarizing apparatus. The design and construction of this apparatus will be presented in the following section.

3.2.1 Design and construction of polarizing apparatus

Polarizing unit consists of an external high voltage power supply (PS350 High voltage power supply, Ps 50 to 5000 Volts, 5mA, Stanford research system), a modified desiccator box with a locking mechanism, an internally mounted hot plate and the polarizing apparatus. Modified desiccator box was an important part of this research, as to ensure the safety of the operation and in the vicinity of the polarizing unit. The construction of the box (brief) was made in such a way that no high voltage was to pass through the polarizing apparatus while the desiccator door was open. To complete this brief, a safety interlock switch was attached to the side of the desiccator box and a control feedback circuit was created to control the current going to the high voltage power supply.



Figure-3.6: High voltage power supply and desiccators box with locking mechanism

High voltage can only be passed through hydroxyapatite ceramic pellets when the door of the desiccator is fully closed. When the interlock key on the door is inserted into the door interlock, it is held in position with a locking force of 2000N. The insertion of interlock key also closes the circuit to allow the high voltage power unit to power up. Without the key being inserted into the interlock no current will flow through the system. To open the door the high voltage power unit must be fully turned off. This in turn kills power to the interlock switch and switches the locking motor to the off position. The door of the desiccator cannot be opened without firstly turning the power off to the high voltage supply.

A keyed emergency stop button is attached to the side of the control unit, as shown in figure - 3.7. This button may be pressed if immediate shut down is required. By pressing emergency stop button all power is stopped from going into the high voltage supply, which in turn powered down the door interlock switch allowing the door to be opened. To re- start the system, after the emergency stop has been pressed, the key must be turned to the ON position. If the key is removed before turning it to the ON position, the system will remain shut down and no current will flow through it.

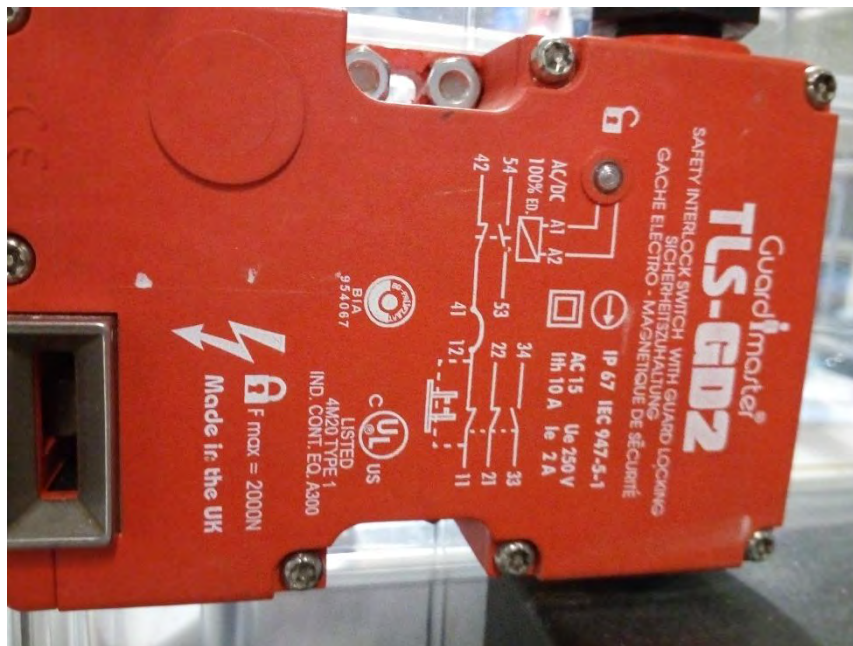


Figure- 3.7: Interlocked key attached with desiccators

These modifications in the desiccator box allows for the safe polarizing of ceramic up to very high voltages due to thickness and high insulating properties of the desiccator walls along with the control polarizing conditions. The desiccator box was also modified to allow for the safe and easy use of hot plate during the polarizing.

3.2.2 Polarizing procedure

Ceramic sample of hydroxyapatite were prepared for electrical polarization by mechanically polishing each of these 10 mm diameter of ceramic pellets into thickness of 1mm. To ensure an even distribution of charge and to avoid any electrical discharge due to un-even surface during the polarization, each sample was given a smooth/flat surface. To achieve this condition and characteristic, samples were mechanically polished using a phoenix 4000 polisher with tungsten carbide paper.

The hydroxyapatite ceramic samples were then placed into the polarizing apparatus as shown in the figure-3.8. The apparatus consists of a positive and negative aluminum electrode of 15 mm in diameter. A spring was attached to the top negative electrode to ensure constant contact between the electrode and the sample during the polarizing process. The positive and negative sections of the polarizing apparatus were separated by a ceramic insulator to avoid shorting during the polarizing process. Samples were polarized in air medium for low voltages and silicon oil was also used as insulating medium for the application of high voltages. In the time of poling process below 150°C, the sample along with the polarizing unit was placed into a beaker filled with silicon oil and then placed on the top of the hot plate within the modified desiccator box. Silicon oil was used during the polarization to ensure an even thermal distribution throughout the polarizing unit and the sample. This silicon oil also allows to apply greater electric fields over the 1 mm thick ceramic pellets due to its higher dielectric constant in comparison to air by reducing the risk of electrical arcing occurs at elevated fields.

When these samples were tried to polarize at comparatively high temperature then silicon oil was avoided because of the tendency of silicon oil to get evaporated at temperature above 200°C. The entire unit was enclosed in the desiccator box and then connected to the high voltage power supply. To ensure enough motion of crystallographic domains, a temperature range 100-200°C was chosen for the polarization process. DC contact electrical poling was then carried out by heating the sample to the poling temperature at a heating rate of 10 °C/min. A DC electric field of between 10KV/cm to 35KV/cm was then applied to these pellets for 90 min to 150 min to know best sintering condition.

Experimental steps involved in high voltage contact electrical poling technique

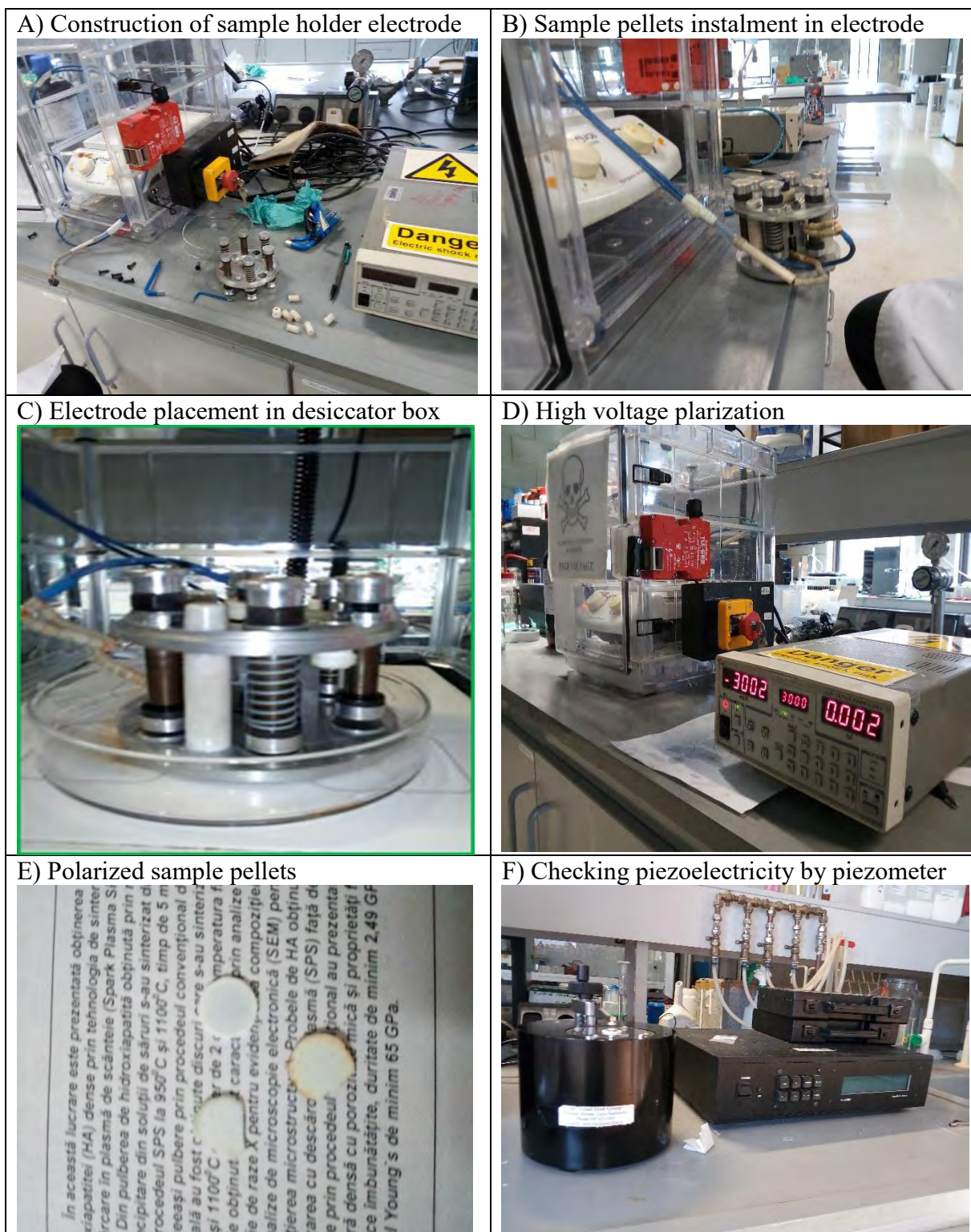


Figure-3.8: Polarizing Apparatus and Electrodes

Before poling, all samples were heated to temperature 200°C and hold at this temperature for one hour then cooled down to reduce surface charge induced in the sample during sintering. Therefore, steps that were taken to polarize HA samples can be summarized as follows-

1. Heating at Temperature 200°C just before poling
2. Holding at temperature 200°C for 90 min without poling
3. Cooling them to room temperature
4. Reheating HA pellets again at temperature 90°C to 150°C
5. Poling for 1-1.5hr using voltage 2-3kV at temperature referred temperature range.
6. Turning off heating device but poling continued for one more hour to cool samples under continuous poling
7. Poling device was kept on for 20 min under low electrical voltage (38 Volt)
8. Piezoelectric constant measured after 1 hour of poling

To ensure permanent alignment of dipole after poling, heating system was turned off 60 min before stopping electrical poling to allow the sample to cool down to room temperature within the electric field. Finally, D_{33} piezoelectric measurements were then carried out on each HA ceramic pellet after 1hr of polling using piezometer.

3.3: Characterization Methods

3.3.1 Optical Characterization using UV visible spectroscopy

UV-Vis spectrophotometer was used to measure the transmittance of sintered HA samples. This spectrometer contains a spectrophotometer that measured the intensity of light absorbed. When ultraviolet light is projected through samples or compounds then some of it gets absorbed, some part of light gets reflected, and the rest transmits through the sample. So, UV / Vis spectrophotometer measures the absorption and then transmission through the sample, which is measured directly as a percent transmittance from absorption by using the following equation-

$$A = 2 - \log_{10} \%T$$

Where, A= absorbance,

T= transmittance



Figure-3.9: UV-Visible spectrometer

Here, transmittance of prepared samples was measured by UV- visible spectrometer in the range of wavelength 200nm to 1000nm to see maximum transmittance. To measure the transmittance of HA, sample were properly cleaned and then placed inside the chamber. Light of visible spectral range were passed through the sample. Before applying to the measurement process of transmittance, every sample was thin down to 1mm in thickness and polished it properly by tungsten carbide polishing paper.

3.3.2 Optical microscopic imaging

Optical micrograph of transparent, translucent and opaque HA samples were taken by using optical microscope. It is a very powerful tool for understanding grain size, shape, morphology of sample. Prepared transparent hydroxyapatite sample were taken under optical microscope to see grain size, shape and distribution. Before watching the surface of hydroxyapatite sample, they were polished properly by using different grade of tungsten carbide paper for several min and finally 1 micrometer diamond suspension and 0.6 micrometer silicon suspension along with polishing cloth were used. Finally, 0.5% acetic acid solution was used as an etching agent to reveal grain boundary. Every sample were downed in acetic acid solution for 3 min and washed by distilled water and then took under optical microscope to see grain and grain boundary.



Figure-3.10: Optical microscope

3.3.3 X-ray diffraction

The X-ray diffraction (XRD) patterns of the samples were recorded in a PAN analytical X'Pert instrument using Cu $K_{\alpha 1}$ radiation. Rietveld refinement was used to calculate the cell parameters of HA. Obtained XRD patterns were used to texture sintered HA samples and to verify if there any decomposition would have taken place during the sintering. In the time of experimental analysis, X-ray of a known wavelength was passed through a sample to investigate its structure. The wave nature of X-rays allowed itself to be diffracted by the lattice structure of the crystal following Bragg's law and reflected to give a unique pattern of peaks at different angles and of different intensity depend on the lattice structure. The diffracted beams from atoms in successive planes cancel out one another through destructive interference unless they are in phase and the condition for this is given by the Bragg equation.

$$n\lambda = 2d \sin \theta$$

Where λ denotes wavelength of X- ray used, d denotes distance between different plane of atom within the crystal lattice and θ is the angle of diffraction.

An X-ray detector, in the XRD machine, moves around the sample stage and measures the intensity and the position (diffraction angle 2θ) of this reflected peak. The highest peak intensity measured is considered as 100% peak and the intensity of all other peaks are measured as a ratio of it.



Figure-3.11: XRD machine

XRD analysis was carried out on all samples using X'Pert PRO MPD X- ray diffraction diffractometer (Philips, Almelo, The Netherland) using graphite-chromatize Cu K_{α} radiation ($L=0.15406\text{\AA}$) at 40KV and 35 mA. A scanning range(2θ) from 20° from 60° with a step size

of 0.02 $2\theta/s$ was used throughout the entire process. XDR analysis was used to texture sintered HA sample and to determine purity of produced sample as well as its crystallographic orientation such lattice parameters.

SPS sintered HA sample pellets were sectioned perpendicular and parallel to the applied SPS pressure to know their structural orientation with respect to the pressure.



Figure-3.12: Prepared samples for placing in XRD chamber

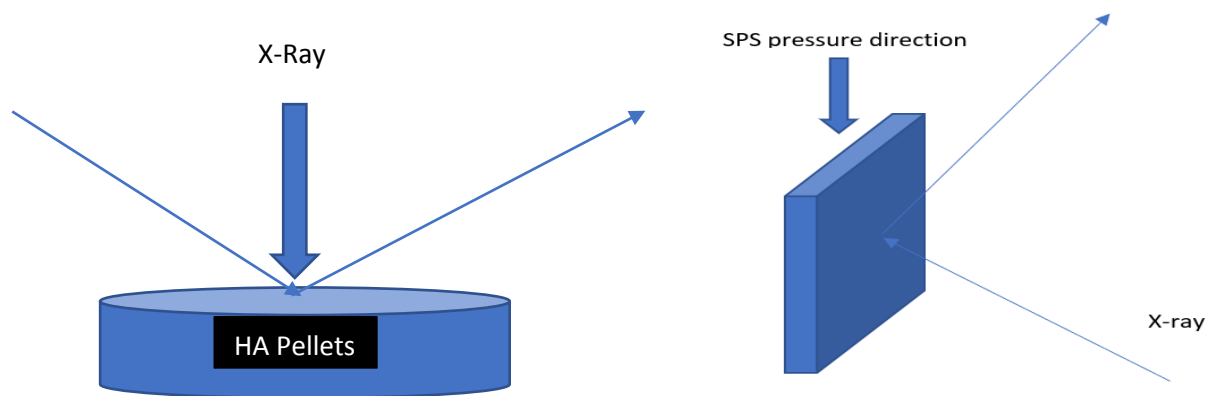


Figure-4.13: XRD direction on HA pellets as per SPS pressure

Phase identification of each sample was performed using a reference to the library database supplied by the International Centre for Diffraction Data (ICDD) by directly comparing the X-ray diffraction patterns to the joint Committee for Powder Diffraction Standard (JCPDS) for hydroxyapatite and other common phases formed during the synthesis and related high temperature decomposition of hydroxyapatite. The list of peaks of hydroxyapatite and most important peaks of other calcium phosphate commonly found within hydroxyapatite. The phase identification was also checked against that the database supplied by the ICDD, using software, X'Pert HighScore plus version.

Chapter-4

Results and Discussion

4.1 XRD Characterization

4.1.1 XRD profile of sintered HA pellets along the perpendicular direction of SPS pressure

Fig-4.1 to Fig-4.5 shows XRD peak profile of 5 samples taken perpendicular surface of applied SPS pressure; where, 3 of them were transparent, one translucent and another one was opaque. It is noticed from these figure that (211) plane at the position $2\theta = 30^\circ$ is comparatively intense for transparent samples, while, (211) plane for translucent sample gets comparatively weak, (300) plane along a-axis get intensified for both transparent and translucent samples, (112) plane get totally disappeared. Others plane for transparent and translucent sample are apparently similar in position and intensity.

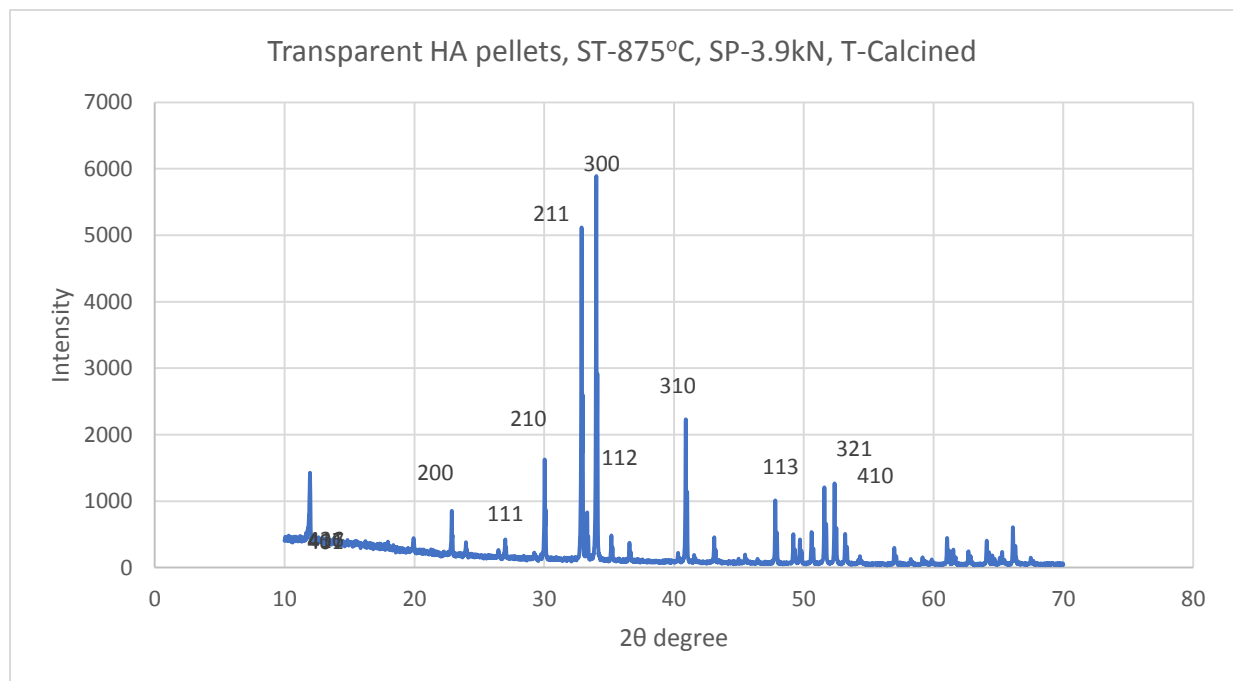


Figure-4.1: Transparent HA pellets, ST-875°C, SP-3.9kN, powder type-Calcined

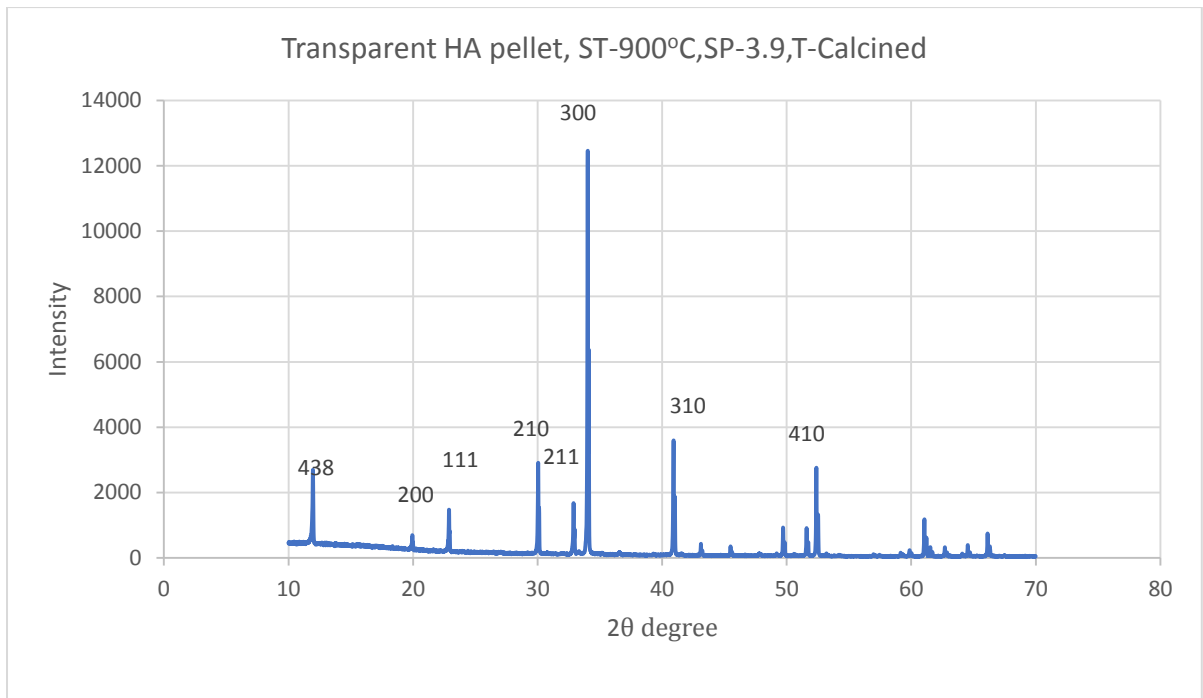


Figure-4.2: Transparent HA pellet, ST-900°C, SP-3.9, powder type-calcined

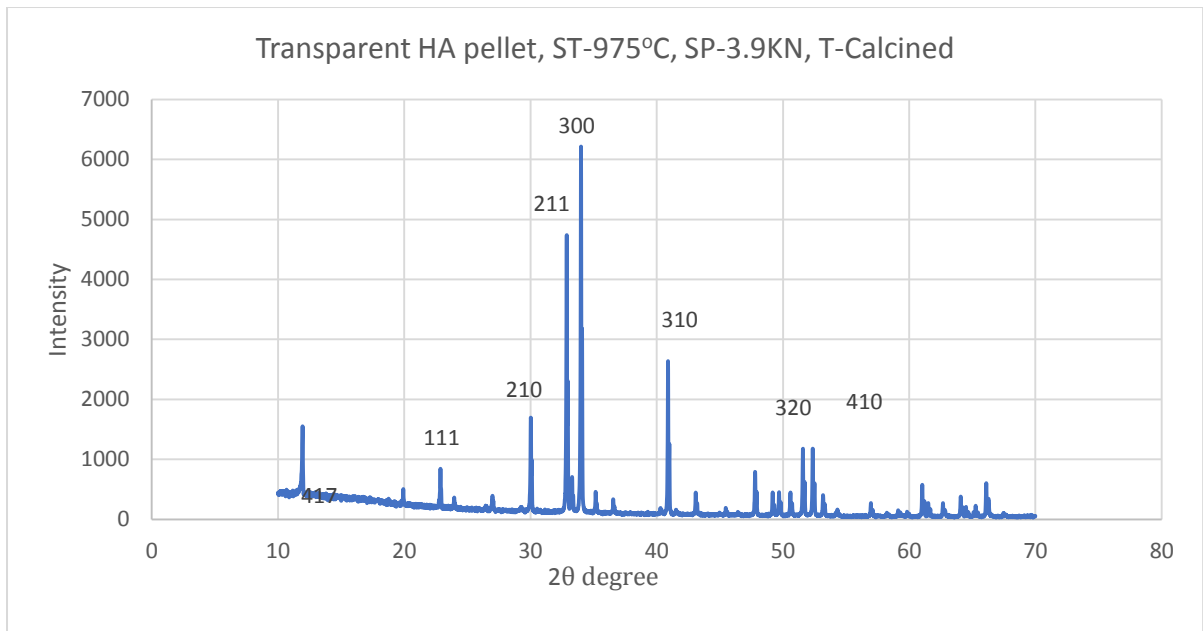


Figure-4.3: Transparent HA pellet, ST-975°C, SP-3.9KN, powder type-calcined

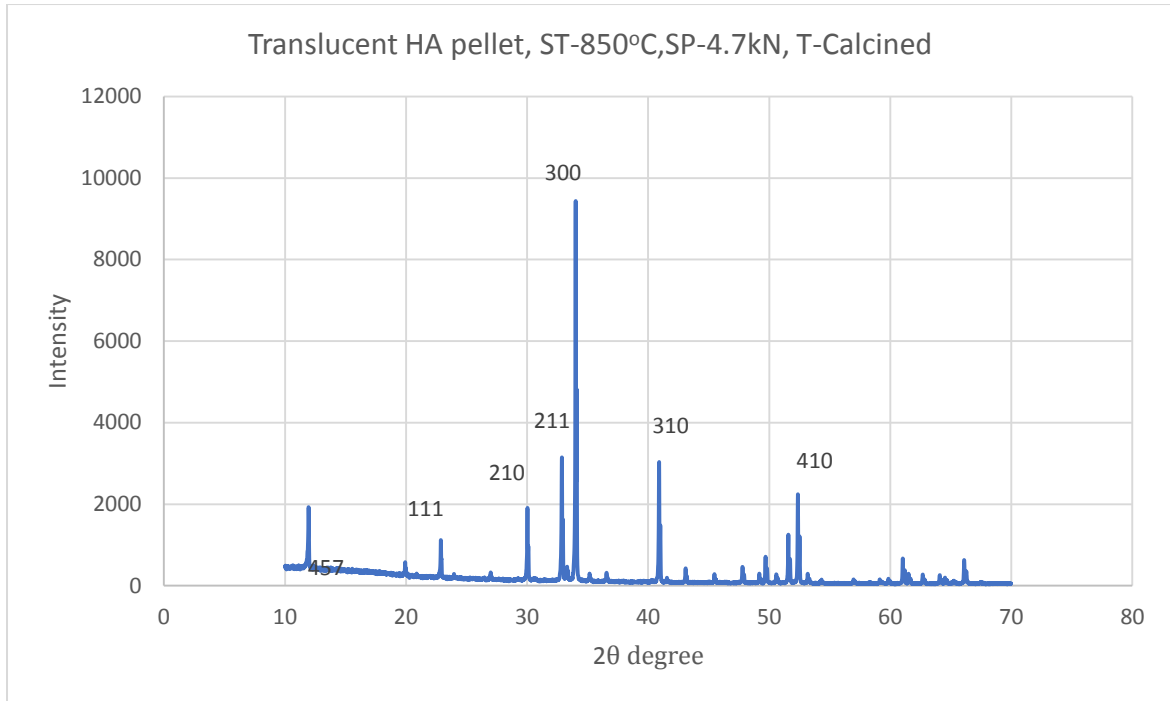


Figure-4.4: Translucent HA pellet, ST-850°C, SP-4.7kN, powder type-calcined

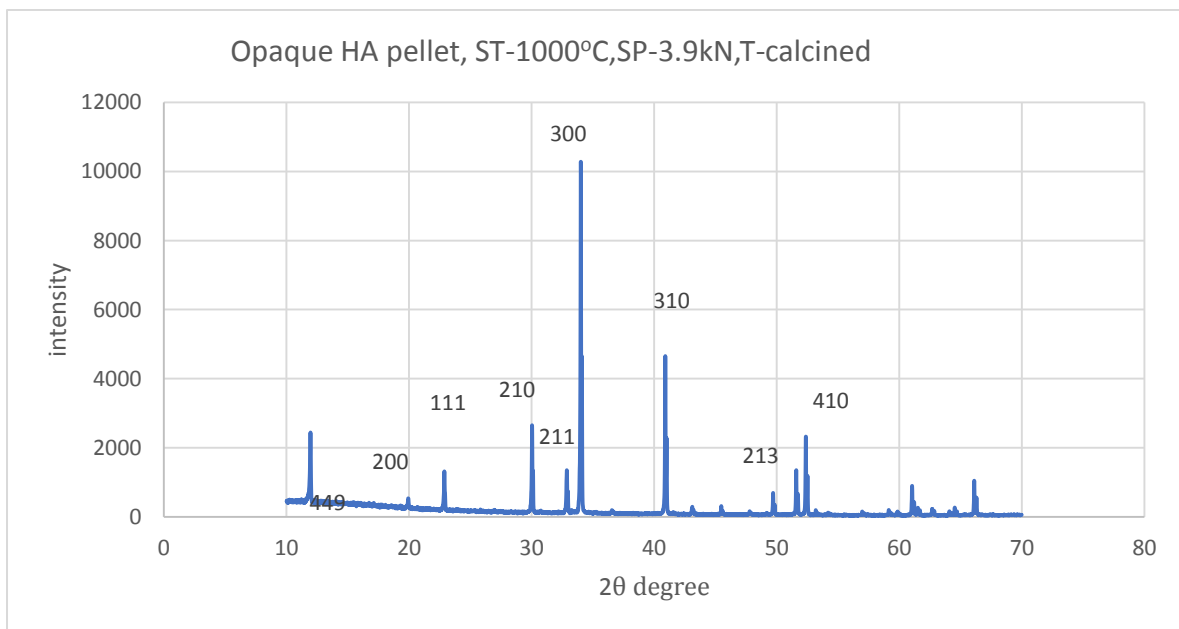


Figure-4.5: Opaque HA pellet, ST-1000°C, SP-3.9kN, powder type-calcined

Table-4.1: XRD data of transparent HA pellets, ST-875 °C, SP-3.9kN, powder type-Calcined

Pos. [°2θ]	Height [cts]	FWHM Left [°2θ]	d-spacing [Å]	Rel. Int. [%]	hkl
30.0355	1460.85	0.0468	2.97277	25.94	210
32.8785	4975.95	0.0468	2.72192	88.34	211
32.9570	2441.03	0.0468	2.72236	43.34	112
34.0102	5632.73	0.0468	2.63389	100.00	300
34.1032	2574.50	0.0312	2.63345	45.71	202
40.9054	2053.84	0.0624	2.20442	36.46	310
41.0071	1047.92	0.0468	2.20465	18.60	310
51.5893	1129.50	0.0624	1.77020	20.05	130
52.3698	1139.16	0.0624	1.74564	20.22	410

Table-4.2: XRD data of transparent HA pellet, ST-900 °C, SP-3.9, powder type-calcined

Pos. [°2θ]	Height [cts]	FWHM Left [°2θ]	d-spacing [Å]	Rel. Int. [%]	hkl
22.8816	1088.13	0.0512	3.88664	11.31	200
30.0393	2420.83	0.0468	2.97240	25.16	210
32.8724	1179.94	0.0624	2.72241	12.26	211
34.0158	9621.64	0.0624	2.63347	100.00	300
34.0977	4428.02	0.0468	2.63386	46.02	202
40.9100	4337.79	0.0468	2.20418	45.08	310
41.0120	2107.41	0.0624	2.20440	21.90	130
51.5936	1199.89	0.0468	1.77007	12.47	113
52.3777	2260.89	0.0624	1.74540	23.50	321
52.5128	1088.73	0.0624	1.74555	11.32	410

Table-4.3: XRD data of transparent HA pellet, ST-975 °C, SP-3.9KN, powder type-calcined

Pos. [°2θ]	Height [cts]	FWHM Left [°2θ]	d-spacing [Å]	Rel. Int. [%]	hkl
22.8859	1287.73	0.0384	3.88593	10.57	200
30.0441	2695.53	0.0468	2.97194	22.12	102
30.1252	1305.63	0.0312	2.97149	10.71	210
32.8864	1444.84	0.0468	2.72128	11.85	112
34.0207	12188.18	0.0468	2.63310	100.00	300
34.1045	5795.32	0.0468	2.63335	47.55	202
40.9132	3424.00	0.0624	2.20402	28.09	310
41.0166	1783.18	0.0468	2.20416	14.63	130
52.3826	2589.00	0.0624	1.74525	21.24	321
52.5214	1244.56	0.0624	1.74529	10.21	410

Table-4.4: XRD data of translucent HA pellet, ST-850 °C, SP-4.7kN, powder type-calcined

Pos. [°2θ]	Height [cts]	FWHM Left [°2θ]	d-spacing [Å]	Rel. Int. [%]	hkl
30.0307	1743.92	0.0468	2.97323	19.03	210
32.8707	2927.16	0.0624	2.72255	31.95	211
32.9592	1397.73	0.0312	2.72219	15.25	112
34.0096	9163.09	0.0468	2.63393	100.00	300
34.0919	4448.92	0.0468	2.63429	48.55	202
40.9029	2865.81	0.0624	2.20455	31.28	310
41.0041	1375.96	0.0468	2.20481	15.02	130
51.5849	1161.09	0.0624	1.77034	12.67	321
52.3710	2081.21	0.0624	1.74560	22.71	220
52.5081	1109.08	0.0624	1.74570	12.10	410

Tab4-4.5: XRD data of opaque HA pellet, ST-1000 °C, SP-3.9kN, powder type-calcined

Pos. [°2θ]	Height [cts]	FWHM Left [°2θ]	d-spacing [Å]	Rel. Int. [%]	hkl
30.0245	1516.66	0.0624	2.97384	26.04	210
32.8665	4451.42	0.0468	2.72288	76.44	211
32.9446	2154.98	0.0468	2.72336	37.00	112
33.9988	5823.77	0.0468	2.63475	100.00	300
34.0902	2723.69	0.0312	2.63442	46.77	202
40.8939	2358.92	0.0624	2.20501	40.50	310
40.9962	1109.20	0.0468	2.20521	19.05	130
51.5783	1059.95	0.0624	1.77055	18.20	321
52.3587	1077.66	0.0624	1.74599	18.50	410

Calcined HA Power XRD profile:

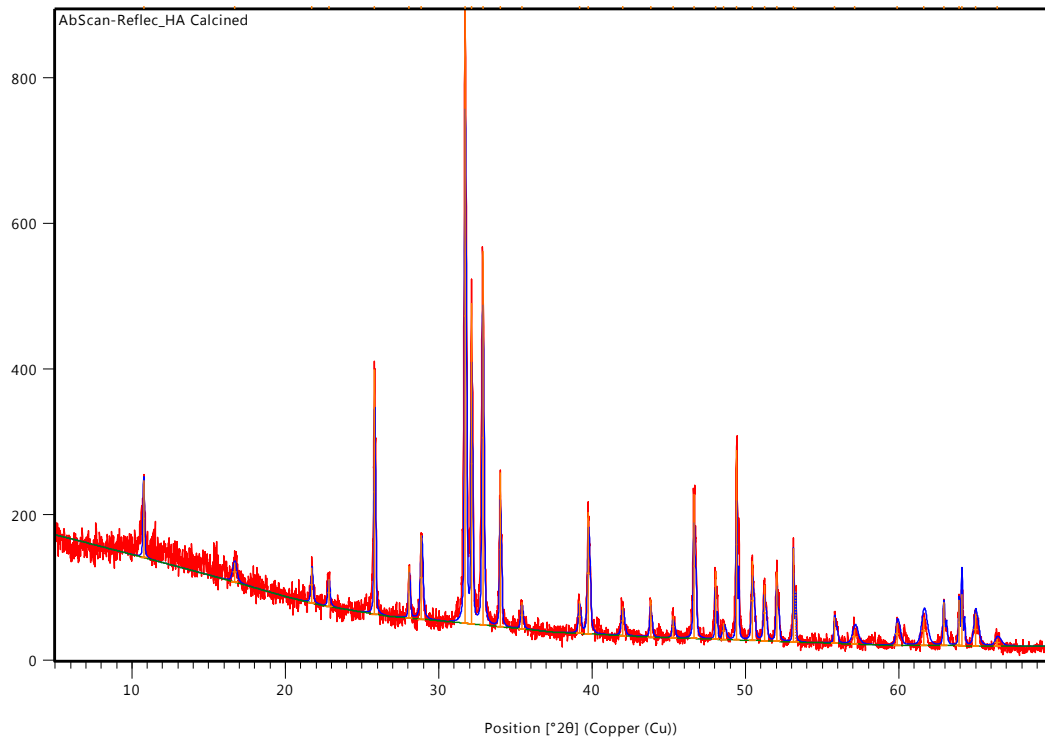


Figure-4.6: XRD of calcined HA powder

Table-4.6: XRD data of calcined HA Powder

Pos. [$^{\circ}2\theta$]	Height [cts]	FWHM Left [$^{\circ}2\theta$]	d-spacing [\AA]	Rel. Int. [%]	hkl
25.8388	335.88	0.0895	3.44814	39.74	002
28.8969	115.05	0.1791	3.08982	13.61	210
31.7444	845.27	0.1023	2.81886	100.00	211
32.1595	440.91	0.0895	2.78341	52.16	112
32.8891	513.17	0.1151	2.72332	60.71	300
34.0343	211.47	0.1023	2.63426	25.02	202
39.7841	167.01	0.1535	2.26580	19.76	310
46.6680	198.06	0.1279	1.94637	23.43	113
49.4396	260.78	0.0768	1.84355	30.85	321
50.4671	108.59	0.1535	1.80840	12.85	410
53.1420	128.60	0.0780	1.72208	15.21	402

4.1.2 XRD profile of sintered HA pellets in parallel direction of SPS pressure

Figure- 4.7 to figure-4.11, shows the XRD pattern of 5 sintered samples at parallel surface of applied SPS pressure. XRD pattern shows that peaks at the position $2\theta = 27^\circ$ and 54° are highly intense. These intense peaks are responsible for 002 and 004 plane. In the previous case, when sintered perpendicular to SPS pressure, they were totally missing.

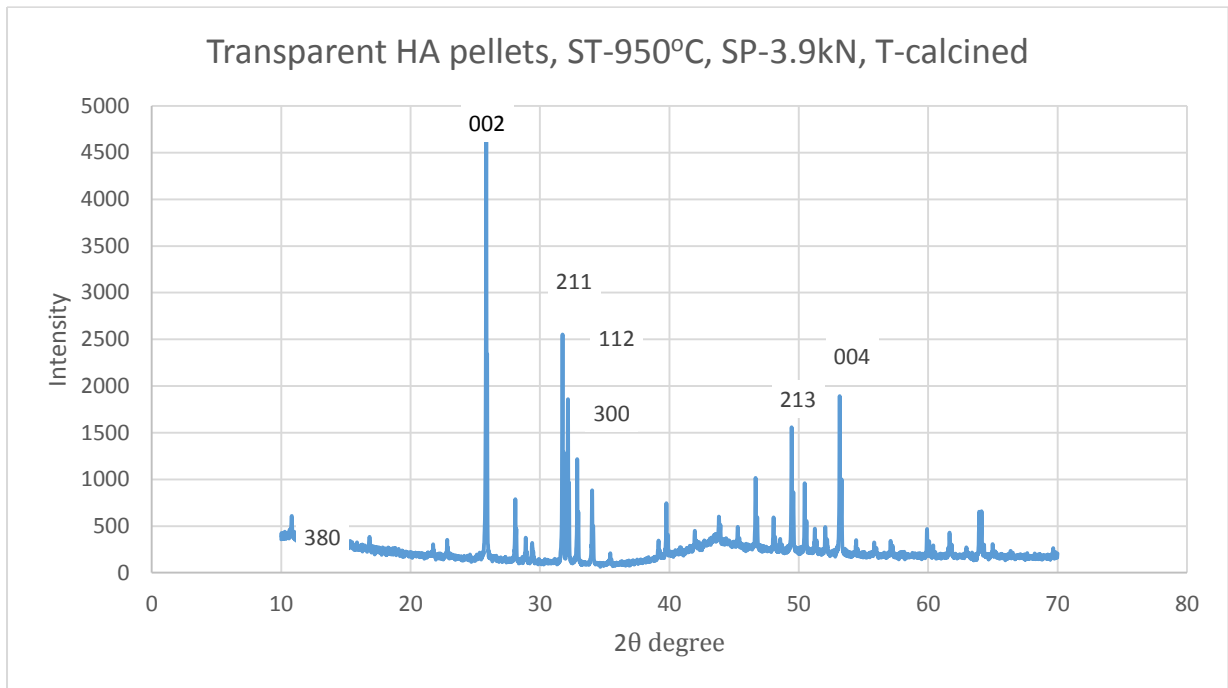


Figure-4.7: Transparent HA pellets, ST-950 °C, SP-3.9kN, powder type-calcined

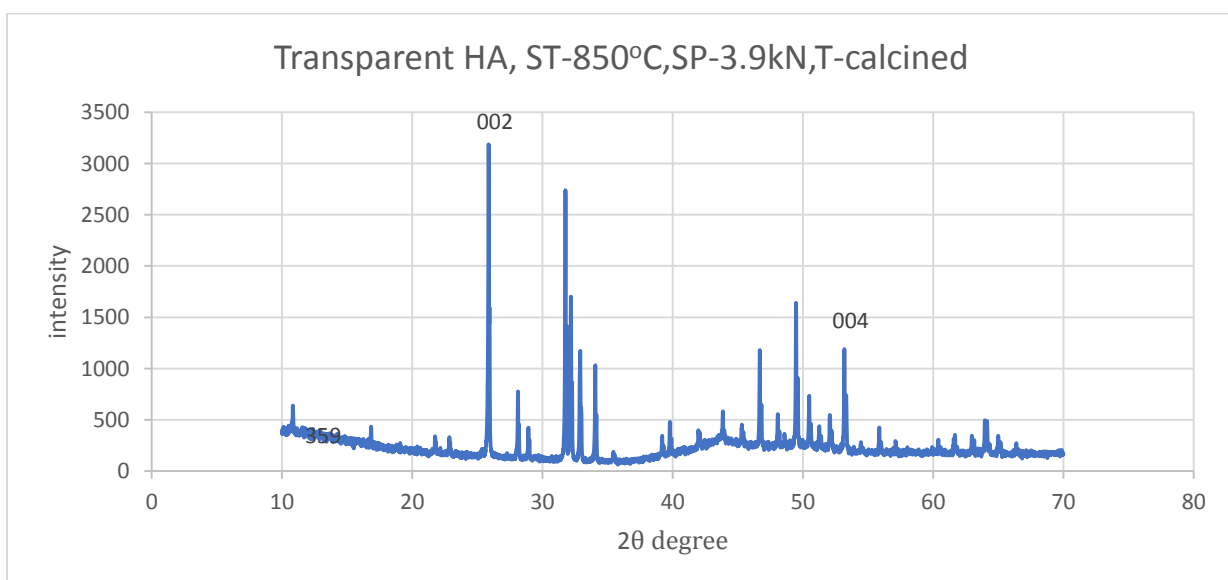


Figure-4.8: Transparent HA pellets, ST-850 °C, SP-3.9kN, powder type-calcined

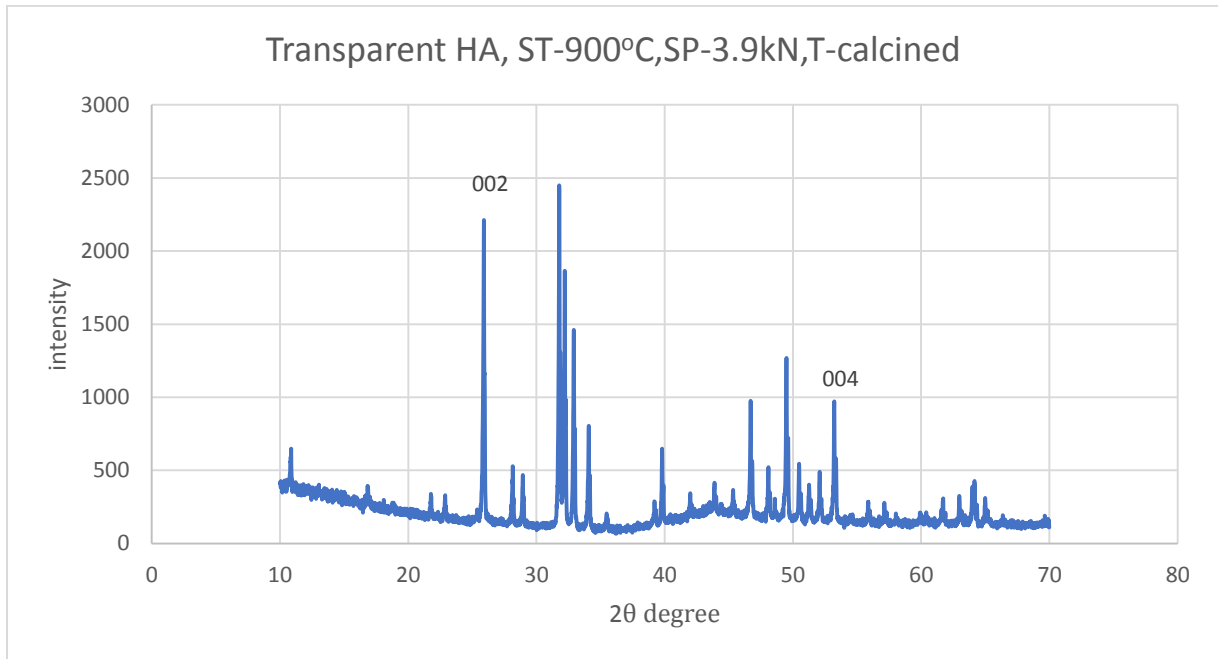


Figure-4.9: Transparent HA pellets, ST-900 °C, SP-3.9kN, powder type-calcined

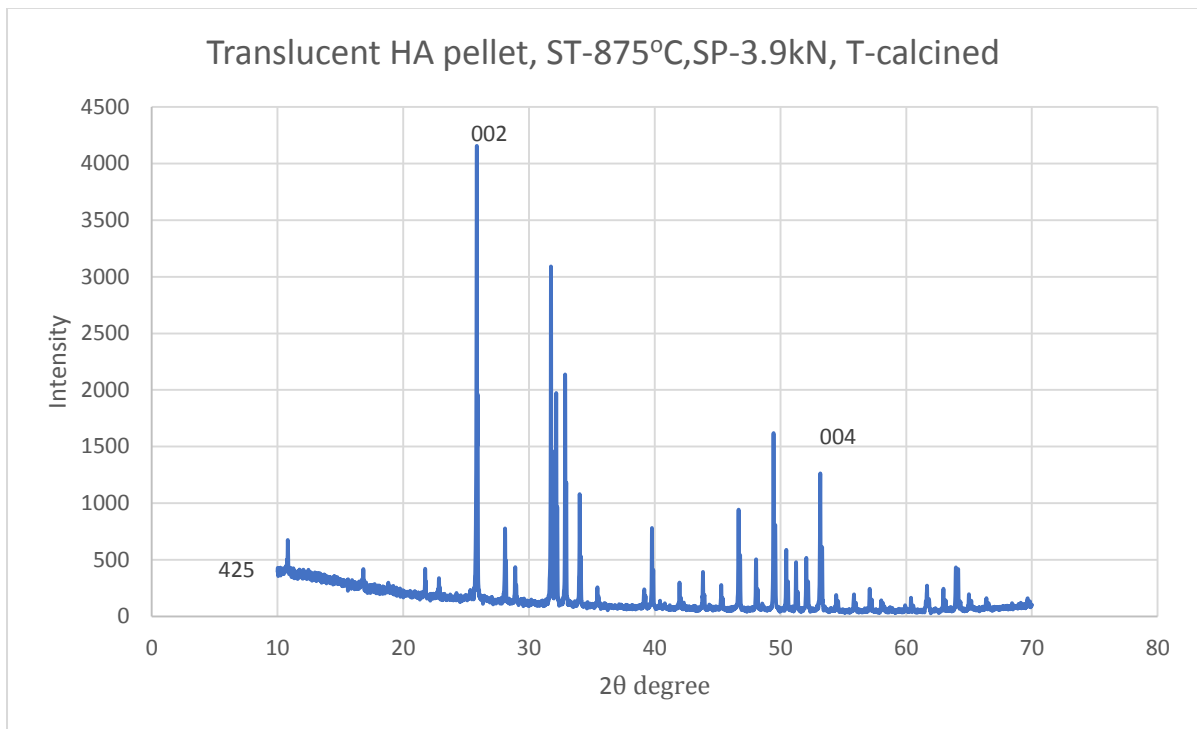


Figure-4.10: Translucent HA pellets, ST-875 °C, SP-3.9kN, powder type-calcined

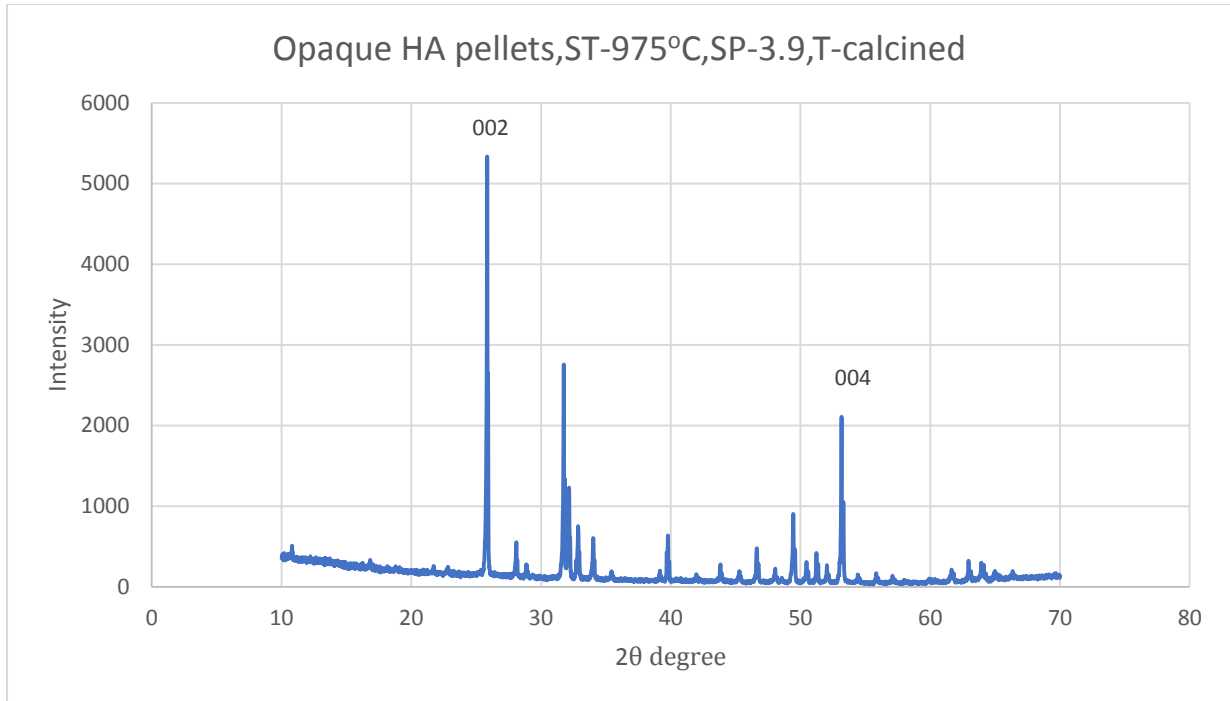


Figure-4.11: Opaque HA pellets, ST-975^o C, SP-3.9kN, powder type-calcined

XRD results from figure-4.7 to figure-4.11 represent orientation indexes where 002 and 004 along the parallel section which are the diffractions corresponding to the *c* plane and it were found much higher than those of the other planes. Regarding the perpendicular section (figure-4.1-4.5), the orientation indexes of 100, 200, 210, 300, and 310 diffractions, corresponding to the *a* and *b* planes, were much higher than those of other planes.

4.1.3. XRD for identification of decomposition product

The XRD patterns (Fig-4.12-4.13) were also used to verify if there any decomposition of HA occurs in the time of sintering, because HA ceramics may experience high temperature related decomposition. Here, these peaks were identified for pure HA phase because there wasn't observed appreciable decomposed materials peaks. Most common high temperature related decomposed materials for HA are tricalcium phosphate (TCP) or other phosphates compounds. Here, no appreciable TCP phase was detected in the produced samples, which is probably due to the short sintering time. The prevention of HA decomposition might enhance the density and thereby transparency of the sintered body.

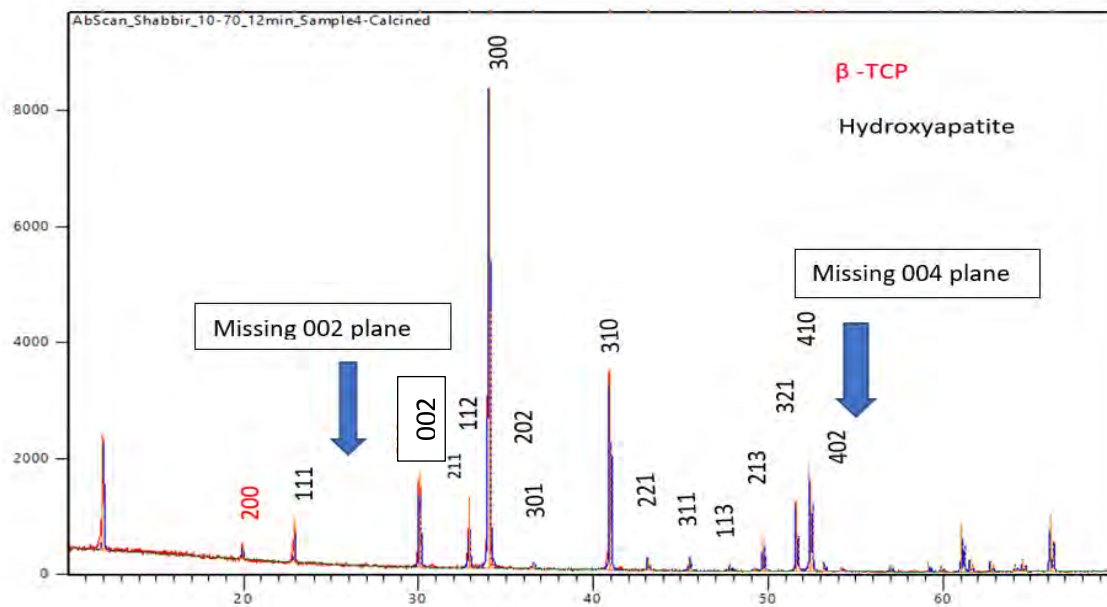


Figure-4.12: XRD peaks and plane taken perpendicular direction of SPS pressure

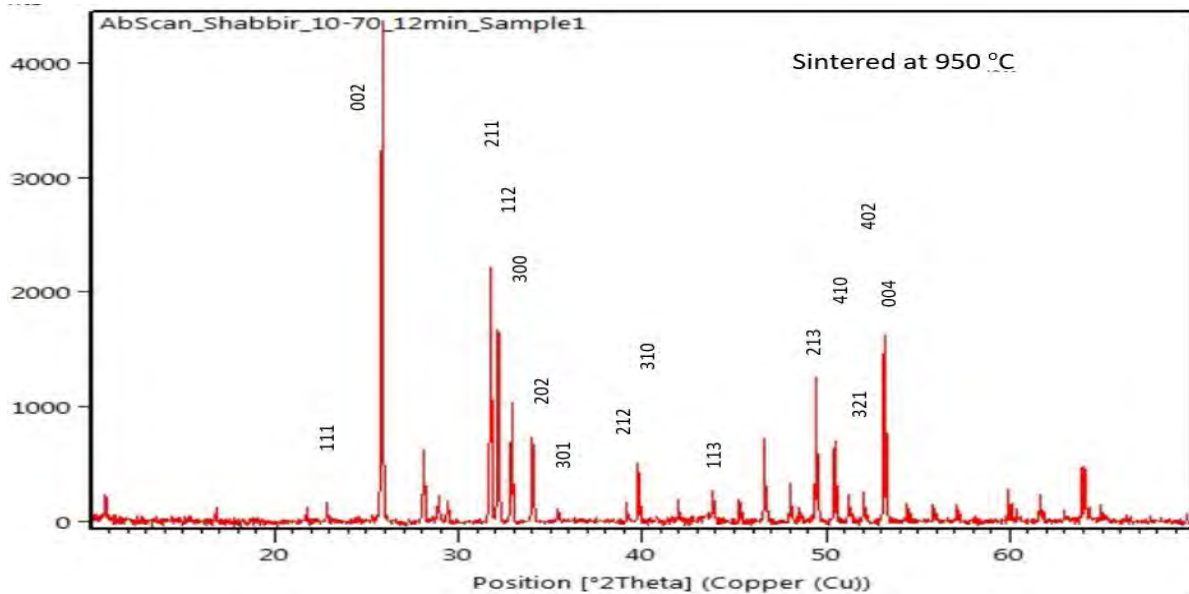


Figure-4.13: XRD peaks and plane taken parallel direction of SPS pressure

Figure-4.14 shows the comparison of the XRD pattern of hydroxyapatite powder and prepared hydroxyapatite pellets together. From the figure, it is noticed that very little peak shift by the amount 1.19° occurred for sintered sample from hydroxyapatite powder. From the figure 4.12 to 4.13, most intense peak (211) of hydroxyapatite powder at $2\theta = 32^\circ$ loses its intensity in the sintered sample and (300) plane of SPS sintered sample became the most intense among all the peaks, (210) and (200) peaks also get intensified in sintered sample. Another most noticeable peak of powder hydroxyapatite (002) is totally absent in sintered hydroxyapatite pellets.

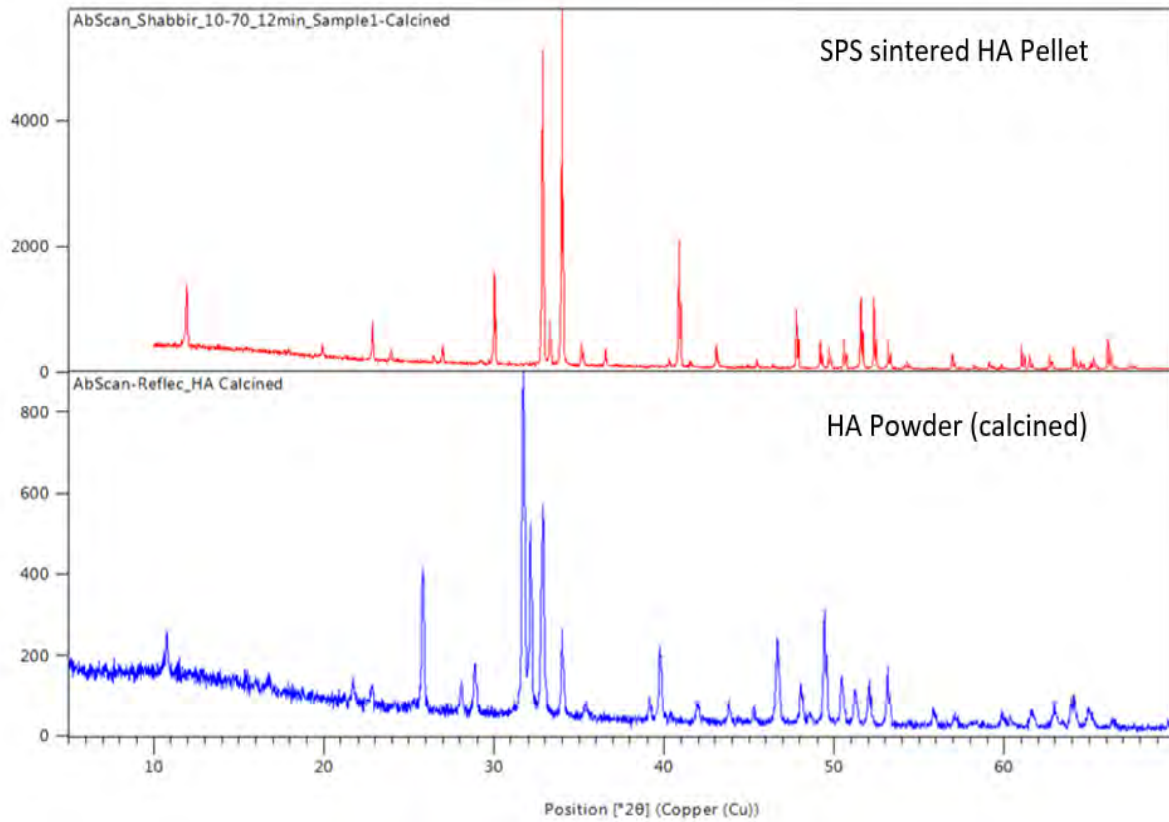


Figure-4.14: XRD peak of calcined HA powder and prepared HA pellet together

4.1.4 XRD peak profile- perpendicular and parallel surface of SPS pressure.

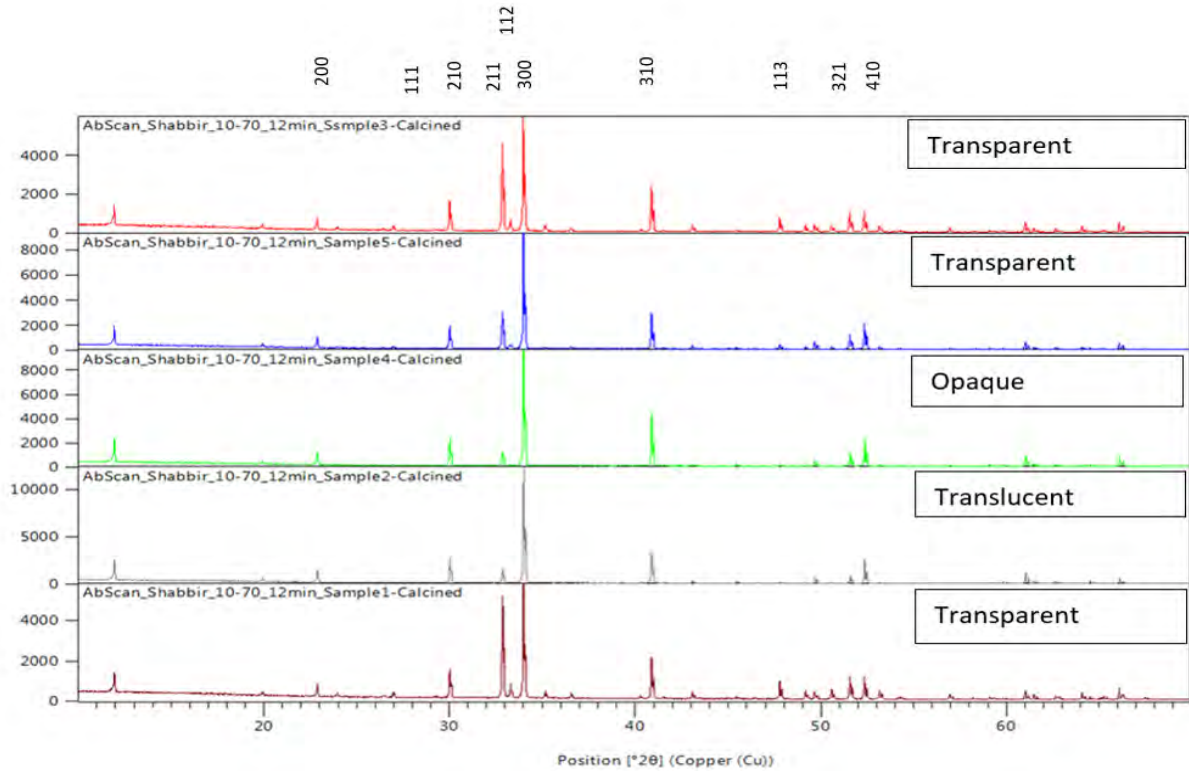


Figure-4.15: XRD at the perpendicular surface of pellet with respect to SPS pressure

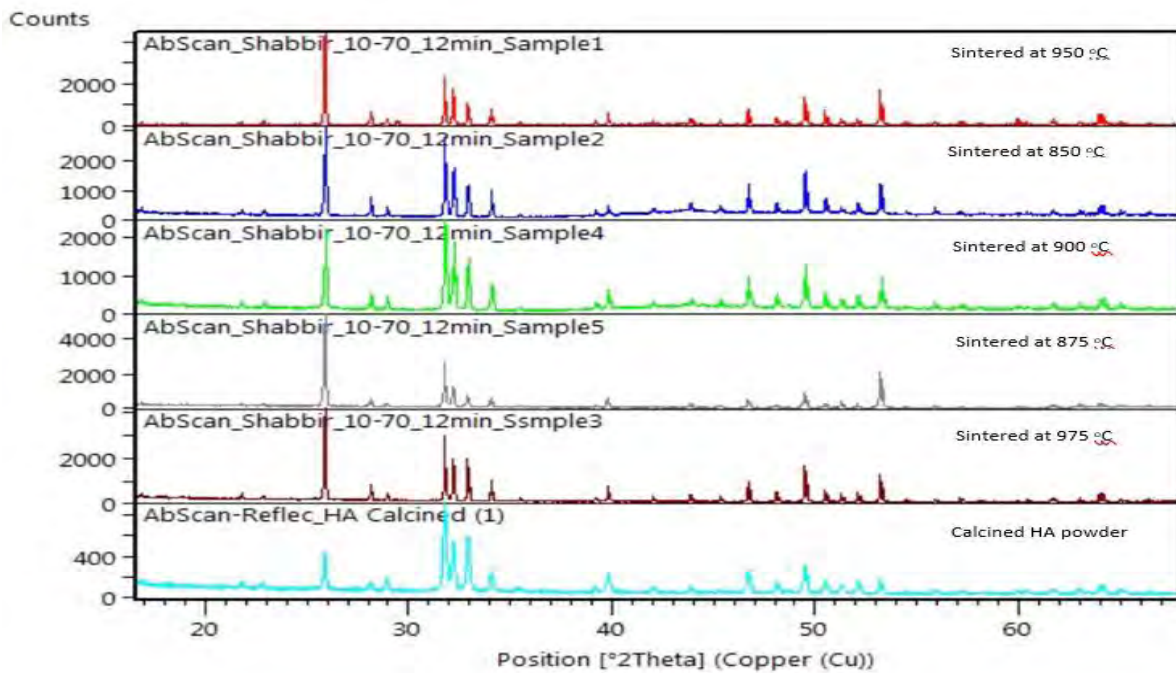


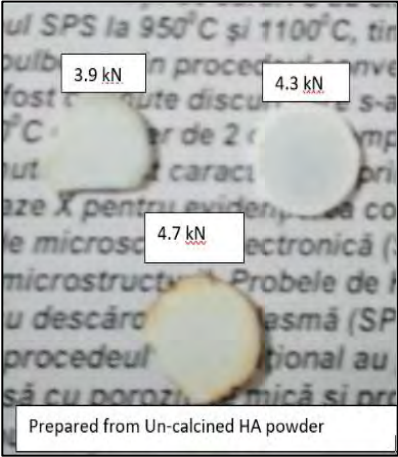
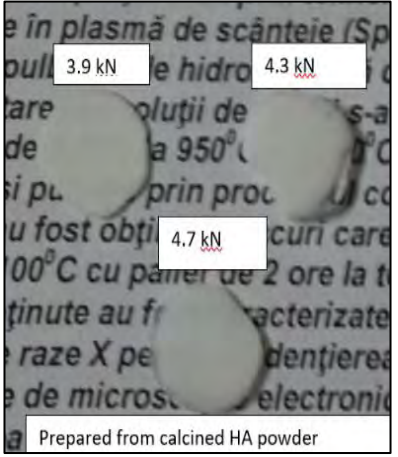
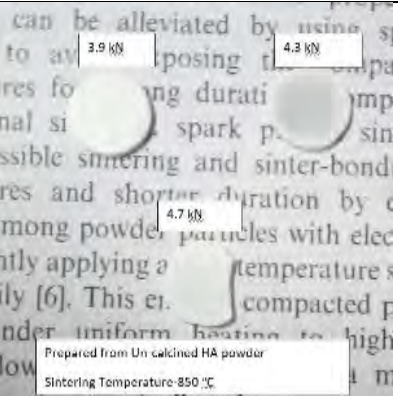
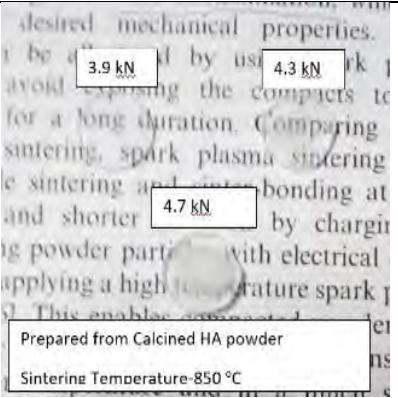
Figure-4.16: XRD at the parallel surface of pellet with respect to SPS pressure.

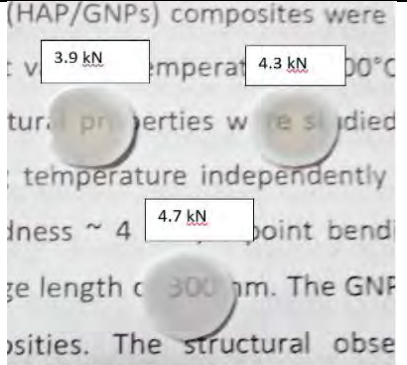
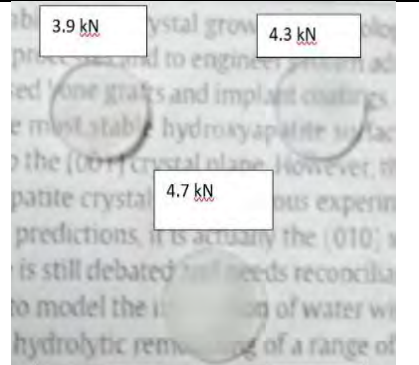
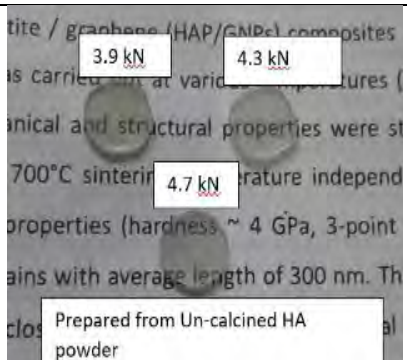
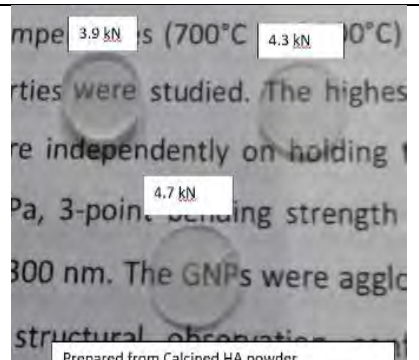
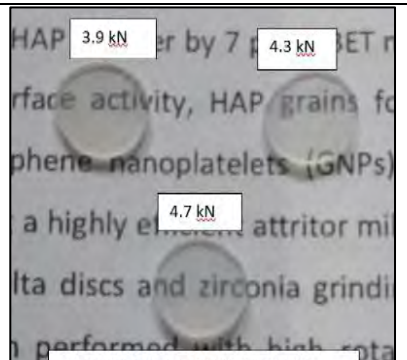
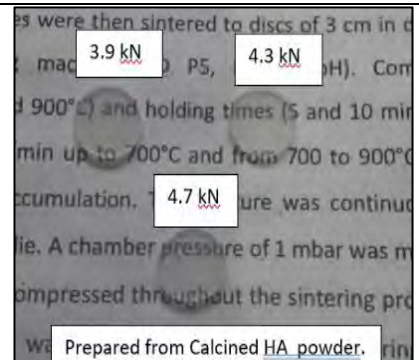
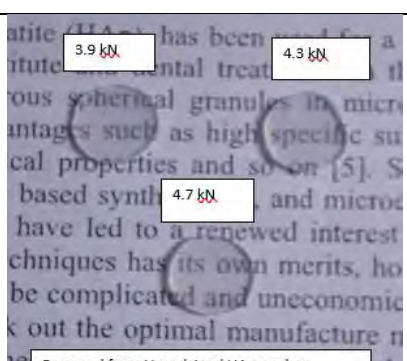
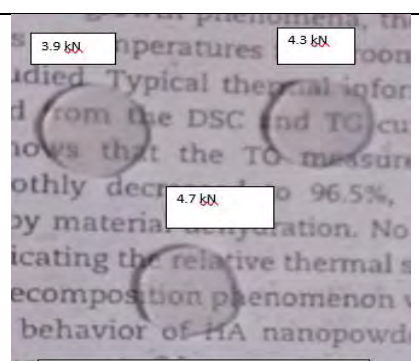
4.2 Transparent hydroxyapatite samples

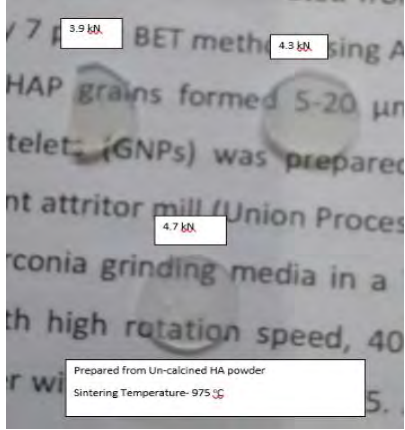
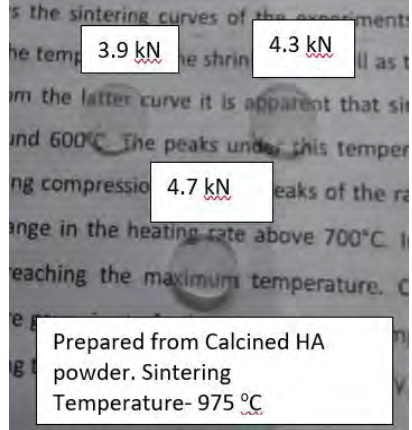
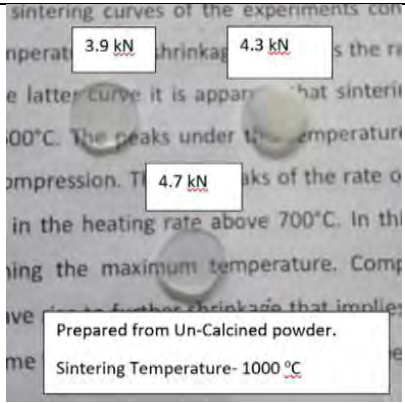
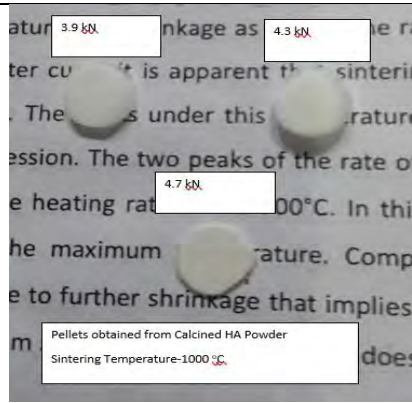
Sintered pellets of hydroxyapatite were sectioned parallel and perpendicular direction of applied SPS pressure. It is observed that types or nature of samples varied based on sintering temperature, pressure and type of powder used in this sintering process both in parallel and perpendicular direction of applied SPS pressure as shown in the table-4.7.

Transparent hydroxyapatite samples were obtained at prolonged temperature range. For calcined HA powder (Set-A) transparent samples were started producing from 850°C and ended up at sintering temperature 975°C. For un-calcined powder (Set-B), it was started 875°C and terminated at 1000°C. Pellets prepared from calcined and un-calcined powder showed % transmittance around 75% and 70% at wavelength 700nm prepared at temperature 900°C and pressure 3.9kN respectively. It was also observed that samples prepared from calcined HA powder at temperature 1000°C were quite opaque. Highly transparent samples were obtained at temperature 900°C, but after crossing the sintering temperature 900°C, transmittance got reduced and raised again when the sintering temperature was chosen 975°C.

Table-4.7: Samples obtained at different sintering temperatures and pressures are shown below-

Sin. Temperature	SPS Pressure	Un-calcined (Set-A)	Calcined (Set-B)
825°C	a) 3.9kN b) 4.3kN c) 4.7kN	 <p>Prepared from Un-calcined HA powder</p>	 <p>Prepared from calcined HA powder</p>
850°C	a) 3.9kN b) 4.3kN c) 4.7kN	 <p>Prepared from Un-calcined HA powder Sintering Temperature-850 °C</p>	 <p>Prepared from Calcined HA powder Sintering Temperature-850 °C</p>

875°C	a) 3.9kN b) 4.3kN c) 4.7kN	 <p>Prepared from Un-Calcined powder. Sintering Temperature- 875 °C</p>	 <p>Prepared from Un-Calcined powder. Sintering Temperature- 875 °C</p>
900°C	a) 3.9kN b) 4.3kN c) 4.7kN	 <p>Prepared from Un-calcined HA powder</p>	 <p>Prepared from Calcined HA powder Sintering Temperature-900 °C</p>
925°C	a) 3.9kN b) 4.3kN c) 4.7kN	 <p>Prepared from Un-Calcined powder. Sintering Temperature- 925 °C</p>	 <p>Prepared from Calcined HA powder. Sintering Temperature- 925 °C</p>
950°C	a) 3.9kN b) 4.3kN c) 4.7kN	 <p>Prepared from Un-calcined HA powder Sintering Temperature- 950 °C</p>	 <p>Prepared from Calcined HA powder Sintering Temperature- 950 °C</p>

975°C	a) 3.9kN b) 4.3kN c) 4.7kN		
1000°C	a) 3.9kN b) 4.3kN c) 4.7kN		

4.3 Microscopic Images of Transparent, Translucent and Opaque HA samples

Figure-4.17 to 4.23 shows the optical microscope photographs of sintered samples along the perpendicular and parallel sections of applied SPS pressure. Figure-4.17 shows the surface of sintered pellets before and after etching in 0.5% acetic acid solution, which revealed the microstructure of milky white HA pellets. Microscopic image (figure-4.18) of the perpendicular section of applied SPS pressure shows intergrowth of columnar crystallites corresponding to the a - , b - axes of HA crystallite. On the other hand, microscopic image (Figure-4.22 to 4.23) of the parallel section of sample with respect to the SPS pressure shows intergrowth of fine hexagonal plate crystallites, corresponding to the c - axis of HA crystallite. These results confirm that the c - axis of HA crystals is aligned perpendicular to the pressure direction.

Optical micrograph of HA pellets before and after etching

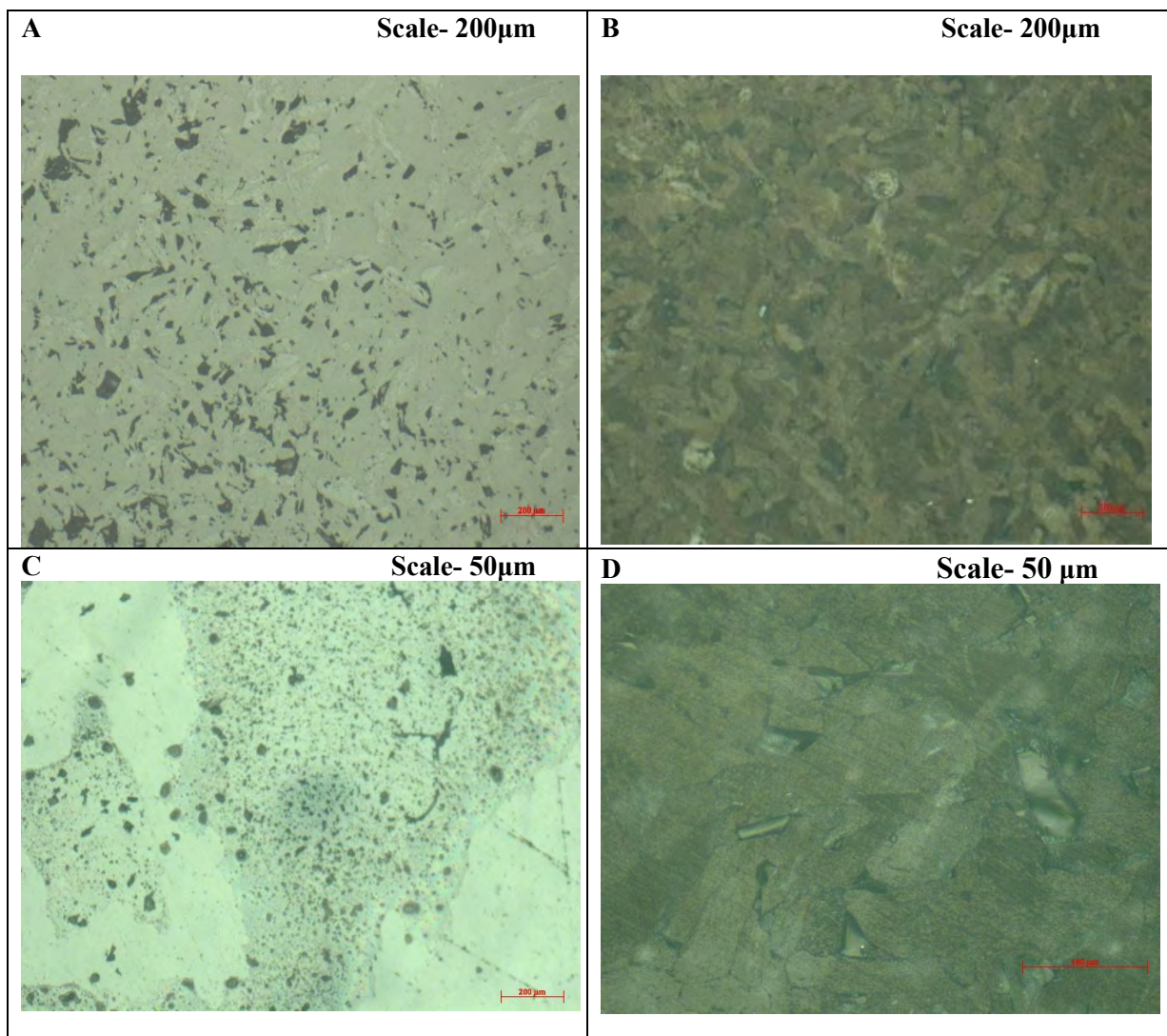


Figure-4.17: Un-calcined powder sintered at pressure 3.9kN, temperature-825°C and sectioned perpendicular to SPS pressure (A) before etching (B) after etching. Calcined powder sintered at pressure 3.9kN, temperature-825°C and sectioned perpendicular to SPS pressure (C) before etching (D) after etching.

Optical Micrograph HA pellets along the edge portion

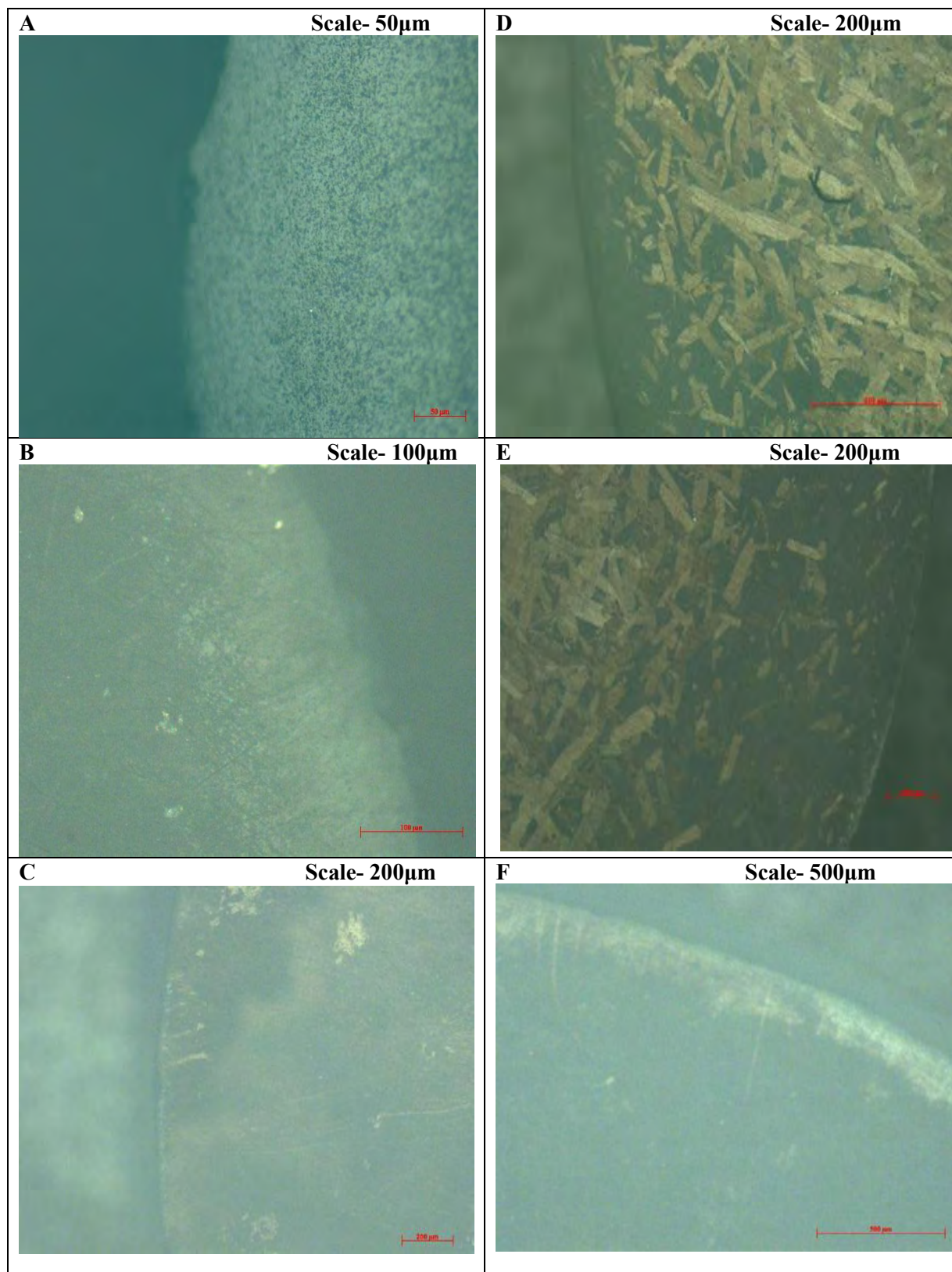


Figure-4.19: Optical micrograph of SPS sintered HA pellets along the edge portion prepared at (A) 875 $^{\circ}\text{C}$ and 4.3kN (B) 900 $^{\circ}\text{C}$ and 4.3kN (C) 9250 $^{\circ}\text{C}$ and 4.3kN from un calcined powder, (D) 825 $^{\circ}\text{C}$ and 4.3kN (E) 825 $^{\circ}\text{C}$ and 4.7kN (F) 900 $^{\circ}\text{C}$ and 4.3kN from calcined powder

Optical Micrograph of transparent HA pellets.

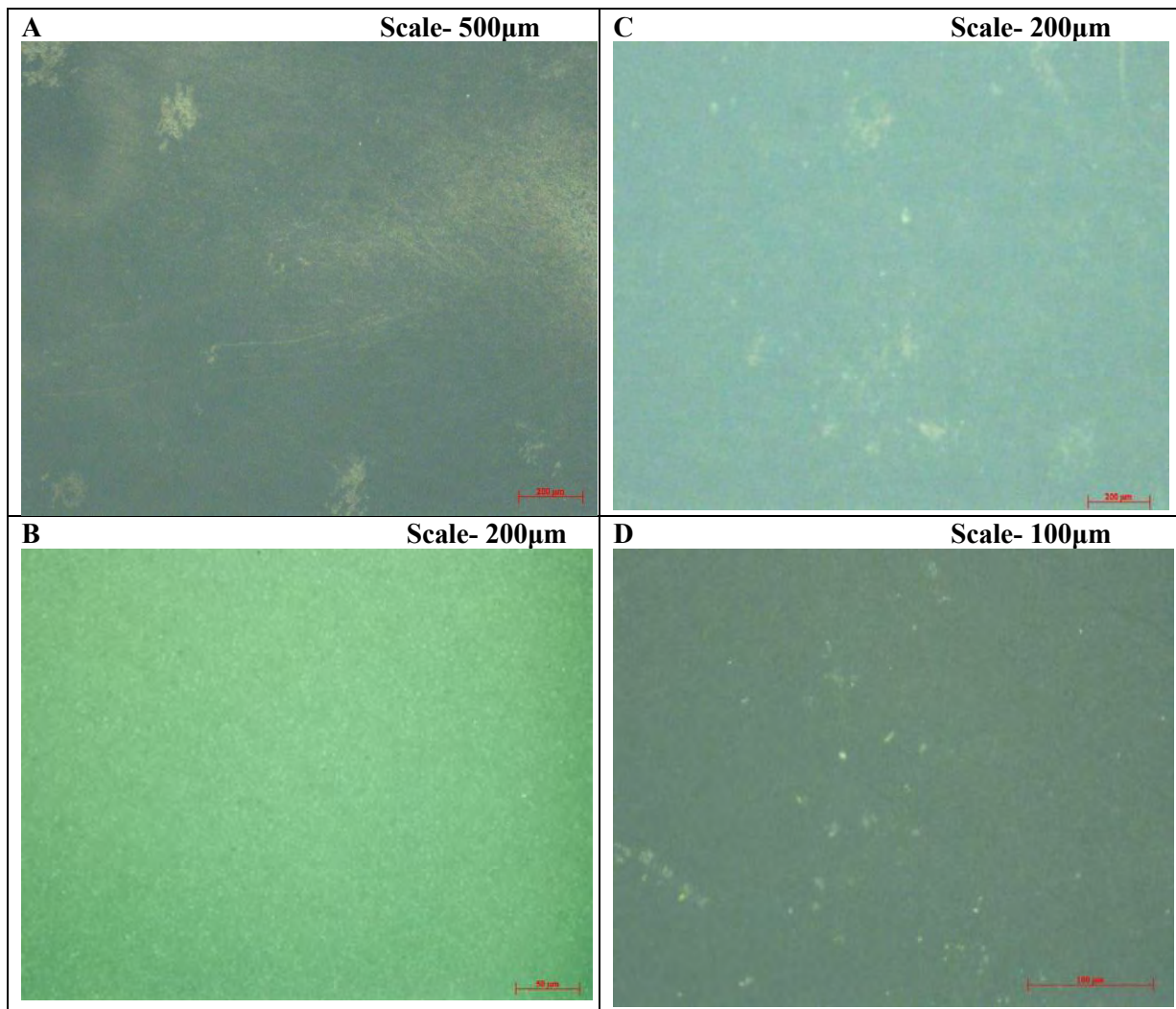


Figure-4.20: Optical micrograph of SPS sintered transparent HA pellets prepared at (A)900⁰C and 3.9kN (B) 975⁰C and 3.9kN from un calcined powder (C) 900⁰C and 3.9kN (D) 975⁰C and 3.9kN from calcined powder

Optical Micrograph of translucent HA pellets

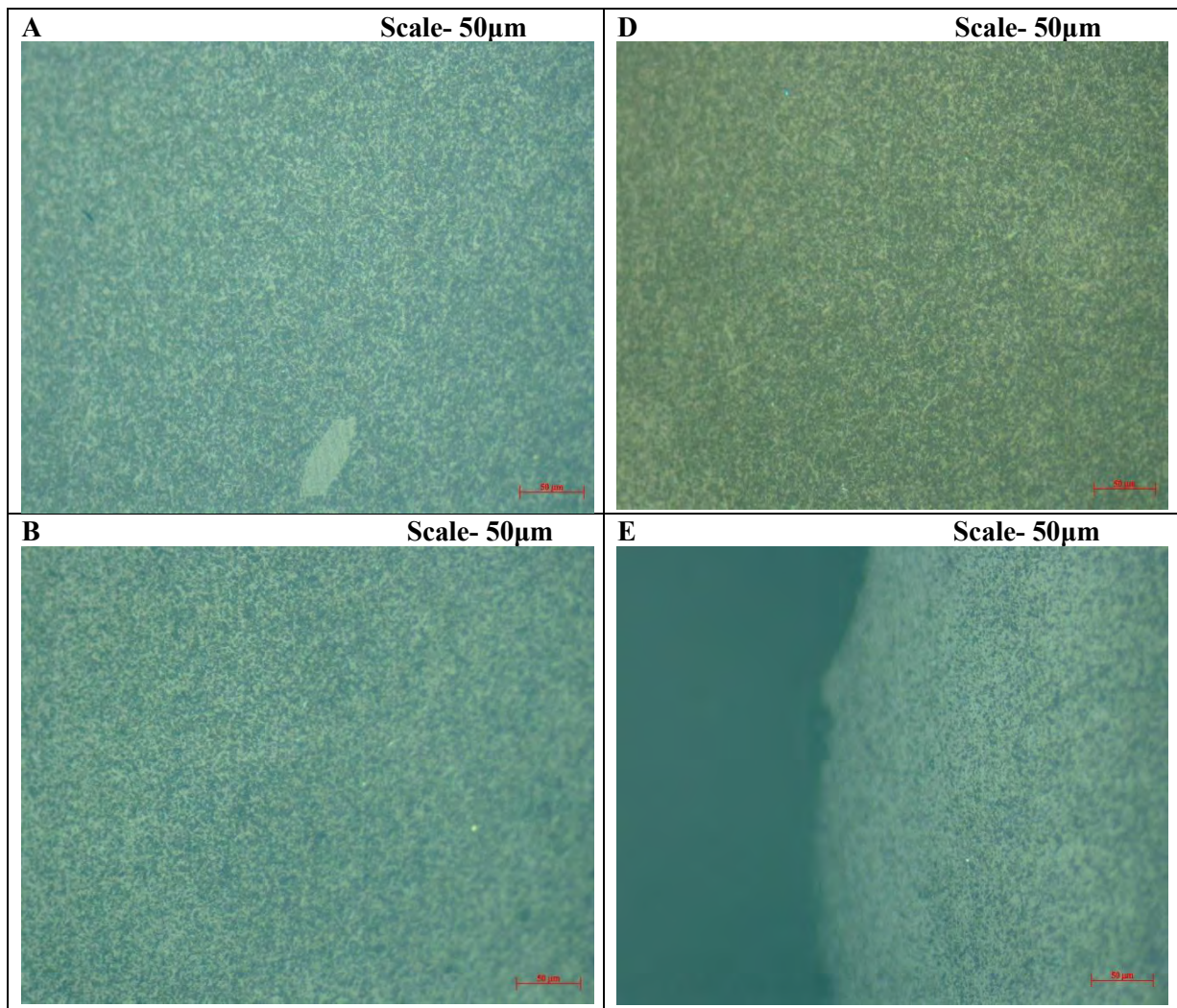


Figure-4.21: Optical micrograph of SPS sintered mildly transparent HA pellets prepared at (A) 850⁰C and 4.7kN (B) 875⁰C and 4.7kN from calcined powder (C) 875⁰C and 3.9kN (D) 875⁰C and 4.3kN from un calcined powder

Optical micrograph of translucent and opaque sample in the parallel direction of SPS pressure:

Figure-4.22 shows optical microscopic images of translucent HA pellets surface along the direction parallel to applied SPS pressure. Its clearly shows intergrowth of fine hexagonal plate crystallites.

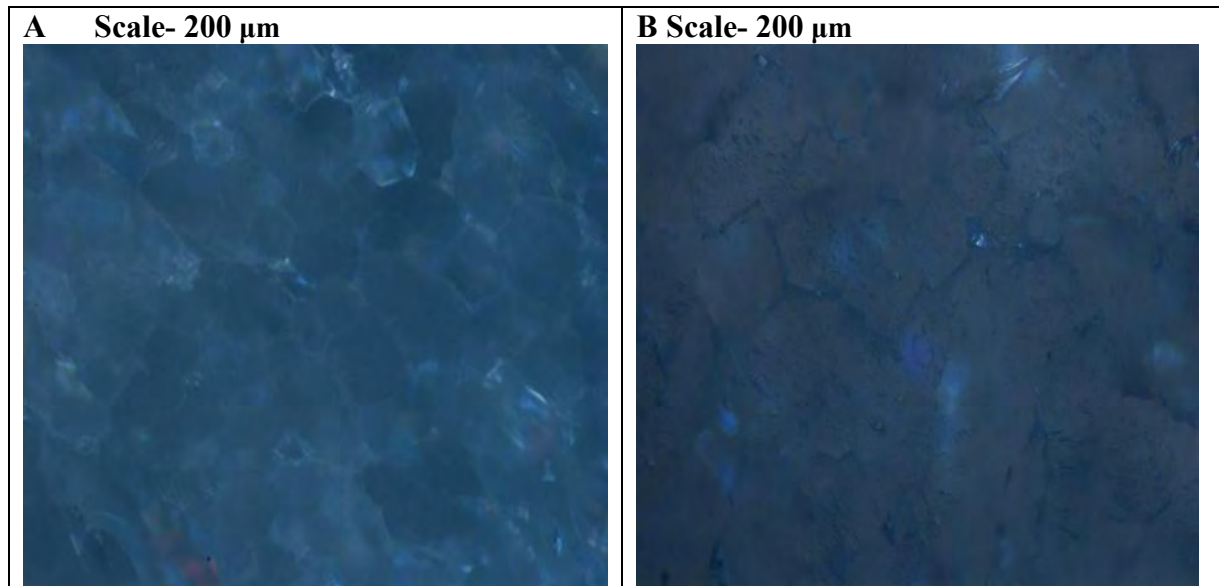


Figure-4.22: Optical micrograph of SPS sintered (A) translucent HA pellets prepared at 875⁰C, 4.7kN (B) Opaque HA pellets prepared at 825⁰C, 4.7kN from un calcined powder sectioned along the parallel direction of SPS pressure

Optical micrograph transparent sample in the parallel direction of SPS pressure:

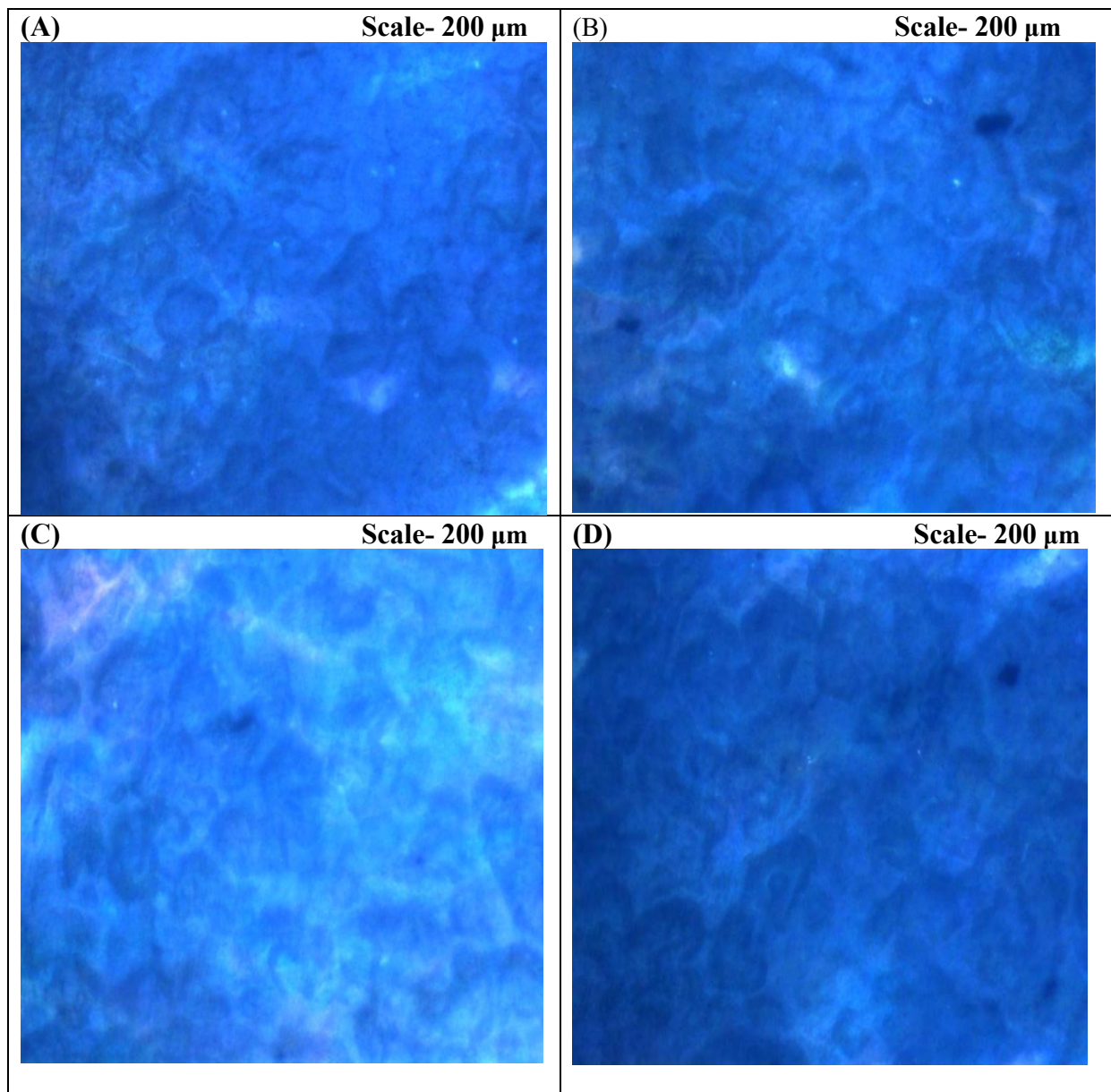


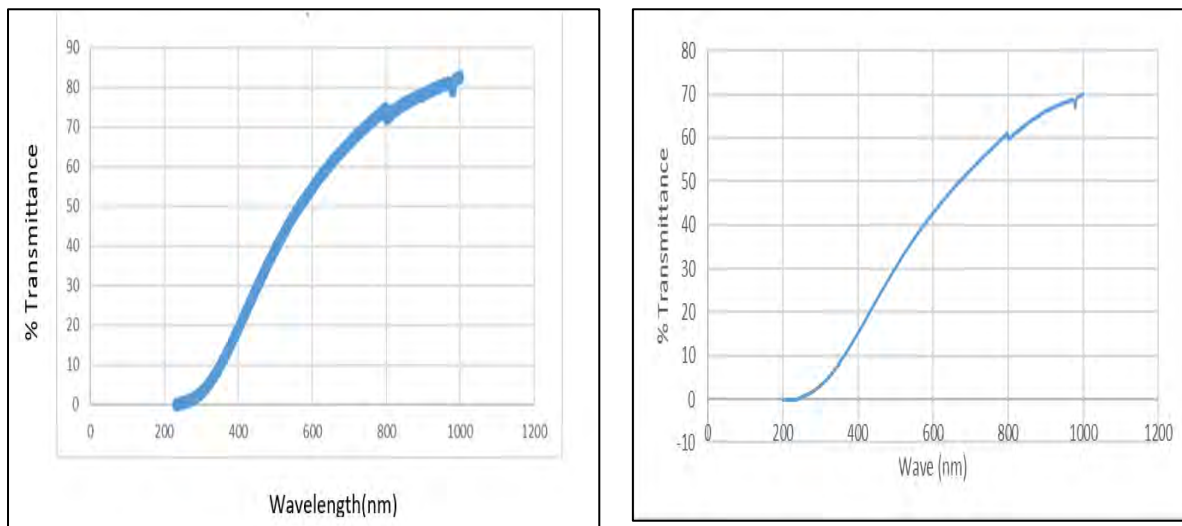
Figure-4.23: Optical micrograph of SPS sintered transparent HA pellets prepared at(A) 900⁰C, 3.9kN (B) 900⁰C, 3.4kN(C) 900⁰C, 4.7kN(D) 925⁰C, 4.7kN and sectioned parallel to SPS pressure.

4.4 Measurement of transmittance in UV visible spectrometer.

Transmittances of clear samples were measured in UV visible spectrometer. Samples that were converted to 1 mm in thickness showed transmittance more than 60% at 800 nm. Maximum transparency of clear samples was found 75% at wavelength 800nm. In all cases, transmittance increased with the increasing wavelength, it would be owing to the relative increase in wavelength with respect to the fixed grain and pore sizes. Transmission also increases due to decreasing light scattering according to the theory of Rayleigh scattering.

Results obtained from UV vis spectrometer for sintered transparent HA pellets prepared from both calcined and un-calcined powder are presented below-

Sintering Temperature-850°C:

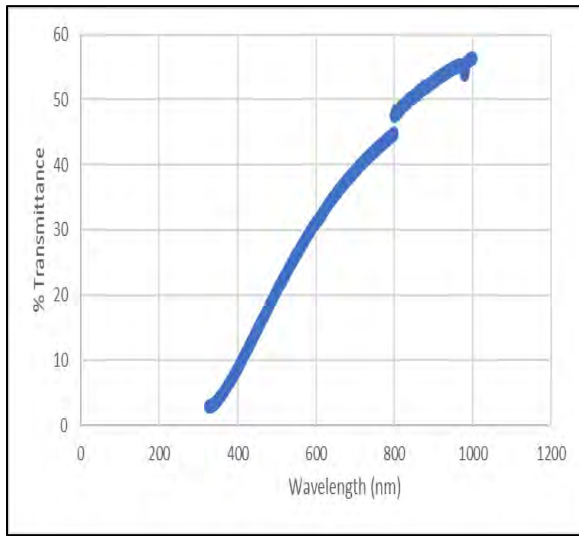


(a)

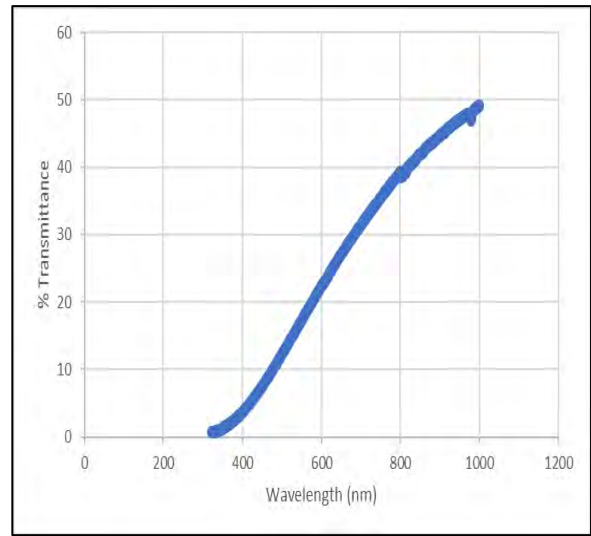
(b)

Figure-4.24: Transparent HA pellets from calcined powder (a) SPS pressure-3.9kN (b) SPS pressure 4.7kN, sintering temperature 850°C

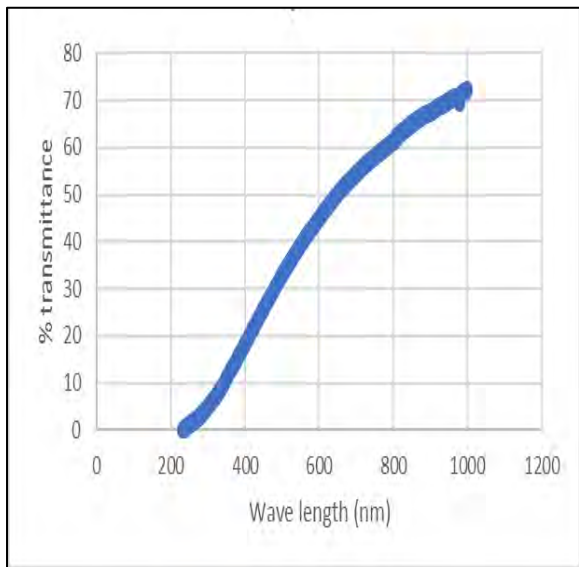
Sintering Temperature-875°C:



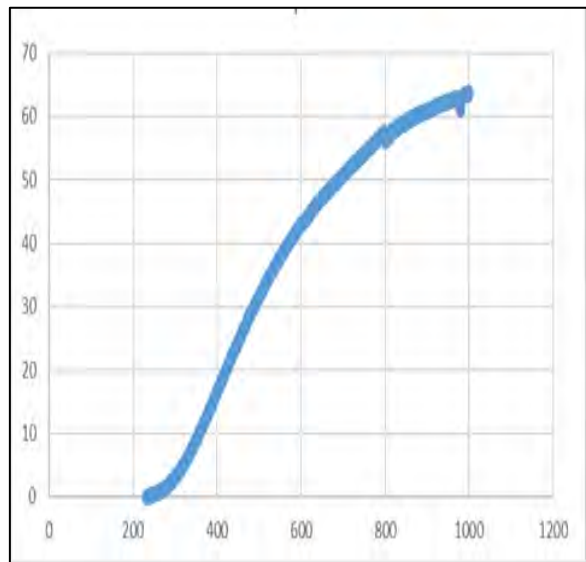
(a)



(b)



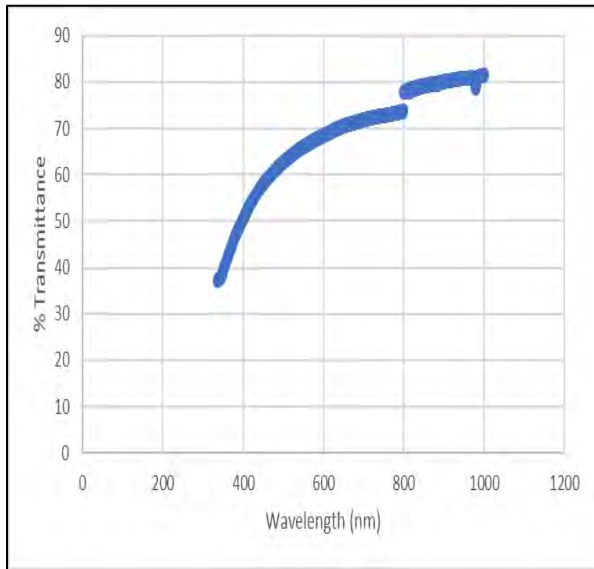
(c)



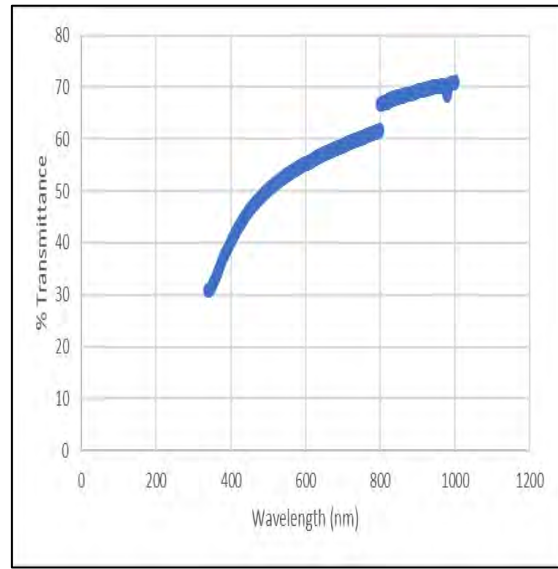
(d)

Figure-4.25: Transparent HA pellets from un-calcined powder (a) SPS pressure-3.9kN (b) SPS pressure-4.7kN, pellets from calcined powder (c) SPS pressure-3.9kN (d) SPS pressure-4.7kN, sintering temperature 875°C

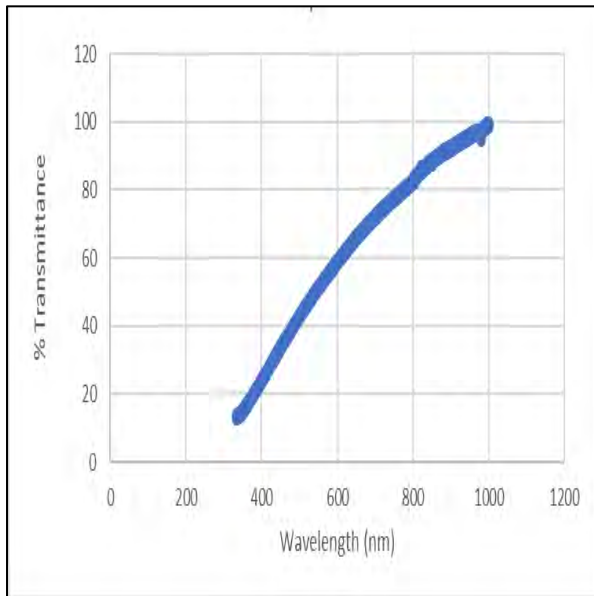
Sintering Temperature-900°C:



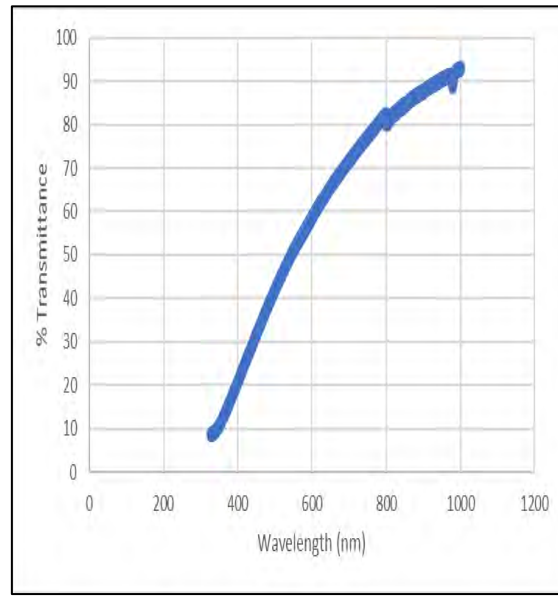
(a)



(b)



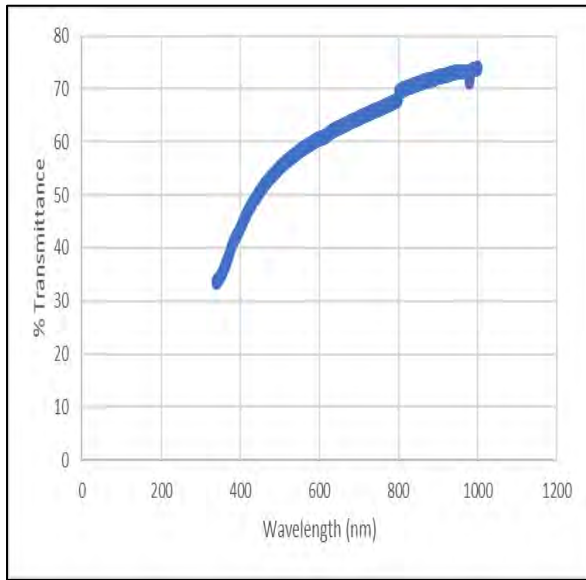
(c)



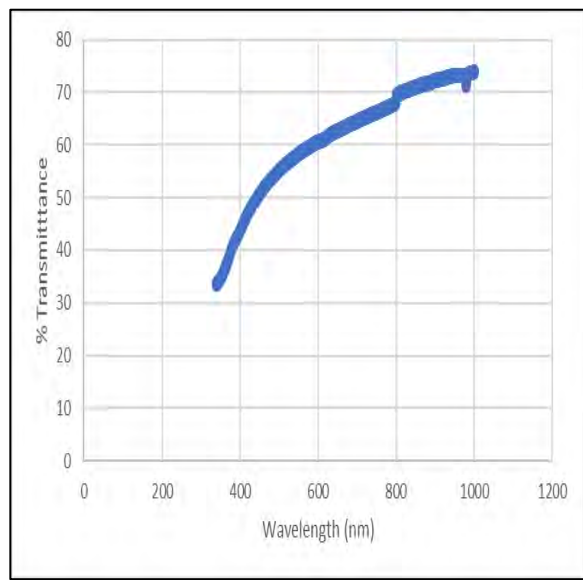
(d)

Figure-4.26: Transparent HA pellets from un-calcined powder (a) SPS pressure-3.9kN (b) SPS pressure-4.7kN, pellets from calcined powder (c) SPS pressure-3.9kN (d) SPS pressure-4.7kN, sintering temperature 900°C

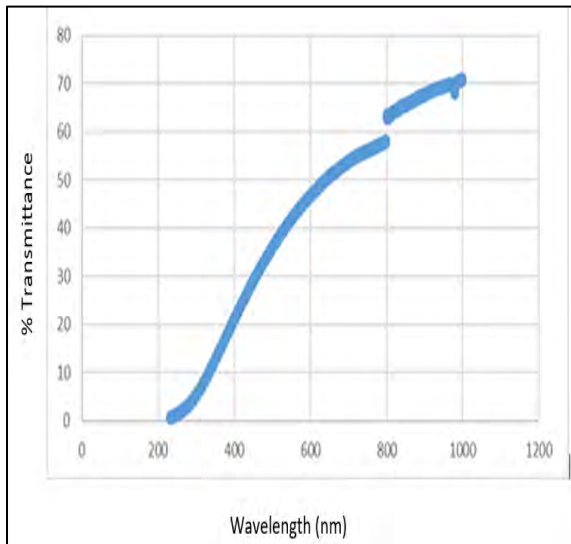
Sintering Temperature-925°C:



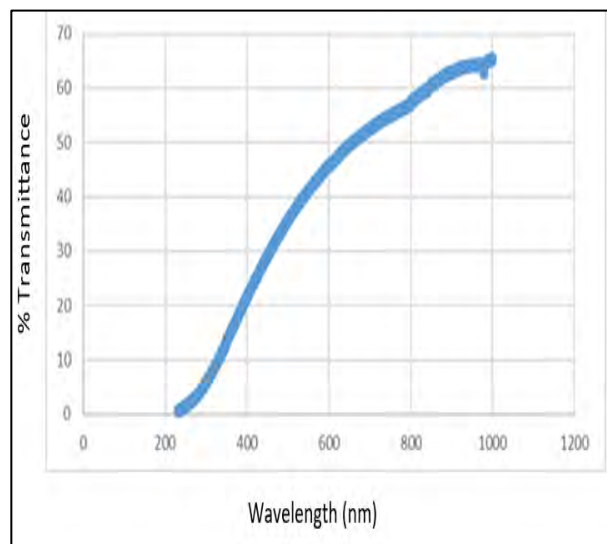
(a)



(b)



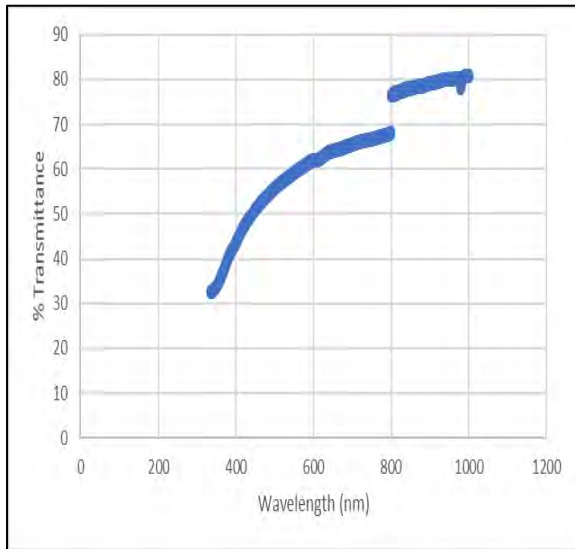
(c)



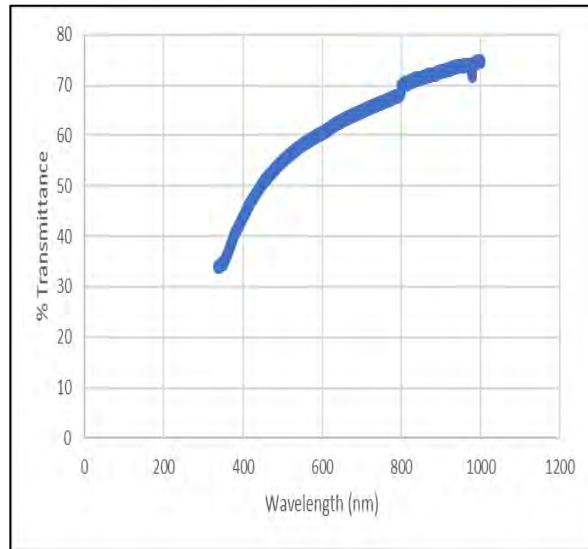
(d)

Figure-4.27: Transparent HA pellets from un-calcined powder (a) SPS pressure-3.9kN (b) SPS pressure-4.7kN, pellets from calcined powder (c) SPS pressure-3.9kN (d) SPS pressure-4.7kN, sintering temperature 925°C

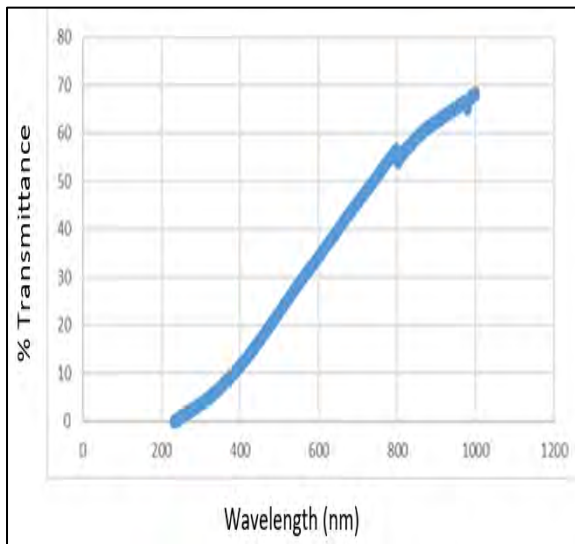
Sintering Temperature-950°C:



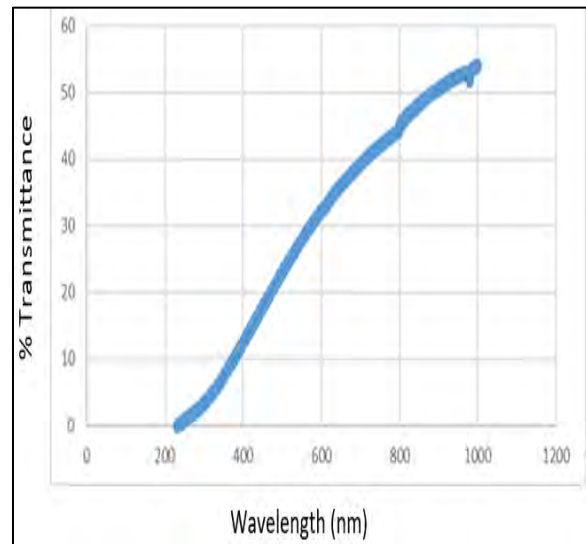
(a)



(b)



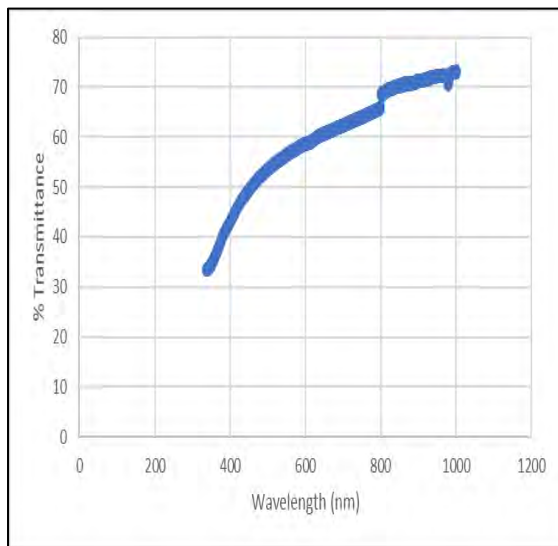
(c)



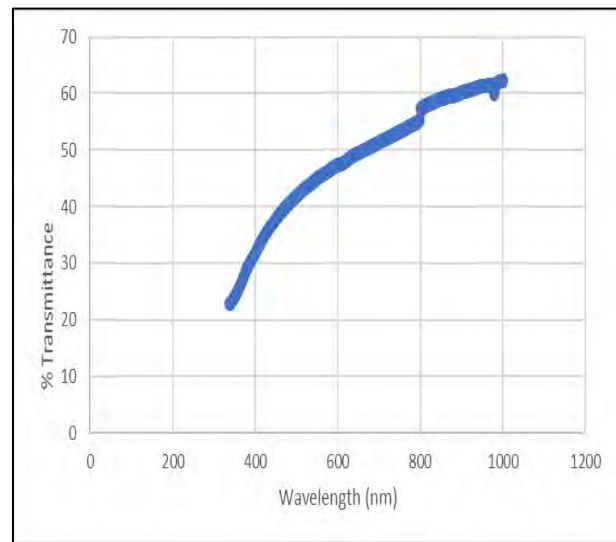
(d)

Figure-4.28: Transparent HA pellets from un-calcined powder (a) SPS pressure-3.9kN (b) SPS pressure-4.7kN, pellets from calcined powder (c) SPS pressure-3.9kN (d) SPS pressure-4.7kN, sintering temperature 950°C

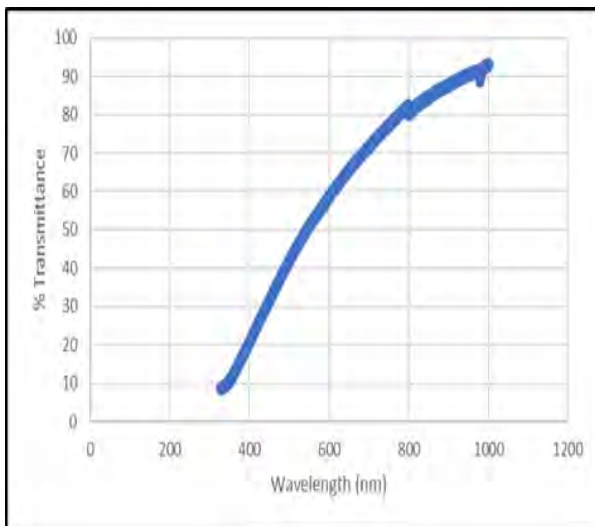
Sintering Temperature-975°C:



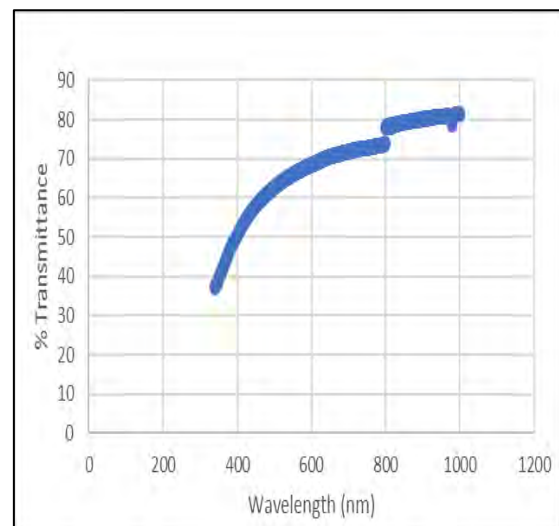
(a)



(b)



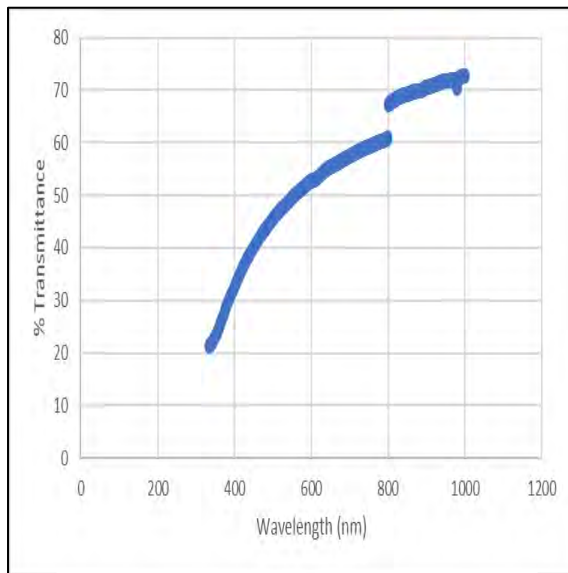
(c)



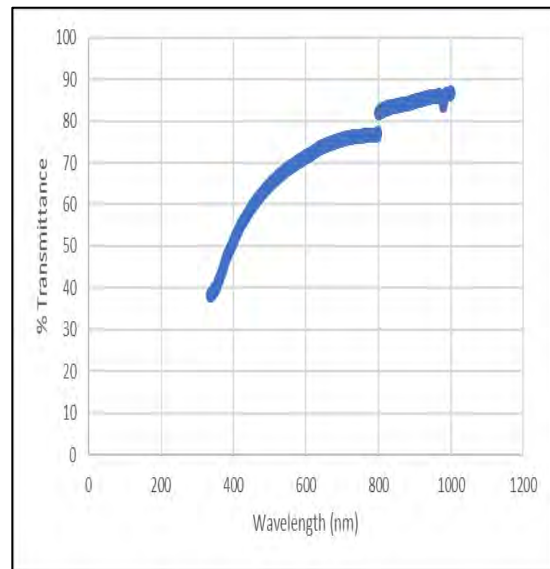
(d)

Figure-4.29: Transparent HA pellets from un-calcined powder (a) SPS pressure-3.9kN (b) SPS pressure-4.7kN, pellets from calcined powder (c) SPS pressure-3.9kN (d) SPS pressure-4.7kN, sintering temperature 975°C

Sintering Temperature-1000°C:



(a)



(b)

Figure-4.30: Transparent HA pellets from un-calcined powder (a) SPS pressure-3.9kN (b) SPS pressure-4.7kN, sintering temperature 975°C

4.5 Effects of sintering parameters on transmittance

4.5.1 Effect of sintering temperature on transmittance

Temperature has profound effect on transmittance of hydroxyapatite pellets. In the time of sintering, it was found that transparent hydroxyapatite samples started to produce at temperature 825°C and ended up 975°C for calcined HA powder. For un calcined powder, it was started at temperature 875°C and continued through 1000°C. Those sample were prepared at temperature 1000°C and at pressure 3.9kN, they were comparatively less transparent for calcined powder. Highly transparent samples were obtained at temperature 900°C, but after crossing the sintering temperature 900°C, transmittance got reduced and raised again when the sintering temperature was chosen 975°C as shown in figure-4.31.

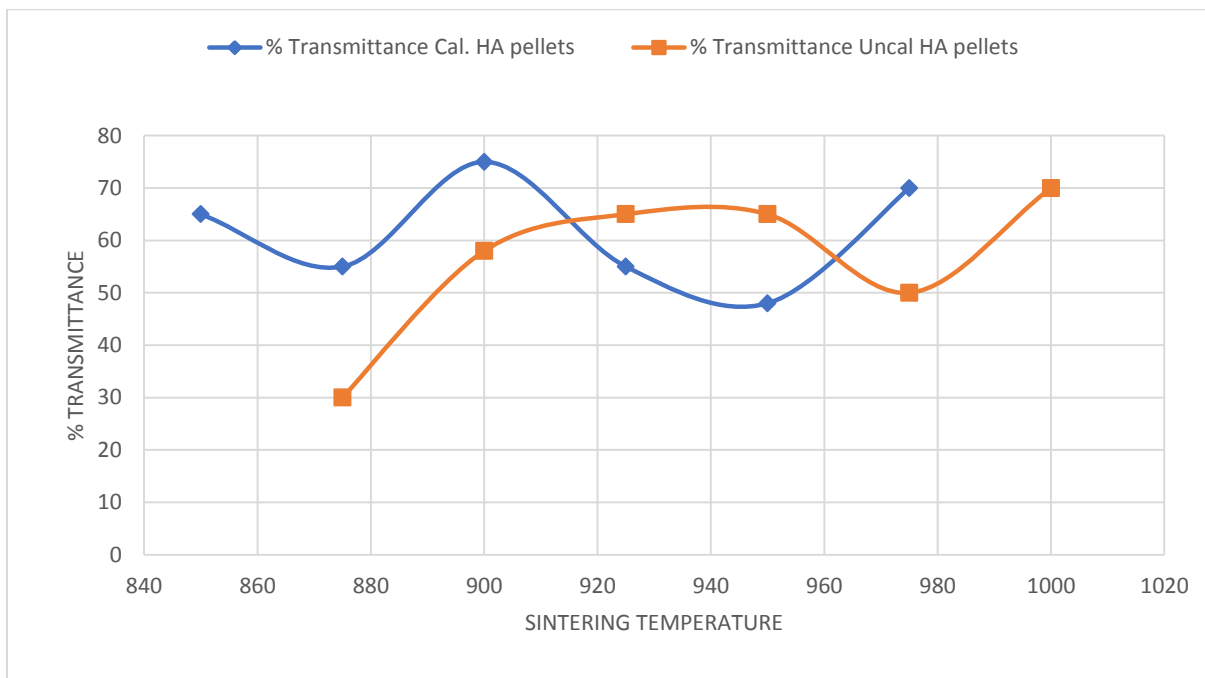


Figure- 4.31: Sintering Temperature Vs Transmittance

Temperature has an immense effect on the microstructures. It is studied from the principle of sintering that with the rising of temperature, the open porosity is replaced by the closed porosity which leads toward the reduction in the density of porosity of the sintered body. Temperature plays greater role than other parameters as it is directly linked with D.C current, pulse intensity and die size which facilitated the heat transport across the sample boundaries efficiently. A drastic change in microstructures occurs with increasing temperatures.

4.5.2 Effect of pressure on transmittance

To see the role of spark plasma sintering pressure on transmittance, HA samples that were prepared from calcined powder in different sintering pressure were considered. Figure -4.32 shows the effect of SPS pressure on transmittance of HA samples sintered at different pressure by SPS machine. It is observed from the figure that % transmittance of prepared HA samples is comparatively high at low sintering pressure 3.9kN and transmittance decreased gradually with increasing pressure from 4.3kN to 4.7kN in temperature range 850°C to 925°C. After crossing the sintering temperature 950°C, opposite effect was observed, transmittance increased with increasing sintering pressure in SPS machine.

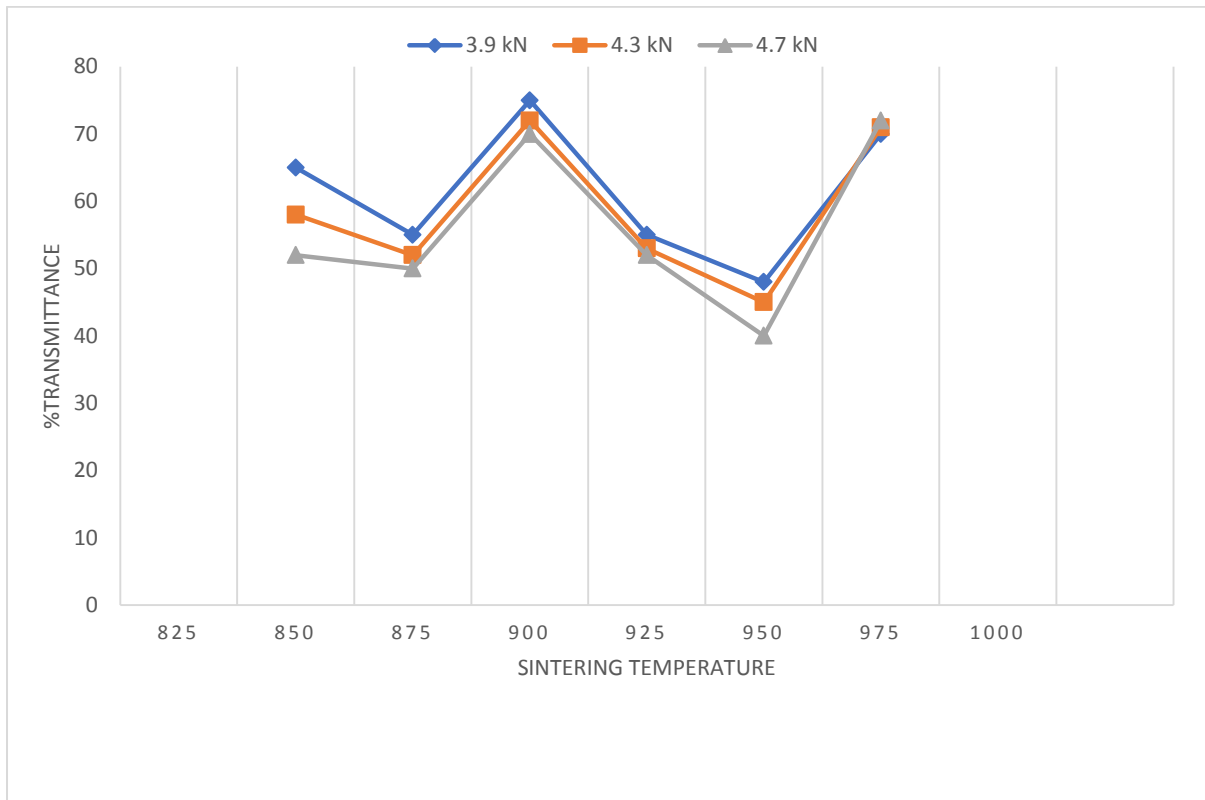


Figure-4.32: Transmittance of HA pellets prepared from calcined powder at different SPS pressures.

Optical transmittance of obtained samples was measured by UV- visible spectrometer in the wavelength range 200-800 nm and found that % transmittance of HA sample was around 75% when sintered at pressure 3.9kN. On the other hand, this transmittance was around 70% at sintering pressure 4.7kN; both these samples were sintered at sintering temperature 900°C.

4.5.3 Effect of hydroxyapatite powder on transmittance

Types of powder play an influential role on transmittance of spark plasma sintered hydroxyapatite sample. Figure-4.31 shows %transmittance of sparked plasma sintered Hydroxyapatite pellets at different sintering temperature synthesized from both calcined and un-calcined powder. It shows that pellets prepared from calcined powder having higher transmittance at sintering temperature 900°C and 975°C comparing HA pellets sintered from un-calcined powder.

4.5.4 Effect of sintering time on transmittance

Sintering time also plays a dominating role to make hydroxyapatite pellets transparent. In the time of sintering, powder was hold in the corresponding sintering temperature for 3 min after crossing temperature 825°C. It would be assumed that from the figure-4.33, extended time after crossing the temperature 825°C allows HA atoms to get rearranged and reshaped in their position which is probably influences on the changes of transmittance.

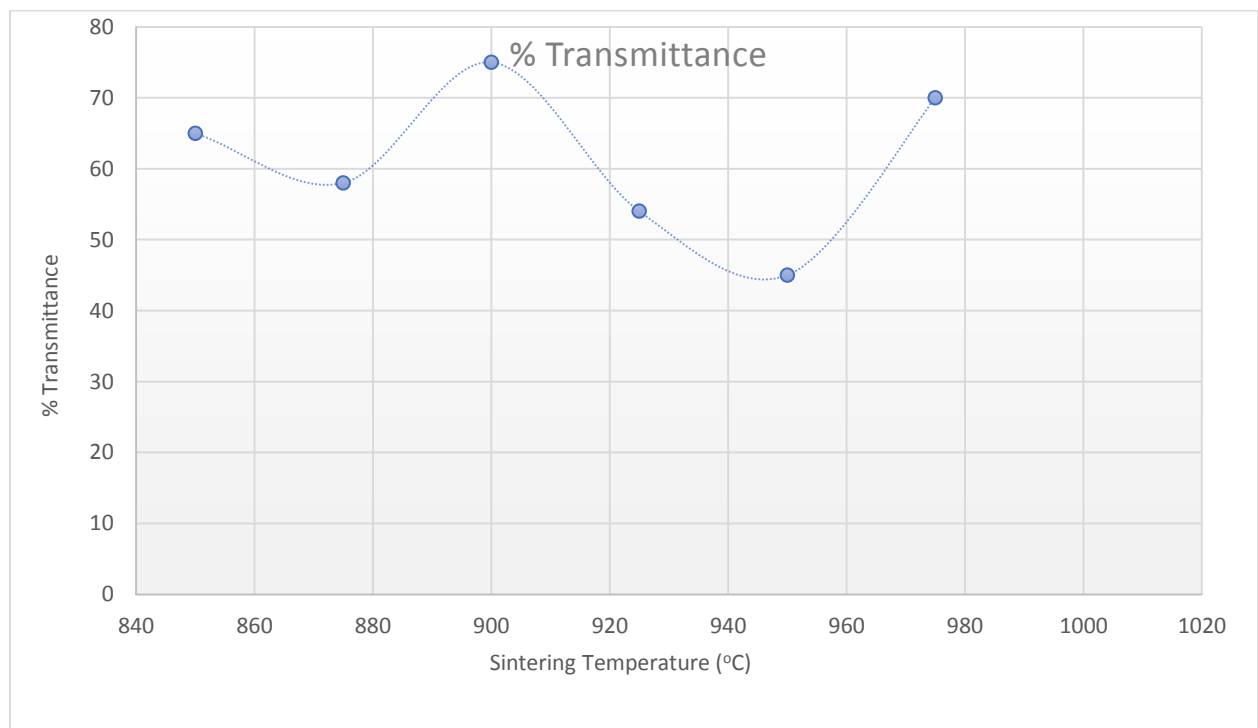


Figure-4.33: Changes of transmittance

4.6 Piezoelectric responses

Contact Electrical poling experiment was carried out on those transparent samples that were prepared by using calcined powder and sintering pressure 3.9kN. Longitudinal piezoelectric constant (D_{33}) of sintered hydroxyapatite pellets were measured after sintering or before applying them in contact electrical poling devices. But did not show any appreciable piezoelectric response in piezometer along parallel or perpendicular direction of applied pressure, as shown in the table-4.8, below-

Table-4.8: Longitudinal piezoelectric constant (D_{33}) before poling.

Sample Profile- Sintering Temperature (ST) Sintering Pressure (SP)	D_{33} values along the parallel direction of SPS pressure	D_{33} values along perpendicular direction of SPS pressure
ST-850°C, SP-3.9kN	0.01	0.01
ST-875°C, SP-3.9kN	0.01	0.02
ST-900°C, SP-3.9kN	0.02	0.00
ST-925°C, SP-3.9kN	0.02	0.01
ST-950°C, SP-3.9kN	0.01	0.00
ST-975°C, SP-3.9kN	0.02	0.01
ST-1000°C, SP-3.9kN	0.00	0.00

After electrical poling (Applied Voltage: 2V, Applied Current: 0.003mA, Temperature: 95-105°C, Time: 1.5hr) few pellets showed piezoelectric values which were sintered at certain specific temperatures and fixed direction as shown in table-4.9.

Table-4.9: Piezoelectric responses of transparent HA pellets (prepared at different sintering temperature) measured by its D_{33} values, under same applied poling condition.

Sample Profile- Sintering Temperature (ST) Sintering Pressure (SP)	D_{33} values along the parallel direction of SPS pressure		D_{33} values along perpendicular direction of SPS pressure	
	Before poling	After poling	Before poling	After poling
ST-850°C, SP-3.9kN	0.01	0.02	0.01	0.09
ST-875°C, SP-3.9kN	0.01	0.85	0.02	0.15
ST-900°C, SP-3.9kN	0.02	0.04	0.00	0.03
ST-925°C, SP-3.9kN	0.02	0.02	0.01	0.03
ST-950°C, SP-3.9kN	0.01	0.04	0.00	0.04
ST-975°C, SP-3.9kN	0.02	0.12	0.01	0.52
ST-1000°C, SP-3.9kN	0.00		0.00	

Obtained D_{33} constants for different samples prepared at different temperature were found to be different. Polarizability of samples were also varied with respect to poling direction. Samples that were sintered at temperature 875°C and pressure 3.9kN found to show noticeable piezoelectric constant (D_{33}) around 0.85, when polled in the parallel direction of SPS pressure. Those samples were prepared at same sintering condition but polled in perpendicular direction didn't show any piezoelectricity in piezometer. On the other hand, samples that were sintered at 975°C showed higher piezoelectric value after poling in the perpendicular direction of SPS pressure and found to exist after 24 hours. Samples sintered at 875°C showed piezoelectricity when polled along parallel direction of SPS pressure but

didn't last after 24 hours. Samples prepared at 900°C didn't any response in contact electrical poling in perpendicular or parallel direction of SPS pressure.

Piezoelectric responses also depend on applied voltage and poling temperature. D_{33} value increased with increasing voltage as shown in the figure-4.34, here, contact electrical poling was carried out at temperature 105°C for 2 hours for two type of samples.

Sample-A: Sintering Temp- 975 °C, SPS pressure-3.9kN: Longitudinal Piezoelectric constant D_{33} Vs Applied Voltage Graph.

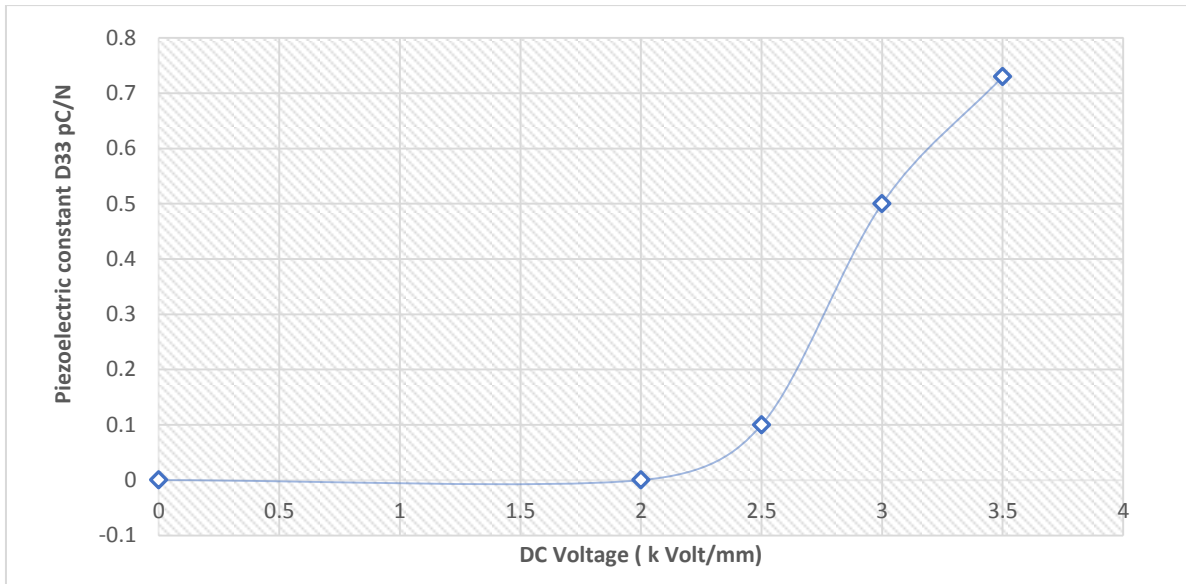


Figure-4.34: Contract Electrical Poling along SPS Pressure Direction

Sample-B: Sintering Temp- 900 °C, SPS pressure-3.9kN: Longitudinal Piezoelectric constant D_{33} Vs Applied Voltage Graph.

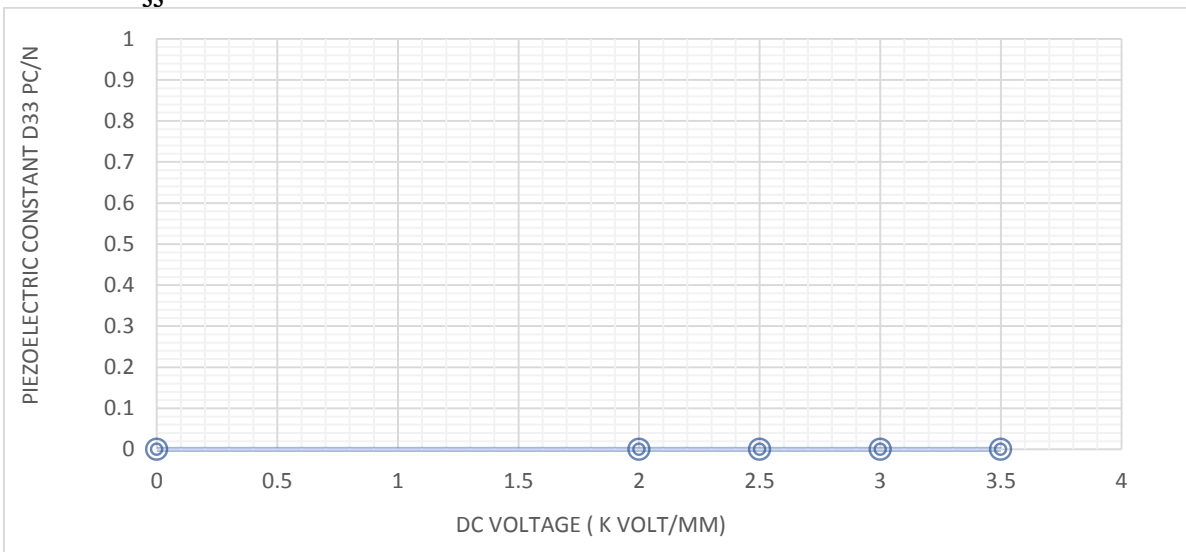


Figure-4.35: Contract Electrical Poling perpendicular to SPS Pressure Direction.

Ceramics consist of grains and grain boundaries. If there are differences in properties (e.g. compositions) between grains and grain boundaries, the interfaces between them will become scattering sites of light. To be transparent, the difference in optical behaviors between grains and grain boundaries should be minimized. Transparent HA ceramics showed less clear grain boundaries than opaque HA ceramics. The presence of a second phase at the grain boundaries in general is the most common reason for opacity. XRD peaks confirmed the absence of second phase Tri-calcium phosphate (TCP) or any other high temperature decomposition related phases in transparent HA ceramics.

Therefore, to fabricate transparent HA ceramics, it is necessary to use raw material of high purity and elongated high temperature of sintering.

Optical transparency of HA is also influenced by texture and densification. The highest transmittance in HA is a combined effect of densification and texture through an in-plane *c*-axis orientation. The sintering parameters (e.g., temperature, time, and pressure) at which this occurs is critical as an increase/decrease in these parameters may in turn affect the texture and/or densification, with the result that transmittance changes. The overall trend in the optical transmittance behavior is dominated by texture, especially when the effect of densification saturates. Thus, careful control of densification and texture, one can tune optical transparency in HA.

Crystal structure plays an important role in determining whether a ceramic can be optically transparent or not. In ceramics of optically anisotropic crystals, an additional scattering of light arises at the boundaries when the light travels from one grain to another. This is the reason why transparent ceramics generally have a cubic lattice structure, which is isotropic, such as MgO, Y₂O₃, YAG, and MgAl₂O₃(spinel), but in the case of HA the reason behind the transparency is different because it has non-cubic crystal symmetry.

Besides those internal factors, there are also external factors that affect the transparency of a ceramic sample, including thickness and surface finish. A rough surface means a significant diffuse scattering, so the sample surface should be as smooth as possible. Generally, transparency decreases with increasing thickness, but it was noticed that produced transparent HA ceramic in this research didn't lose its high transmittance when its thickness was reduced to 1mm or 0.5mm.

Thickness independent transparency is only possible when the material reaches its theoretical maximum of in-line transmission.

In contrast, SPS produced highly transparent HA ceramics optimizing sintering parameter and using highly pure HA powder which reduced all the possible scattering sites of light, attained high density, reduced pores at grain boundaries or made pores with much smaller size than the wavelength of light. Short sintering time suppressed the production of second phase avoiding thermal decomposition. This entire phenomenon jointly contributed to produce transparent hydroxyapatite ceramic.

On basis of XRD results, it is observed that orientation indexes of 002 and 004 diffractions corresponding to the *c* plane were much intense than those of the other planes. At perpendicular section of prepared pellets, the orientation indexes of 100, 200, 210, 300, and 310 diffractions corresponding to the *a* and *b* planes were much intense than those of other planes. These phenomena are indicating that *c* plane of HA unit cell expands along the

parallel direction of applied SPS pressure following the assumed structural changes shown in figure-4.36.

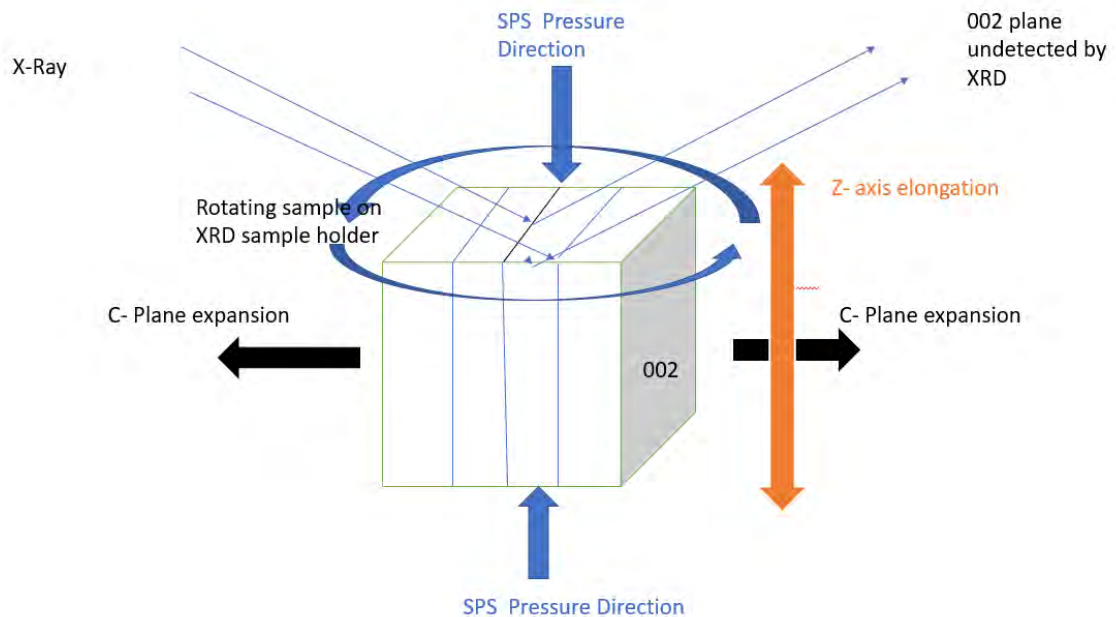


Figure- 4.36: Microstructural changes in sintered sample.

This proposition is also proposing that high voltage contact electrical poling along the parallel direction of SPS pressure applied during sintering would be more favourable to have piezoelectricity in produced transparent hydroxyapatite samples so as to expedite its application as an implant and in implantable biomedical devices.

Transparent HA pellets prepared at different sintering temperatures showed peculiar piezoelectric responses after high voltage contact electrical poling along parallel and perpendicular directions of SPS pressure. It would happen due to sintering temperature and relative structural changes that occurred in the microstructure of sintered pellets. In the previous experiment it was also observed that the transmittance property of HA pellets goes up and down throughout the whole range of sintering temperature fixed for SPS machine.

In the microstructure of hydroxyapatite, hydroxyl ion arrangement in monoclinic structure of hydroxyapatite having space group $p2_1/b$ may render the crystal structure antiferroelectric as each calcium triangle along with the adjacent hydroxyl ions create a local dipole within the crystal lattice with the hydroxyl ion sitting above the calcium triangle at $z = 0.44$ and 0.94 .

In each specific ion channel, all dipoles are oriented in the same direction and these channel orientations alternate along the crystallographic b direction rendering the entire unit cell antiferroelectric. As antiferroelectricity is a physical property closely related with ferroelectricity. It has ordered crystal dipoles, but adjacent dipoles are oriented in opposite directions, that is why antiferroelectricity can appear and disappear depending on temperature, pressure, growth method, external electric field. When temperature is raised to the Curie point,

antiferroelectricity get totally disappeared. Antiferroelectric property is more steady than ferroelectric property. Entire macroscopic spontaneous polarization in antiferroelectric material is zero due to closest opposite dipole, they cancel each other. The antiferroelectric property is not piezoelectric, that means there is no change in mechanical character of the material by the application of external field.

Therefore, by considering all the experimental work, this research work is also assuming that transparent hydroxyapatite possessed both antiferroelectric and ferroelectric properties by its microstructural changes influenced by sintering temperature, pressure and applied time for sintering.

Chapter-5

Conclusion

This thesis work can be divided into two steps:

- Synthesis and characterization of transparent hydroxyapatite ceramic.
- Evaluation of piezoelectric responses of prepared HA samples applying high voltage in contact electrical poling device.

Synthesis and characterization of transparent hydroxyapatite ceramic

When HA powder, both calcined and uncalcined were sintered in fully computerized and current assisted SPS machine at temperature range 825°C to 1000°C and pressure range 3.9kN to 4.7kN keeping the holding time 3 min at selected sintering temperature then following observations were recorded-

- Transparent HA samples were found to obtain at prolonged temperature ranges 850°C to 975°C for calcined HA powder and 875°C to 1000°C for un-calcined HA powder respectively.
- Hydroxyapatite samples that were prepared from calcined powder showed maximum transmittance nearly 75% at sintering temperature 900°C. For un-calcined powder, maximum transmittance was found to be around 70% at sintering temperature 900°C following same sintering condition.
- This transparent HA sintered body showed high crystal orientation while examined by XRD. The orientation indexes of the planes parallel and perpendicular to the pressure direction were investigated. The *c*- plane and *a*- , *b*- plane of the sintered body were aligned perpendicular and parallel to the pressure direction respectively. The direct observations using microscopic images were also coincident to the XRD result.
- Influences of different sintering parameters (temperature, time, and pressure) over transmittance were evaluated. It is observed from result that transmittance varied with sintering temperature but lower sintering pressure 3.9kN was more favorable for producing higher transparent HA ceramic samples.
- A combination of texturing and optical micrograph confirms the possibility of enhancing the magnitude of piezoelectric values in transparent hydroxyapatite ceramics.

Piezoelectric responses of HA samples under high voltage contact electrical poling device

Longitudinal piezoelectric constant (D_{33}) of sintered hydroxyapatite pellets were checked out just after sintering or before applying them in contact electrical poling devices, then these samples were applied in high voltage contact electrical poling device, where recorded observations are-

- Before poling, prepared HA sample from SPS machine didn't show any piezoelectricity.
- Samples sintered at temperature 975°C showed piezoelectricity where longitudinal piezoelectric constant (D_{33}) was found to be around 0.52pC at applied Voltage: 2V , Applied Current: 0.003mA , Temperature: $95\text{-}105^{\circ}\text{C}$, Time: 1.5hr , in the perpendicular direction of SPS pressure and found to exist after 24 hours.
- Samples sintered at 875°C showed longitudinal piezoelectric constant (D_{33}) around 0.8pC when polled along parallel direction of applied SPS pressure but didn't last after 24 hours.
- Samples prepared at 900°C didn't show any response in contact electrical poling in perpendicular or parallel direction of applied SPS pressure.

Recommended Future Work

This work studied about the optimum conditions for producing transparent hydroxyapatite ceramic by SPS machine and piezoelectric responses of produced transparent HA ceramic under high voltage contact electrical poling device. Here, sintering temperature range was chosen up to 1000°C. Based on the present work, some future work would also be considered-

1. Possibility of producing transparent hydroxyapatite should also be checked out at temperatures more than 1000°C and pressure less than 3.9kN. Because, it was observed that lower SPS pressure was better for introducing higher transmittance in sintered HA ceramic.
2. Secondly, some peculiar behaviors of transparent samples were observed after sintering and applying them in high voltage contact electrical poling device and that's why suspecting its structural changes from antiferroelectric to ferroelectric nature depending on the corresponding sintering temperature, pressure and time.
3. Thirdly, it was noticed that piezoelectric property was introduced in few of these transparent samples, but they didn't last for long time. So, it is needed to find out a method that will ensure permanent piezoelectricity in these sample to expedite it's uses for biomedical purposes.

References

1. Mostafa, N.Y., 2005. Characterization, thermal stability and sintering of hydroxyapatite powders prepared by different routes. *Materials chemistry and physics*, 94(2-3), pp.333-341.
2. Paul, W. and Sharma, C.P., 1999. Development of porous spherical hydroxyapatite granules: application towards protein delivery. *Journal of Materials Science: Materials in Medicine*, 10(7), pp.383-388
3. Woodard, J.R., Hildore, A.J., Lan, S.K., Park, C.J., Morgan, A.W., Eurell, J.A.C., Clark, S.G., Wheeler, M.B., Jamison, R.D. and Johnson, A.J.W., 2007. The mechanical properties and osteoconductivity of hydroxyapatite bone scaffolds with multi-scale porosity. *Biomaterials*, 28(1), pp.45-54.
4. Oliveira, S.M., Barrias, C.C., Almeida, I.F., Costa, P.C., Ferreira, M.R.P., Bahia, M.F. and Barbosa, M.A., 2008. Injectability of a bone filler system based on hydroxyapatite microspheres and a vehicle with in situ gel- forming ability. *Journal of Biomedical Materials Research Part B: Applied Biomaterials: An Official Journal of The Society for Biomaterials, The Japanese Society for Biomaterials, and The Australian Society for Biomaterials and the Korean Society for Biomaterials*, 87(1), pp.49-58
5. Wang, Ai- Juan, Yu- Peng Lu, Rui- Fu Zhu, Shi- Tong Li, Gui- Yong Xiao, Guang- Feng Zhao, and Wen- Hua Xu. "Effect of sintering on porosity, phase, and surface morphology of spray dried hydroxyapatite microspheres." *Journal of Biomedical Materials Research Part A: An Official Journal of The Society for Biomaterials, The Japanese Society for Biomaterials, and The Australian Society*
6. Gandhi, A.A., Wojtas, M., Lang, S., Kholkin, A.L. and Tofail, S.A., 2014. Piezoelectricity in poled hydroxyapatite ceramics. *Journal of the American Ceramic Society*, 97(9), pp.2867-2872
7. Gandhi, A.A., Gunning, R.D., Ryan, K.M. and Tofail, S.A., 2010. The role of texturing and densification on optical transmittance of hydroxyapatite ceramics. *Journal of the American Ceramic Society*, 93(11), pp.3773-3777
8. Baxter, F.R., Bowen, C.R., Turner, I.G. and Dent, A.C., 2010. Electrically active bioceramics: a review of interfacial responses. *Annals of biomedical engineering*, 38(6), pp.2079-2092.
9. Fukada, E. and Yasuda, I., 1957. On the piezoelectric effect of bone. *Journal of the physical society of Japan*, 12(10), pp.1158-1162
10. Anderson, J.C. and Eriksson, C., 1970. Piezoelectric properties of dry and wet bone. *Nature*, 227(5257), p.491
11. Lang, S.B., Tofail, S.A.M., Kholkin, A.L., Wojtaś, M., Gregor, M., Gandhi, A.A., Wang, Y., Bauer, S., Krause, M. and Plecenik, A., 2013. Ferroelectric polarization in nanocrystalline hydroxyapatite thin films on silicon. *Scientific reports*, 3, p.2215
12. Lang, S.B., Tofail, S.A.M., Gandhi, A.A., Gregor, M., Wolf-Brandstetter, C., Kost, J., Bauer, S. and Krause, M., 2011. Pyroelectric, piezoelectric, and photoeffects in hydroxyapatite thin films on silicon. *Applied Physics Letters*, 98(12), p.123703
13. Chaim, R., Marder-Jaeckel, R. and Shen, J.Z., 2006. Transparent YAG ceramics by surface softening of nanoparticles in spark plasma sintering. *Materials Science and Engineering: A*, 429(1-2), pp.74-78. Messing, G.L. and Stevenson, A.J., 2008. Toward pore-free ceramics. *Science*, 322(5900), pp.383-395.

14. Messing, G.L. and Stevenson, A.J., 2008. Toward pore-free ceramics. *Science*, 322(5900), pp.383-384.
15. M. Tofail, S.A., Haverty, D., Stanton, K.T. and McMonagle, J.B., 2005. Structural order and dielectric behaviour of hydroxyapatite. *Ferroelectrics*, 319(1), pp.117-123.
16. Elliott, J.C. and Young, R.A., 1968, January. Dielectric measurements on single crystals of synthetic chlorapatite. In *BULLETIN DE LA SOCIETE CHIMIQUE DE FRANCE* (p. 1763). 23 RUE LINOIS, 75724 PARIS CEDEX 15, FRANCE: EDITIONS SCIENTIFIQUES MEDICALES ELSEVIER
17. Wang, S.F., Zhang, J., Luo, D.W., Gu, F., Tang, D.Y., Dong, Z.L., Tan, G.E., Que, W.X., Zhang, T.S., Li, S. and Kong, L.B., 2013. Transparent ceramics: Processing, materials and applications. *Progress in Solid State Chemistry*, 41(1-2), pp.20-54.
18. Anderson, J.C. and Eriksson, C., 1970. Piezoelectric properties of dry and wet bone. *Nature*, 227(5257), p.491
19. Elliott, J.C., 2013. *Structure and chemistry of the apatites and other calcium orthophosphates* (Vol. 18). Elsevier.
20. Martin, R.B., Burr, D.B. and Sharkey, N.A., 1998. *Skeletal tissue mechanics* (Vol. 190). New York: Springer
21. De Jong, W.F., 1926. La substance minerale dans les os. *Recueil des Travaux Chimiques des Pays- Bas*, 45(6), pp.445-448.
22. Neuman, W.F. and Neuman, M.W., 1958. The chemical dynamics of bone mineral. *The chemical dynamics of bone mineral*.
23. Legros, R., Balmain, N. and Bonel, G., 1987. Age-related changes in mineral of rat and bovine cortical bone. *Calcified tissue international*, 41(3), pp.137-144.
24. Labarthe, J.C., Bonel, G. and Montel, G., 1973, January. Structure and properties of B-type phosphocalcium carbonated apatites. In *Annales De Chimie France* (Vol. 8, No. 5, pp. 289-301).
25. Nasiri-Tabrizi, B., Fahami, A. and Ebrahimi-Kahrizangi, R., 2013. Effect of milling parameters on the formation of nanocrystalline hydroxyapatite using different raw materials. *Ceramics International*, 39(5), pp.5751-5763
26. Elliot, J.C., 1994. Structure and chemistry of the apatites and other calcium orthophosphates. *Studies in inorganic chemistry 18*
27. Martz, E.O., Goel, V.K., Pope, M.H. and Park, J.B., 1997. Materials and design of spinal implants—a review. *Journal of Biomedical Materials Research*, 38(3), pp.267-288.
28. Rao, R.R., Roopa, H.N. and Kannan, T.S., 1997. Solid state synthesis and thermal stability of HAP and HAP- β -TCP composite ceramic powders. *Journal of Materials Science: Materials in Medicine*, 8(8), pp.511-518
29. Tas, A.C., Korkusuz, F., Timucin, M. and Akkas, N., 1997. An investigation of the chemical synthesis and high-temperature sintering behaviour of calcium hydroxyapatite (HA) and tricalcium phosphate (TCP) bioceramics. *Journal of Materials Science: Materials in Medicine*, 8(2), pp.91-96
30. Dorozhkin, S.V., 2010. Calcium orthophosphates as bioceramics: state of the art. *Journal of functional biomaterials*, 1(1), pp.22-107.
31. Junqueira, L.C. and Carneiro, J., 2005. *Basic Histology Text & Atlas*, McGra-Hill Medical; ISBN 978-0071440912. USA, 502p.

32. Hui, P., Meena, S.L., Singh, G., Agarawal, R.D. and Prakash, S., 2010. Synthesis of hydroxyapatite bio-ceramic powder by hydrothermal method. *Journal of Minerals & Materials Characterization & Engineering*, 9(8), pp.683-692.
33. Haverty, D., Tofail, S.A., Stanton, K.T. and McMonagle, J.B., 2005. Structure and stability of hydroxyapatite: density functional calculation and Rietveld analysis. *Physical Review B*, 71(9), p.094103.
34. Greenblatt, M., Pifer, J.H. and Banks, E., 1977. Electron spin resonance of CrO₄³⁻ in fluoroapatite Ca₅(PO₄)₃F. *The Journal of Chemical Physics*, 66(2), pp.559-562.
35. Mackie, P.E., 1980. *Location and structural role of water in tooth enamel*. Georgia Institute of Technology.
36. Fleet, M.E. and Pan, Y., 1994. Site preference of Nd in fluorapatite [Ca₁₀(PO₄)₆F₂]. *Journal of Solid State Chemistry*, 112(1), pp.78-81.
37. Wei, G. and Ma, P.X., 2004. Structure and properties of nano-hydroxyapatite/polymer composite scaffolds for bone tissue engineering. *Biomaterials*, 25(19), pp.4749-4757.
38. Kalita, S.J., Bhardwaj, A. and Bhatt, H.A., 2007. Nanocrystalline calcium phosphate ceramics in biomedical engineering. *Materials Science and Engineering: C*, 27(3), pp.441-449.
39. Nasiri-Tabrizi, B., Fahami, A. and Ebrahimi-Kahrizsangi, R., 2013. Effect of milling parameters on the formation of nanocrystalline hydroxyapatite using different raw materials. *Ceramics International*, 39(5), pp.5751-5763
40. Gandhi, A.A., Wojtas, M., Lang, S., Kholkin, A.L. and Tofail, S.A., 2014. Piezoelectricity in poled hydroxyapatite ceramics. *Journal of the American Ceramic Society*, 97(9), pp.2867-2872
41. Gandhi, A.A., Gunning, R.D., Ryan, K.M. and Tofail, S.A., 2010. The role of texturing and densification on optical transmittance of hydroxyapatite ceramics. *Journal of the American Ceramic Society*, 93(11), pp.3773-3777
42. Bone, S. and Pethig, R., 1985. Dielectric studies of protein hydration and hydration-induced flexibility. *Journal of molecular biology*, 181(2), pp.323-326
43. Boyan, B.D., McMillan, J., Lohmann, C.H., Ranly, D.M. and Schwartz, Z., 2003. Bone graft substitutes: basic information for successful clinical use with special focus on synthetic graft substitutes. *Bone Graft Substitutes*, pp.231-259
44. German, R.M., 1996. Sintering theory and practice. *Solar-Terrestrial Physics*, p.568
45. Kelly, J.P. and Graeve, O.A., 2015. Spark plasma sintering as an approach to manufacture bulk materials: feasibility and cost savings. *JOM*, 67(1), pp.29-33
46. Ioku, K., Kawagoe, D., Toya, H., Fujimori, H., Goto, S., Ishida, K., Mikuni, A. and Mae, H., 2002. OH-designed transparent apatite ceramics prepared by spark plasma sintering. *TRANSACTIONS-MATERIALS RESEARCH SOCIETY OF JAPAN*, 27(2), pp.447-450
47. Fang, Y., Agrawal, D.K., Roy, D.M. and Roy, R., 1995. Fabrication of transparent hydroxyapatite ceramics by ambient-pressure sintering. *Materials Letters*, 23(1-3), pp.147-151.
48. Pawlikowski, M., 2017. Electric phenomenon in bones as a result of piezoelectricity of hydroxyapatite. *Arch Clin Biomed Res*, 1, pp.132-139.
49. Jacobson-Kram, D., Tepper, J., Kuo, P., San, R.H., Curry, P.T., Wagner, V.O. and Putman, D.L., 1997. Evaluation of potential genotoxicity of pulsed electric and electromagnetic fields used for bone growth stimulation. *Mutation Research/Genetic Toxicology and Environmental Mutagenesis*, 388(1), pp.45-57.

50. Pawlikowski, M., 2014. Osteoporosis as a source of tissue mineralization research on osteoporosis therapy and dissolution of arterial mineralization. *Journal of Life Sciences*, 8(7).
51. Wilson, E.R.M. and Dowker, S.E.P., 2002. Apatite structure. *Advances in X-ray Analysis*, 45, pp.172-181.
52. Boyde, A., Wolfe, L.A., Maly, M. and Jones, S.J., 1995. Vital confocal microscopy in bone. *Scanning*, 17(2), pp.72-85.
53. Kotobuki, N., Ioku, K., Kawagoe, D., Fujimori, H., Goto, S. and Ohgushi, H., 2005. Observation of osteogenic differentiation cascade of living mesenchymal stem cells on transparent hydroxyapatite ceramics. *Biomaterials*, 26(7), pp.779-785.
54. Fox, M., 2002. Optical properties of solids
55. Patel, P.J., Gilde, G.A., Dehmer, P.G. and McCauley, J.W., 2000, October. Transparent ceramics for armor and EM window applications. In *Inorganic Optical Materials II* (Vol. 4102, pp. 1-15). International Society for Optics and Photonics.
56. Bohren, C.F. and Huffman, D.R., 1983. Absorption and scattering of light by small particles. Research supported by the University of Arizona and Institute of Occupational and Environmental Health. New York, Wiley-Interscience, 541, pp.1-3.
57. Gandhi, A.A., Gunning, R.D., Ryan, K.M. and Tofail, S.A., 2010. The role of texturing and densification on optical transmittance of hydroxyapatite ceramics. *Journal of the American Ceramic Society*, 93(11), pp.3773-3777
58. Kim, B.N., Prajatelista, E., Han, Y.H., Son, H.W., Sakka, Y. and Kim, S., 2013. Transparent hydroxyapatite ceramics consolidated by spark plasma sintering. *ScriptaMaterialia*, 69(5), pp.366-369.
59. Kim, B.N., Hiraga, K., Morita, K. and Yoshida, H., 2007. Spark plasma sintering of transparent alumina. *ScriptaMaterialia*, 57(7), pp.607-610.
60. Chaim, R., Marder-Jaekel, R. and Shen, J.Z., 2006. Transparent YAG ceramics by surface softening of nanoparticles in spark plasma sintering. *Materials Science and Engineering: A*, 429(1-2), pp.74-78.
61. Watanabe, Y., Ikoma, T., Monkawa, A., Suetsugu, Y., Yamada, H., Tanaka, J. and Moriyoshi, Y., 2005. Fabrication of transparent hydroxyapatite sintered body with high crystal orientation by pulse electric current sintering. *Journal of the American Ceramic Society*, 88(1), pp.243-245.
62. Nakahira, A., M. Tamai, H. Aritani, S. Nakamura, and K. Yamashita. "Biocompatibility of dense hydroxyapatite prepared using an SPS process." *Journal of Biomedical Materials Research: An Official Journal of The Society for Biomaterials, The Japanese Society for Biomaterials, and The Australian Society for Biomaterials and the Korean Society for Biomaterials* 62, no. 4 (2002): 550-557.
63. Nakahira, A., Tamai, M., Eguchi, K., Nakamura, S. and Yamashita, K., 2003. Preparation and evaluation of dense hydroxyapatite by PECS method. In *Key Engineering Materials* (Vol. 240, pp. 551-554). Trans Tech Publications
64. Eriksson, M., Liu, Y., Hu, J., Gao, L., Nygren, M. and Shen, Z., 2011. Transparent hydroxyapatite ceramics with nanograin structure prepared by high pressure spark plasma sintering at the minimized sintering temperature. *Journal of the European Ceramic Society*, 31(9), pp.1533-1540.
65. Webster, T.J., Ergun, C., Doremus, R.H., Siegel, R.W. and Bizios, R., 2000. Enhanced functions of osteoblasts on nanophase ceramics. *Biomaterials*, 21(17), pp.1803-1810.

66. Kotobuki, N., Ioku, K., Kawagoe, D., Fujimori, H., Goto, S. and Ohgushi, H., 2005. Observation of osteogenic differentiation cascade of living mesenchymal stem cells on transparent hydroxyapatite ceramics. *Biomaterials*, 26(7), pp.779-785.
67. Ioku, K., Yoshimura, M. and Sōmiya, S., 1990. Microstructure and mechanical properties of hydroxyapatite ceramics with zirconia dispersion prepared by post-sintering. *Biomaterials*, 11(1), pp.57-61.
68. Suchanek, W. and Yoshimura, M., 1998. Processing and properties of hydroxyapatite-based biomaterials for use as hard tissue replacement implants. *Journal of Materials Research*, 13(1), pp.94-117.
69. Yadoji, P., Peelamedu, R., Agrawal, D. and Roy, R., 2003. Microwave sintering of Ni–Zn ferrites: comparison with conventional sintering. *Materials Science and Engineering: B*, 98(3), pp.269-278.
70. Eriksson, M., Liu, Y., Hu, J., Gao, L., Nygren, M. and Shen, Z., 2011. Transparent hydroxyapatite ceramics with nanograin structure prepared by high pressure spark plasma sintering at the minimized sintering temperature. *Journal of the European Ceramic Society*, 31(9), pp.1533-1540
71. Choi, J.W., Kong, Y.M., Kim, H.E. and Lee, I.S., 1998. Reinforcement of hydroxyapatite bioceramic by addition of Ni₃Al and Al₂O₃. *Journal of the American Ceramic Society*, 81(7), pp.1743-1748.
72. Chaki, T.K. and Wang, P.E., 1994. Densification and strengthening of silver-reinforced hydroxyapatite-matrix composite prepared by sintering. *Journal of Materials Science: Materials in Medicine*, 5(8), pp.533-542
73. Murakami, T., Kitahara, A., Koga, Y., Kawahara, M., Inui, H. and Yamaguchi, M., 1997. Microstructure of Nb–Al powders consolidated by spark plasma sintering process. *Materials Science and Engineering: A*, 239, pp.672-679
74. Yoo, S., Groza, J.R., Yamazaki, K. and Sudarshan, T.S., 1996. Diffusion bonding of boron nitride on metal substrates by plasma activated sintering (PAS) process. *Scripta Materialia*, 34(9).
75. Groza, J.R., 1994. Consolidation of atomized NiAl powders by plasma activated sintering process. *Scripta Metallurgica et Materialia; (United States)*, 30(1)
76. Liao, C.J., Lin, F.H., Chen, K.S. and Sun, J.S., 1999. Thermal decomposition and reconstitution of hydroxyapatite in air atmosphere. *Biomaterials*, 20(19), pp.1807-1813.
77. Tokita, M., 1993. Trends in advanced SPS spark plasma sintering systems and technology. *Journal of the Society of Powder Technology, Japan*, 30(11), pp.790-804
78. Tokita, M., 2006. Innovative sintering process-Spark plasma sintering. *Mater. Intergration*, 19, pp.19-24.
79. Wroe, R. and Rowley, A.T., 1996. Evidence for a non-thermal microwave effect in the sintering of partially stabilized zirconia. *Journal of materials science*, 31(8), pp.2019-2026
80. Sairam, K., Sonber, J.K., Murthy, T.C., Subramanian, C., Fotedar, R.K., Nanekar, P. and Hubli, R.C., 2014. Influence of spark plasma sintering parameters on densification and mechanical properties of boron carbide. *International Journal of Refractory Metals and Hard Materials*, 42, pp.185-192
81. Vanmeensel, K., Laptev, A., Hennicke, J., Vleugels, J. and Van der Biest, O., 2005. Modelling of the temperature distribution during field assisted sintering. *Acta Materialia*, 53(16), pp.4379-4388

82. Kim, D.K., Pak, H.R. and Okazaki, K., 1988. Electrodischarge compaction of nickel powders. *Materials Science and Engineering: A*, 104, pp.191-200
83. Groza, J.R. and Zavaliangos, A., 2000. Sintering activation by external electrical field. *Materials Science and Engineering: A*, 287(2), pp.171-177.
84. Conrad, H., 2002. Thermally activated plastic flow of metals and ceramics with an electric field or current. *Materials Science and Engineering: A*, 322(1-2), pp.100-107
85. Conrad, H., 2000. Effects of electric current on solid state phase transformations in metals. *Materials Science and Engineering: A*, 287(2), pp.227-237.
86. Conrad, H., 2000. Electroplasticity in metals and ceramics. *Materials Science and Engineering: A*, 287(2), pp.276-287
87. Koch, C.C., 2000. Experimental evidence for magnetic or electric field effects on phase transformations. *Materials Science and Engineering: A*, 287(2), pp.213-218.
88. Suárez, M., Fernández, A., Menéndez, J.L., Torrecillas, R., Kessel, H.U., Hennicke, J., Kirchner, R. and Kessel, T., 2013. Challenges and opportunities for spark plasma sintering: a key technology for a new generation of materials. *Sintering Applications*, 13, pp.319-342.